Development of Methods and Technology for Automated High-throughput Multi-parameter Analysis of Single Cells by Fluorescence Microscopy

---

Dissertation

zur

Erlangung der naturwissenschaftlichen Doktorwürde

(Dr. sc. nat.)

vorgelegt der

Mathematisch-naturwissenschaftlichen Fakultät

der

Universität Zürich

von

Michael Zeder

von Buchrain LU

Promotionskomitee

Prof. Dr. Jakob Pernthaler

(Leitung/Vorsitz der Dissertation)

Prof. Dr. Leo Eberl

Prof. Dr. Christian von Mering

Zürich, 2009

Dedicated to my master students.

As an ETH biochemist by education, doing my Ph.D. in the field of aquatic microbial ecology, I often felt uncomfortable with ecological experiments, because the methodologies and results of such experiments generally hardly complied with my demands on precision and accuracy. Moreover, I never dared to even think to be able to understand what is going on out there in reasonable detail. That's why I spent most of my time on the development of novel technology related to the field, trying to render aquatic microbial ecology a bit more accurate. But nevertheless, some amount of 'ecology' swapped over into my thinking as time went by ...

In Church

R. S. Thomas

(1913 - 2000)

Often I try
To analyse the quality
Of its silences. Is this where God hides
From my searching? I have stopped to listen,
After the few people have gone,
To the air recomposing itself
For vigil. It has waited like this
Since the stones grouped themselves about it.
These are the hard ribs
Of a body our prayers have failed
to animate. Shadows advance
From their corners to take possession
Of places the light held
For an hour. The bats resume
Their business. The uneasiness of the pews
Ceases. There is no other sound
In the darkness but the sound of a man
Breathing, testing his faith
On emptiness, nailing his questions
One by one to an untenanted cross.

Table of Contents

1 Summary

One important focus of aquatic microbial ecology lies on the spatial and temporal dynamics of bacterial populations in freshwater and marine systems, as well as on the structure of communities in terms of phylogenetic composition and activity distribution. These questions can be accurately and comprehensive addressed through the investigation of single cells by in-situ staining techniques and subsequent analysis by fluorescence microscopy or flow cytometry. A variety of staining protocols are available to assess abundances, phylogenetic identity and activities on a single cell level. However, while biological preparations can be produced massively parallel, the manual microscopic cell counting and sizing represents the bottleneck of this approach and limits the scope of experimental studies. The main objective of my Ph.D. thesis was to design and establish a fully automated microscopy platform for autonomous image acquisition and analysis of multiple stained microbial cells. This was realized on a commercial microscope by means of object oriented programming and the elaboration of a suitable workflow. The system was subsequently applied for the investigation of bacterioplankton dynamics during phytoplankton spring blooms in Lake Zürich and in other field studies. Particular emphasis was put on basic methodological problems arising in high throughput screening by epifluorescence microscopy in the context of aquatic microbial ecology. For one, a fast and accurate autofocus routine based on live image processing and image subdivision was created. It is able to measure the topology of fields of view to assess image quality prior to image acquisition. Nevertheless, additional post acquisition image quality control was found to be of crucial importance for data precision in high throughput imaging. An automated image quality assessment routine based on artificial neural network analysis was established to efficiently process large image datasets. Thirdly, a contour based, morphology independent algorithm was developed to accurately assess biovolumes of aquatic microbes, because it represents an ecologically important feature that can be readily retrieved by microscopy and image analysis. Currently applied methods were found to be over-simplistic and moreover strongly biased for some bacterial cell morphologies. A final project was focused on *Planktothrix rubescens*, an important constituent of the autotrophic bacterioplankton in many lakes (including Lake Zürich). Since its filamentous morphology and its large size complicate automated quantification and size measurement by conventional

image processing, an object oriented model based image analysis approach was developed for this purpose.

2 Zusammenfassung

Die Untersuchung von bakteriellen Population im Süsswasser sowie im marinen Plankton ist ein wichtiger Schwerpunkt der aquatischen mikrobiellen Ökologie. In diesem Zusammenhang sind die zeitlichen und räumlichen Dynamiken von Populationen sowie die Struktur der mikrobiellen Gemeinschaft im Bezug auf ihre phylogenetische Zusammensetzung und ihre Aktivitätsmuster von grossem Interesse. Als Mittel zur Untersuchung dieser Fragestellungen ist im Besonderen die fluoreszenzmikroskopische Analyse einzelner Zellen oder die Durchflusszytometrie geeignet. Zur Bestimmung von Abundanzen, taxonomischer Zugehörigkeit und Aktivitätslevel von einzelnen Zellen steht eine Vielfalt von etablierten Färbeprotokollen zur Verfügung. Die Produktion von biologischen Präparaten lässt sich in grossem Masse parallel realisieren, die Auswertung hingegen erfolgt generell durch manuelles Mikroskopieren, ist daher sehr zeitaufwändig und stellt den limitierenden Faktor für den Umfang von experimentellen Studien dar. Das Ziel dieser Doktorarbeit war das Konzipieren und Entwickeln einer automatischen Mikroskopie-Platform für die vollautomatische Auswertung von biologischen Präparaten mit mehrfach gefärbten Zellen. Dies wurde verwirklicht mit Hilfe eines kommerziellen motorisierten Mikroskops, objekt-orientierter Programmierung und durch Entwicklung eines spezifischen Arbeitsflusses. Schliesslich kam das System in diversen Forschungsprojekten zum Einsatz, insbesondere bei Untersuchungen zur Bakterioplankton-Dynamik während Frühjahresblüten des Phytoplanktons im Zürichsee. Bei der Systementwicklung wurde besonderer Wert auf die Lösung grundlegender technischer Probleme im Zusammenhang mit der automatisierten Hochdurchsatzmikroskopie für die aquatische Mikrobiologie gelegt. Zum einen wurde ein neues schnelles und zuverlässiges Autofokus-System entwickelt. Dieses erlaubt es, die Qualität eines Bildfeldes vor der Bildaufnahme zu beurteilen, indem an mehreren Stellen fokussiert und damit die lokale Topologie eines Präparates erfasst wird. Zum anderen ist es notwendig, automatisch aufgenommene Bilder auf deren Qualität hin zu überprüfem, um die Präzision der nachfolgenden Zellzählung mittels Bildanalyse zu gewährleisten. Dazu wurde ein vollautomatisches System entwickelt welches auf einem künstlichen neuronalen Netzwerk basiert. Neben diesen rein technischen wurden auch biologische Fragestellungen bearbeitet. Einerseits wurde ein neues, konturbasiertes, bildanalytisches Verfahren entwickelt um das Biovolumen

von Bakterien, eine ökologisch bedeutende Kenngrösse, die mittels Mikroskopie ermittelt werden kann, unabhängig von der bakteriellen Morphologie, genau zu bestimmen. Zum anderen wurde eine neue, model-basierte objekt-orientierte Bildanalysemethode entwickelt, um häufige filamentöse Cyanobakterien, beispielsweise *Planktothrix rubescens*, in der Wassersäule von Seen vollautomatisch zu quantifizieren.

3 Introduction

3.1 Single Cell Analysis in Aquatic Microbiology

Aquatic microbial ecology investigates highly complex environmental systems composed of a vast number of different organisms, namely eukaryotes, bacteria, archaea and viruses, that are altogether linked by various interactions such as competition for nutrient sources and habitats, transformation of organic matter, symbiotic relationships, or predation (Azam et al. 1983, Cole et al. 1988, Pace & Cole 1996, Pernthaler 2005, Pernthaler & Amann 2005). Some of these relationships may be qualitatively depicted as a microbial food web. Moreover, these interactions are superimposed by global physical and chemical conditions such as seasonality (Pernthaler et al. 1998), short term meteorological events, and the in- and efflux of organic and inorganic matter. As a consequence these systems are highly dynamic and hardly understandable at large[1].

One promising strategy to approach the complexity of such systems is the in-situ analysis of single microbial cells (Amann et al. 1995). It allows for addressing central questions of population and community ecology, i.e. the spatial and temporal dynamics of populations, the structure of communities and the specific roles of different organisms. Notably, the single cell analysis methods differ from the classical microbial methodology for the descriptions of microorganisms in that they do not presume the organisms of interest to be cultivable. This is important as most environmental bacteria (> 99.9%) cannot be grown in pure culture (Ferguson et al. 1984, Amann et al. 1995).

However, some of the most wide-spread methods in environmental microbiology use a rather ancient instrumentation for the analysis of cells, the light microscope, whose very development is inextricably linked with the history of microbiology (Nowak 1984, Schlegel 2004). It was invented in 1595 in the Netherlands and subsequently used to observe nature. In 1665, Robert Hooke coined the term ‘cell’ for biological organisms and the first scientific description of microbes was carried out by Antonie van Leeuwenhoek in 1676 (Fig. 1). These early observations were limited

[1] To get an understanding for the cells in the water one should probably first understand the water in the cell, but as stated by P. M. Wiggins: “Anyone attempting to describe the nature of water in the cell must realise that, because our understanding is so incomplete, the description will probably be outmoded in a decade or so.” (Wiggins 1990)

to some larger microbes as the nearly transparent smaller ones were beyond the resolution capacity of the first microscopes. As a next major improvement, microscopic staining techniques evolved over the following 200 years. On one hand, the contrast of organisms and structures could be enhanced, thus rendering them visible, on the other hand, specific stains allowed for the differentiation of microbes, representing another milestone in the history of microbiology. As a prominent example, Hans Christian Gram in 1884 introduced a staining technique for the classification of bacteria that is still widely applied today.

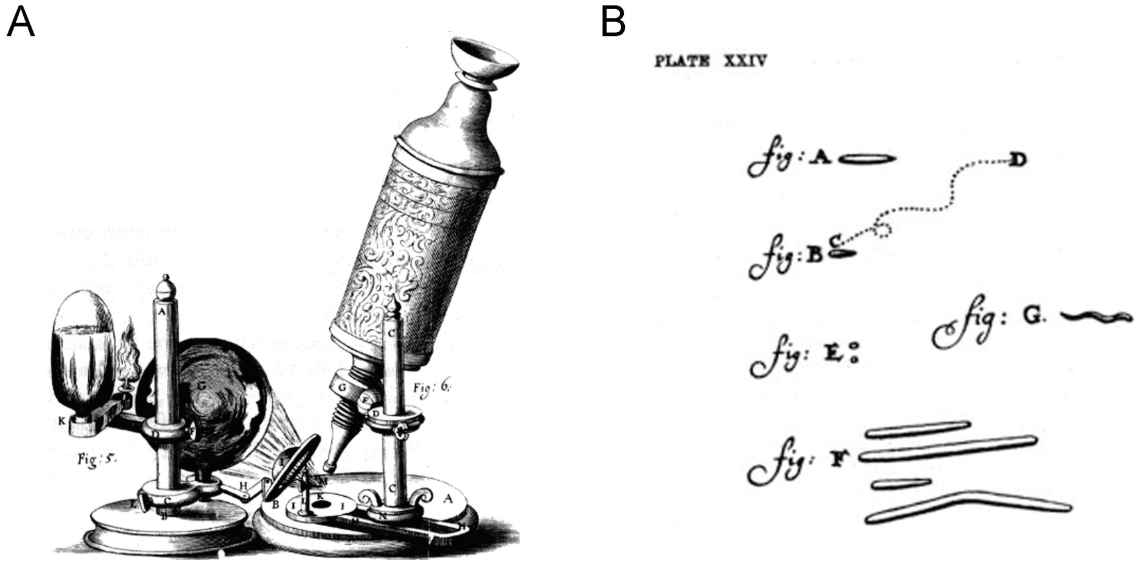

Fig. 1 A: Drawing of a microscope as used by R. Hooke (from Novak, 1984). B: Drawing of bacteria by A. van Leeuwenhoek (from Schlegel, 2004).

In the 20th century, two more revolutions[2] took place, besides to the continuous improvement of the optical instrument *per se*. The first was the introduction of fluorescent stains. In the 1930s they were originally used for histology and histopathology, but became soon universally applied in all fields of life science, also in aquatic ecology. For example, the advent of nucleic acid stains (e.g. acridine orange (Jones 1974), DAPI (Porter & Feig 1980), SYBR-Green (Noble & Fuhrman 1998)) facilitated the visualization and quantification of bacteria and viruses in water

[2] It would go far beyond the scope of this thesis to give an overview on even only the most important developments in the field of microbiology and microscopy in the 20th century, as the rate of discoveries behaves exponentially. Not because scientists are more intelligent today then centuries before, but there are just more of them. J. R. Oppenheimer stated in 1962 that from all scientists in the history of humanity, 93% are currently alive (Oppenheimer 1966).

samples. The second revolution came in the 1990s with the broad availability of digital cameras and computer systems for the acquisition and processing of microscopic images. Firstly it offered a new way for quantitative microscopy by means of both counting and measuring, and secondly, it was the first step in the direction of high-throughput microscopy (Pernthaler et al. 2003). Altogether, in the past two decades, microscopy in combination with fluorescent staining has opened new perspectives in aquatic microbial ecology, in particular also by means of single cell analysis.

But what can single cells tell? Logically, this depends on the question asked, in the figurative sense, i.e. what kind of staining protocol is applied. Notably, it is possible to apply multiple staining on a single cell, thus retrieving complementary information, rendering this approach far more powerful.

3.1.1 Abundance

The membrane filter technique for the analysis of aquatic microbes was introduced in the 1920s (Beling & Jannasch 1955) and has become a standard method nowadays, e.g. for the determination of the number of prokaryotes present in a distinct volume of water. Basically, water is filtered through a polycarbonate track etch membrane filter with a pore size of 0.2 µm, retaining almost all bacteria, and some larger viruses (Hobbie et al. 1977, Noble & Fuhrman 1998). The known filtered volume and filter area allows for a quantification of fluorescently stained microorganisms (Fig. 2).

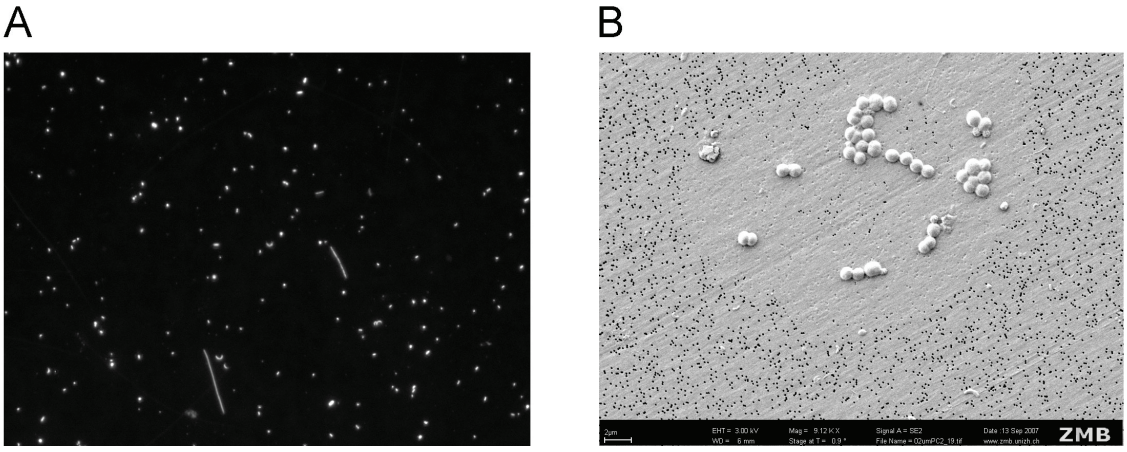

Fig. 2 A: Microscopic image of fluorescently stained cells (DAPI) on a membrane filter (63 × objective). B: Scanning electron micrograph of a membrane filter containing microbial cells. Images by MZ, electron microscopy was kindly supported by the ZMB, University of Zürich.

In addition, there are constituents of the plankton that are visible by fluorescent microscopy without prior staining, e.g. autotrophic algae or cyanobacteria. However, the mere total abundance of microbial cells is, in the context of to the current state of research, not a highly valuable information *per se*, nor is microscopy, even automated microscopy, the fastest and most convenient way to obtain this information. Another very promising technology for this purpose that arose over the last decades is flow cytometry. It was developed by Wolfgang Göhde in 1968 for the analysis of particles suspended in a stream of fluid (Shapiro 1995). Originally used in the field of medicine (e.g. hematology, tumor immunology, or sperm sorting) it also found application in aquatic sciences (Legendre et al. 2001) for counting and sorting (Fuchs et al. 2000, Andreatta et al. 2002, Sekar et al. 2004) of microbial cells in a high throughput manner. However, it is not fully compatible with some important staining protocols in environmental microbiology (e.g. CARD-FISH, MAR-FISH), and thus cannot replace microscopy. A general staining of all bacteria by means of a nucleic acid stain is routinely applied in most multiple staining protocols to link the number of specifically stained cells to the total cell number for retrieving relative abundances.

3.1.2 Cell Biomass and Morphology

As aquatic bacteria exhibit a wide range of cell sizes and morphologies (Henrici 1933, Boyde & Williams 1971, Young 2006, Posch et al. 2009), the mere abundance of cells or specific groups of cells might not be an adequate ecological descriptor, especially when the transfer of organic matter (e.g. carbon fluxes) is the subject of investigation. Therefore, the biomass of single cells is of interest. Microscopy and image analysis allow for the calculation of biovolumes from detected cells on images and then, by the applications of suitable conversion factors, the biomass and carbon content of cells can be estimated (Sieracki et al. 1989, Bloem et al. 1995, Blackburn et al. 1998, Posch et al. 2001, Posch et al. 2009).

Next to the biovolume of a cell, the morphology is another interesting feature that can be quantified by image analysis. While there is a considerable morphological diversity in the microbial world, the underlying reasons and its ecological role are yet poorly understood (Young 2006). At the same time, morphological features seem to be important for bacterial survival, e.g. the ubiquitous marine SAR11 bacteria are vibrioid shaped. The genome of these bacteria has found to be reduced to a

minimum (Giovannoni et al. 2005), but still they possess sub cellular structures to maintain this specific morphology, indicating that this might be of high importance. A promising approach to classify shapes of bacteria is to analyze their cell boundaries by Fourier analysis. The retrieved invariant Fourier descriptors may subsequently be used in a neural network analysis for classification (Blackburn et al. 1998).

3.1.3 Phylogenetic Identification by Fluorescent *in-situ* Hybridization

The above mentioned phenotypic analysis of uncultivable bacteria is, on its own, strongly limited, as it describes the bacterial community as one entity. The introduction of molecular techniques in biology, e.g. amplification (PCR) and sequencing of nucleic acids marked a major breakthrough in biology. The analysis of genomic sequences opened new perspectives and allowed for the identification of prokaryotes on the species level, based on genetic markers, the most prominent of which is the 16S rRNA gene. Fluorescent *in situ* hybridization (FISH) is a molecular staining methodology based on rRNA-targeted oligo- or polynucleotide probes that allows the phylogenetic identification and quantification of single bacteria (Giovannoni et al. 1988, DeLong et al. 1989, Amann et al. 1990, Amann et al. 1995, Glöckner et al. 1996). This approach has been widely applied to study microbes in different environmental habitats but also in experimental investigations (Alfreider et al. 1996, Jurgens et al. 1999, Pernthaler et al. 2001, Pernthaler & Amann 2005). A major disadvantage of FISH with mono-labeled probes is that cells harbouring a low number of ribosomes, as many prokaryotes in the environment do, yield a low fluorescence signals and are thus not detectable. An improved protocol, based on enzymatic signal amplification (CARD: catalyzed reporter deposition, (Pernthaler et al. 2002b, Sekar et al. 2003)) finally resolved this issue. CARD-FISH allows for the detection of small or starving cells and thereby increases the detection rate in environmental samples.

3.1.4 Assessment of Activity by Microautoradiography and BrdU Incorporation

The mere *in situ* quantification of bacterial taxa is often not sufficient to get a detailed understanding about their ecological role, as information about the activity of the organisms is missing (Alonso 2005). From the many methods for studying microbial activity on a single cell level, two examples shall be mentioned here,

microautoradiography (MAR) and the BrdU incorporation method. Notably, they are both compatible with the FISH staining technique and microscopic evaluation.

Microautoradiography is known in biological sciences since the 1960s (Brock 1967) and allows for the visualization of the incorporation of radiolabelled substrates by microbial cells. The use of radioactive isotopes, e.g. tritium, renders this approach highly sensitive and the chemical and physical properties of the labelled substrate largely coincide with those of the original, natural molecule (Smith & del Giorgio 2003, Alonso 2005). The combination of the FISH and the MAR method, subsequently termed MAR-FISH has become popular in the field of aquatic microbial ecology in the last decade (Lee et al. 1999, Ouverney & Fuhrman 1999, Cottrell & Kirchman 2000, Alonso & Pernthaler 2005, Alonso et al. 2008, Salcher et al. 2008). Briefly, bacteria from environmental samples are incubated with a radiolabelled tracer (e.g. glucose, leucine or thymidine) for a defined time span (hours) close to *in situ* conditions and subsequently fixed. Thereafter, the standard FISH protocol is applied and the preparations are finally covered with an autoradiographic emulsion. Cells containing radioactivity then trigger the formation of visible silver grain deposits in close proximity. These can be imaged in bright field illumination and quantified.

Another, eventually more direct measure for activity is the quantification of cell growth, e.g. cell division. In order to proliferate, microbial cells have to duplicate their genome, what involves DNA synthesis. The chemical compound 5-bromo-2'-deoxyuridine (BrdU) is a thymidine analog that is, when offered in incubation, incorporated into the newly synthesized DNA by dividing cells and can be later on visualized by the immuno-fluorescence staining (Pernthaler et al. 2002a). This technique has been applied in environmental studies (Hamasaki et al. 2004, Warnecke et al. 2005, Zeder et al. 2009) to track cell growth. However, it is known that certain bacteria are not able to incorporate this compound (Urbach et al. 1999).

3.2 Automated High-Throughput Microscopy and Image Analysis

The above mentioned staining methodologies and especially their combinations provide a powerful tool to address scientific questions in aquatic microbial ecology. However, the evaluation of such experiments is based upon microscopic analysis of samples and manual counting of microbial cells is a highly time consuming and tedious task. Actually, this part of the procedure represents the bottleneck of the approach and depicts the limiting factor of any large study (Schattenhofer 2009).

Not surprisingly, attempts have been made to automate the microscopic evaluation of fluorescently stained preparations, notably in many areas life sciences. Historically, the first step in automation was carried out in the 1970s by automated analysis of manually acquired digital images (Bartels et al. 1972, Krambeck et al. 1981, Sieracki et al. 1985, Bjornsen 1986, Pernthaler et al. 1997), whereas the second, technically more complex part, the (semi-) automated image acquisition was achieved decades later (Gmür et al. 2000, Singleton et al. 2001, Pernthaler et al. 2003, Daims & Wagner 2007) (Fig. 3). Despite of the obvious advantages, fully automated microscopy platforms are not widely spread in the field of aquatic microbiology today. On the one hand, fully motorized and programmable microscopes have become commercially available off the shelf only recently. On the other hand, the automation of a specific, user-defined, task involves intensive effort, including knowledge on image analysis and high-level programming.

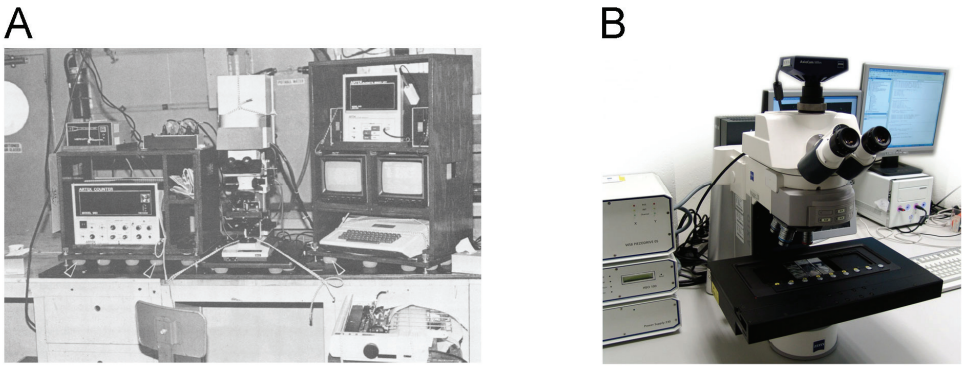

Fig. 3 A: Microscope and image analysis system for the use on a ship as described by Sieracki in 1985. Automated microscope used in this thesis (AxioImager.Z1, Zeiss, Germany).

3.3 Lake Zürich: Phytoplankton Spring bloom and Planktothrix rubescens

The field experiments within this thesis were focussed on the mesotrophic prealpine Lake Zürich. It is located in canton Zürich, Switzerland, at a height of 406 m.a.s.l. and features a maximal depth of 136 m (mean: 51 m), a surface area of 68 km^2 and a water retention time of 1.4 years (Bossard et al. 2001). Besides its quality for recreation it serves as the major source of drinking water for the city Zürich and for several communities located at the shore. As many other lakes in Switzerland, Lake Zürich was strongly affected by anthropogenically induced eutrophication during

the first decades of the 20th century. Since the installation of sewage treatment plants with enhanced phosphorus removal, the weighted annual averages of total phosphorus concentrations decreased from > 100 µg l^{-1} in the 1970ies to stable values around 30 µg l^{-1} in the mid of the 1990s. During the last decades a detailed monitoring of the lake has been conducted by the Zürich Water Supply (http://www.stadt-zuerich.ch/internet/wvz/home.html). However, the knowledge about the ecology of heterotrophic bacteria in Lake Zürich is still scarce[3].

Phytoplankton communities in temperate lakes undergo predictable seasonal transitions (Sommer et al. 1986). As a spring phytoplankton bloom is accompanied by rapid alterations of environmental factors, it represents a highly interesting situation for the short time analysis of changes in the bacterioplankton. Therefore, we investigated the dynamics and growth state of bacterioplankton taxa during a spring bloom event in Lake Zürich. Sampling with high temporal resolution was required to adequately map the development of physicochemical and biological parameters during this dynamic period of plankton succession.

Besides the heterotrophic bacterioplankton, the filamentous cyanobacterium *Planktothrix rubescens* is a highly interesting inhabitant of the pelagic zone of many lakes (Fastner et al. 1999b, Ernst et al. 2001). On the one hand, it is the dominant primary producer in Lake Zürich, and on the other hand, it is known to produce a variety of potent toxins, rendering this organisms important in terms of human health concerns and drinking water quality control (Fastner et al. 1999a, Chorus et al. 2000, Blom et al. 2001, Blom et al. 2003, Hoeger et al. 2005). Thus there is a need for rapid methods for the quantification of this organism in environmental samples, e.g. for monitoring purposes. While automated quantification of small, single-celled bacteria is an established technology, the quantification and sizing of such large filamentous organisms is more difficult to achieve by image analysis.

[3] From the roughly 400 publications on Lake Zürich, there are just three which are concerned with heterotrophic bacteria (Button et al. 1996, Koster & Juttner 2001, Zeder et al. 2009), T. Posch, personal communication.

4 Objectives and Content of the Thesis

The main objective of this Ph.D. thesis was to design and establish an automated high-throughput microscopy platform for imaging and evaluation of preparations of multiple stained bacteria resulting from experimental and explorative studies in aquatic microbial ecology. The second objective was to apply the system to investigate bacterioplankton dynamics in a spring phytoplankton bloom situation in Lake Zürich (Publication 5). The process of technical development lasted three years and is still ongoing. During that period, specific problems related to high-throughput microscopy were encountered and had to be addressed in detail, resulting in two scientific publications. Publication 1 describes the development of an autofocus routine for high-throughput microscopy and Manuscript 2 deals with automated image quality assessment.

The system was operational since 2007 but it has not yet been separately described in a publication and is thus discussed in detail within this thesis. During the time of development, the system was applied in several studies conducted at the Limnological Station of the University of Zürich (Alonso et al. 2008, Salcher et al. 2008, Zeder et al. 2009) or in collaborations with external researchers.

Besides the development of technology related to high-throughput microscopy, special emphasis was given on the elaboration of new image analysis methods in the context of aquatic microbial ecology. Manuscript 3 describes a tool for the quantification and sizing of *Planktothrix rubescens* by object oriented image analysis. Manuscript 4 deals with a contour based algorithm for accurate and morphology independent measurement of bacterial biovolumes. As the manuscript is in preparation, its content is described in the ‘Methods and Results’ part of this thesis.

Software development depicted a substantial part of this work and whenever possible it was made freely available for others to use (freeware / open source). The programs are deposited on my personal website (http://www.technobiology.ch).

4.1 Selected Publications and Manuscripts

The main scientific output of within this thesis is presented by two publications as first author, two co-authored publications, one submitted manuscript and two manuscripts in preparation.

4.1.1 Publications on the Development of Technology related to Microscopy and Image Analysis

Publication 1

Zeder M, Pernthaler J., Multi-spot live-image autofocusing for high-throughput microscopy of fluorescently stained bacteria. Cytom Part A. In press 2009. Own contribution: MZ designed and developed the method and wrote the publication.

Manuscript 2 (submitted to Cytometry A)

Zeder M, Kohler E, Pernthaler J., Automated quality assessment of autonomously acquired microscopic images of bacteria by artificial neural network analysis. Own contribution: MZ supervised the master thesis of EK, designed and developed the method in collaboration with EK and wrote the publication.

Manuscript 3 (in preparation)

Zeder M, Van den Wyngaert S, Felder K, Pernthaler J., Automated quantification and sizing of unbranched filamentous cyanobacteria by model based object oriented image analysis. Own contribution: MZ designed and developed the method and wrote the publication.

Manuscript 4 (in preparation, described in the 'Methods and Results' section)

Zeder M, Kohler E, Zeder L, Pernthaler J., A generic contour based morphology independent algorithm for biovolume determination of microbial cells by image analysis. Own contribution: MZ supervised the master thesis of EK, designed and developed the method in collaboration with EK and wrote the publication.

4.1.2 Publications on the Application of the Developed Technology

Publication 5

Zeder M, Peter S, Shabarova T, Pernthaler J., A small population of planktonic *Flavobacteria* with disproportionally high growth during the springphytoplankton bloom in a prealpine lake. Environ Microbiol. Accepted 2009. Own contribution: MZ co-supervised the master thesis of PS and TS, established the technical basis for imaging and evaluation, evaluated a substantial part of the dataset and participated in the writing of the publication.

Publication 6

Alonso C, Zeder M, Piccini C, Conde D, Pernthaler J., Ecophysiological differences of betaproteobacterial populations in two hydrochemically distinct compartments of a subtropical lagoon. Environ Microbiol. 2009. Own contribution: MZ provided and customized the method for sample imaging, assisted in data evaluation and writing of the publication.

Publication 7

Salcher MM, Pernthaler J, Zeder M, Psenner R, Posch T., Spatio-temporal niche separation of planktonic *Betaproteobacteria* in an oligo-mesotrophic lake. Environ Microbiol. 2008. Own contribution: MZ provided and customized the method for sample imaging, assisted in technical data evaluation and writing of the publication.

5 Methods and Results

5.1 Description of the Automated Microscopy Platform

The automated microscopy platform developed in this thesis is an integrated system consisting of several components and computer programs arranged in a linear workflow (Fig. 4). Firstly, preparations on the microscopic slides are localized and a coordinate list is generated. Secondly, the preparations are imaged and the images are stored as .JPG files. Thirdly, a quality control routine discards images of low quality. Fourthly, images are analyzed and the information (e.g. detected cells) is stored in a metadata file. Fifthly, the metadata file is evaluated by the user and a report is generated. The system was designed to be open and expandable to allow for imaging and evaluation of different kinds of samples, i.e. from different environments, and stained by different techniques.

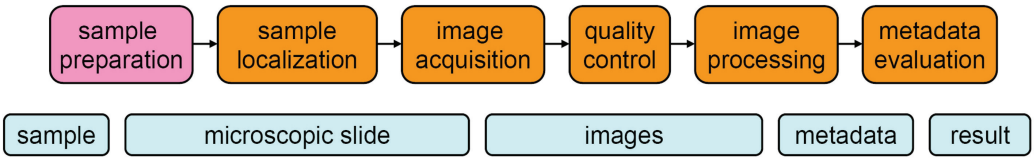

Fig. 4 Schematic representation of the workflow. The upper row depicts the methodological workflow. The orange boxes represent individual program routines. The blue boxes depict the flow of information.

5.1.1 Microscope Hardware

The automated screening platform is based on an AxioImager Z.1 (Fig. 3 (see introduction section) and Fig. 5) epifluorescence microscope (Carl Zeiss, Germany) with a motorized stage for eight microscopic slides (WSB Pieozodrive 05; 225 × 85). The microscope was equipped with a 1 × EC Plan-NEOFLUAR (NA = 0.025), a 10 × EC Plan-NEOFLUAR (NA = 0.3), a 40 × Plan-NEOFLUAR (NA = 1.3), a 63 × Plan-APOCHROMAT (NA = 1.4), and a 100 × EC Plan-NEOFLUAR (NA = 1.3). For both, epi- and transmission illumination, LED devices were used. The COLIBRI system was used for epifluorescence illumination, featuring four LEDs (365 nm, 450-700 nm, 470 nm, and 590 nm). Four filter blocks were employed: 62 HE (Ex.: BP 370/40, BP 474/28, BP 585/35; FT: 395, 495, 610; Em.; BP 425, BP 527, LP 615), 43 (Ex.: BP

545/25; FT 570; Em.: BP 605/70), and 26 (Ex.: BP 575-625; FT 645; Em.: BP 660-710), 49 (Ex.: G 365; FT 395; Em.: BP 445/50).

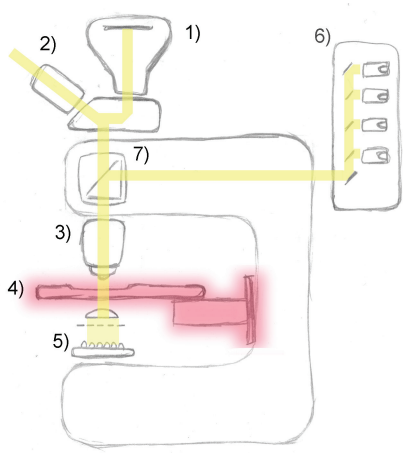

1) CCD camera

2) Ocular

3) Objective

4) Motorized stage

5) LED transmission illumination

6) LED epifluorescence illumination

7) Multi filter set

Fig. 5 Schematic depiction of the automated microscope.

5.1.2 Image Analysis Software and Software Development Environment

Image analysis was either performed using the commercial software AxioVision (Carl Zeiss, Germany) or programmed within Visual Basic .NET (Microsoft). AxioVision 4.7 is an extendable software package and the module “VBA” was used for automation. It allows for controlling the microscope hardware. Furthermore it gives access to the image processing libraries required for automation of image analysis routines. The AxioVision module “MosaiX” was used to create composite images for either the generation of coordinate lists or the imaging of large areas in order to quantify *Planktothrix rubescens* (see Manuscript 3). The “Extended Focus” module was applied to calculate sharp images from z-stacks and thereby compensate for small topological unevenness of preparations (see Publication 1).

5.1.3 Autonomous Image Acquisition

Autonomous image acquisition was realized by creating two programs in AxioVision VBA, a tool for the generation of coordinate lists and a tool for image acquisition.

Generation of coordinate lists: Prior to image acquisition, the locations of fields of view (FOVs) (the preparations, respectively) to be imaged have to be defined

spatially on the microscope stage. Microscopic preparations may feature different geometries. Most typically they are triangular filter segments resulting from cutting polycarbonate membrane filters by a scalpel or using a filter cutter device designed for this purpose by the author and manufactured by Wiederkehr Metallbau AG (Boswil, Switzerland) (for detailed information see: http://www.technobiology.ch). Often, whole filters are subjected to imaging, featuring a circular shape. Additionally rectangular shapes or multiwell slides may occur. The use of predefined coordinate lists with a predefined number of FOV per preparation forcing users to allocate their filter pieces in a well defined way has been proposed (Pernthaler 2003) but renders image acquisition less flexible. Therefore, a generic tool was developed to create user specific coordinate lists. In a first step, all slides on the stage are imaged by a low magnifying objective (1 ×; a single slide is imaged by acquiring and stitching 3 × 11 single images).

On these overview images, image processing is performed to detect filter pieces and to recognize their morphologies (triangle, rectangle, or circle) on the basis of their contours. A user defined number of FOV positions are generated on each recognized preparation for systematic random uniform sampling. Moreover the user is able to add, move or remove preparations (Fig. 6). Importantly, the preparations have to be named by the user at this step of the workflow, and, during the image acquisition step, the names of the preparations are stored within the corresponding .JPG files as tags, for subsequent image identification.

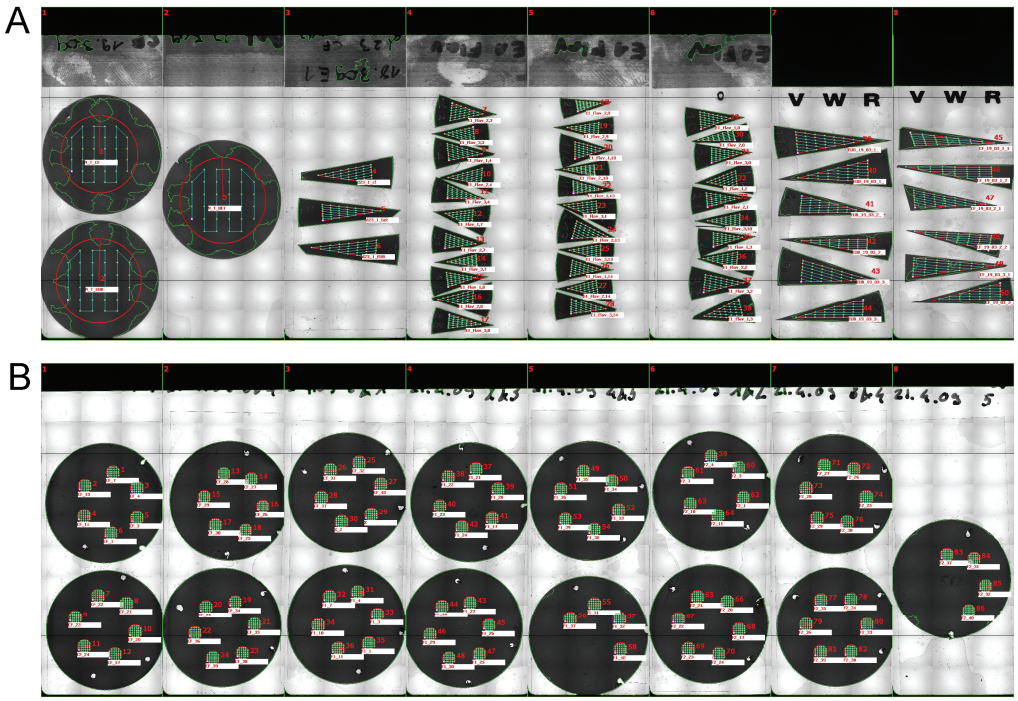

Fig. 6 Two examples of annotated images produced by the coordinate list tool. Each image shows eight slides. A: The first two slides contain entire 25 mm membrane filters, slides 2-6 contain pieces of 25 mm filters and slides 7-8 contain pieces of 47 mm membrane filters. B: Eight slides containing 25 mm membrane filters with six spots of bacterial suspension per filter (obtained from flow cytometric sorting).

Autonomous image acquisition: A program for multi channel image acquisition was created within AxioVision VBA (Fig. 7). The program supports imaging with different magnifications (Fig. 7 A). Up to four images in fluorescence illumination (Fig. 7 B) and one image in bright field illumination (Fig. 7 C) can be acquired per FOV to evaluate different types of experiments: e.g. single staining with DAPI for cell counting, biovolume and morphology assessment, double staining for standard FISH experiments, triple staining for double hybridized FISH or FISH + BrdU experiments, and additional bright field imaging for MAR signal detection.

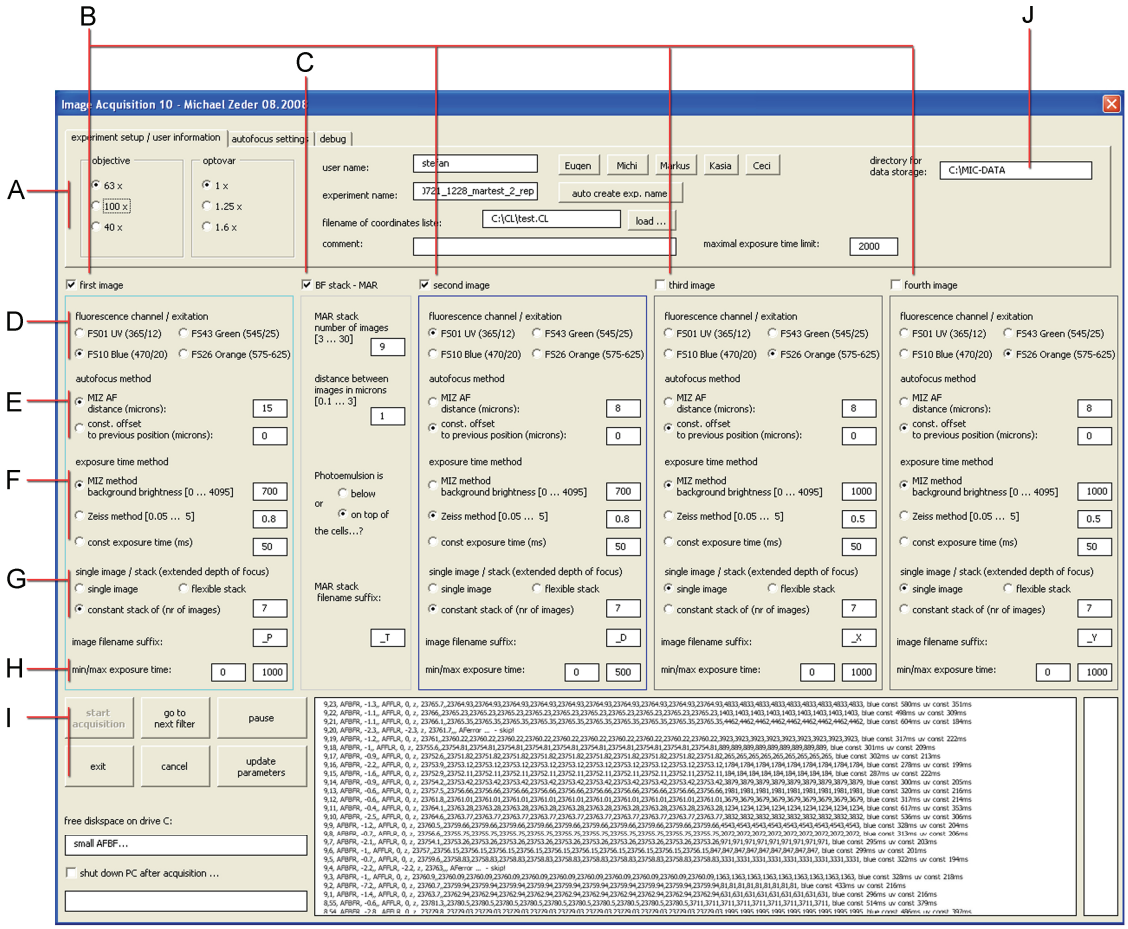

Fig. 7 Graphical user interface of the image acquisition program.

The program allows for the adjustment of settings for excitation wavelength (Fig. 7 D), focusing method (Fig. 7 E), exposure time (Fig. 7 F), and z-stacking extent (Fig. 7 G) for each channel. The exposure time can be set to a constant time, or dynamically adjusted, by either choosing the auto-exposure method by AxioVision or by setting a constant mean gray level intensity of the image, determined by exposure bracketing on the live image. In addition, a minimal and a maximal time can be set to limit the range of the automatically determined exposure time (Fig. 7 H). The program provides two possibilities to adjust the focus: it can be set in relation to the previously found focus position by an offset value or the autofocus routine can be applied. The autofocus routine developed by the author is described in detail in Publication 1. Z-stacking and subsequent application of the extended focus algorithm (which calculates a single, optimized image from a z-stack (Forster et al. 2004)) provided in AxioVision has been shown to significantly improve cell counting accuracy, but at the cost of extended duration of the imaging procedure (as multiple images have to be

acquired per FOV). Therefore, the number of images per z-stack as well as the distance between images can be set by the user. Importantly, while the system is running, the user has the possibility to interrupt the image acquisition, skip preparations, or change the imaging settings mentioned before (Fig. 7 I). Images are stored in the .JPG format (grayscale, 8 Bit) in a user specified directory (Fig. 7 J), together with a report and the overview image with an annotation of the recognized preparations and the FOVs. A fully loaded stage, comprising 8 slides, 8 FISH preparations per slide and 36 FOVs per preparation can be imaged within about 12 hours, e.g. overnight. The here used microscope was equipped with LED illumination devices for transmission- and, more importantly, for epiillumination (COLIBRI, Zeiss). LED devices are of high value in automated systems that exhibit long operation times, as they can be readily switched on and off during different stages of imaging, have a long lifetime, need no maintenance and consume less energy than conventional illumination devices. Moreover, the availability of four LEDs with distinct wavelengths and a multi filter set eliminates the need of mechanically switching filter sets in order to image different fluorescent dyes, which reduces the mechanical load of the system and hence renders the process of imaging significantly faster.

5.1.4 Image Quality Control

Prior to image analysis, autonomously acquired images have to be checked for their quality in order to exclude low quality images. Low quality images significantly lower counting precision and accuracy, as shown in Manuscript 2. Because manual assessment and sorting of images is a time consuming and tedious task, the author developed a computer program in VB.NET for automated assessment of image quality by neural network analysis. The program and its underlying concepts are described in detail in Manuscript 1.

5.1.5 Image Analysis and Metadata Concept

The ultimate goal of high throughput imaging is to gain quantitative data. Depending on the scientific question, different parameters have to be measured on images. In the field of microbial ecology, fundamental variables to be extracted include: The absolute cell numbers on a preparation, the relative abundance of multiple stained cells, cell morphologies and biovolumes of cells.

Conventional image analysis tools are based on image processing, object detection, object measurement and report generation in a linear workflow. As a consequence, images have to be reprocessed, if an image dataset has to be evaluated multiple times, e.g. to revise results of object detection or to obtain additional data (e.g. cell sizes). As image processing is the most time consuming step in the entire procedure, the author has introduced the concept of metadata, in analogy with the data evaluation strategy realized in flow cytometry. By this approach, images have to be processed only once and all possible objects are detected. For each object, characteristic features are measured and saved in text format as a metadata file. These features are densitometric (e.g. mean object brightness, brightest pixel intensity etc.) as well as geometrical parameters (e.g. length, width, area, perimeter, contour coordinates, Fourier descriptors, circularity etc.). The program for the generation of metadata files was created within AxioVision VBA and allows for analysis of single image experiments, double staining experiments and triple staining experiments such as MAR-FISH and BrdU-FISH. The computer program for the evaluation of the metadata files was developed in VB.NET using an object oriented programming approach. By loading a metadata file, an object structure is build up in the RAM of the computer, containing preparations, FOV per preparation and cells per FOV for each channel. The program provides functionality to select cells to be counted by setting gates for area and brightness (Fig. 8). Preloading of all data into the RAM allows for fast data processing (i.e. re-analysis of images is approx. 1000 times faster than conventional re-processing of images).

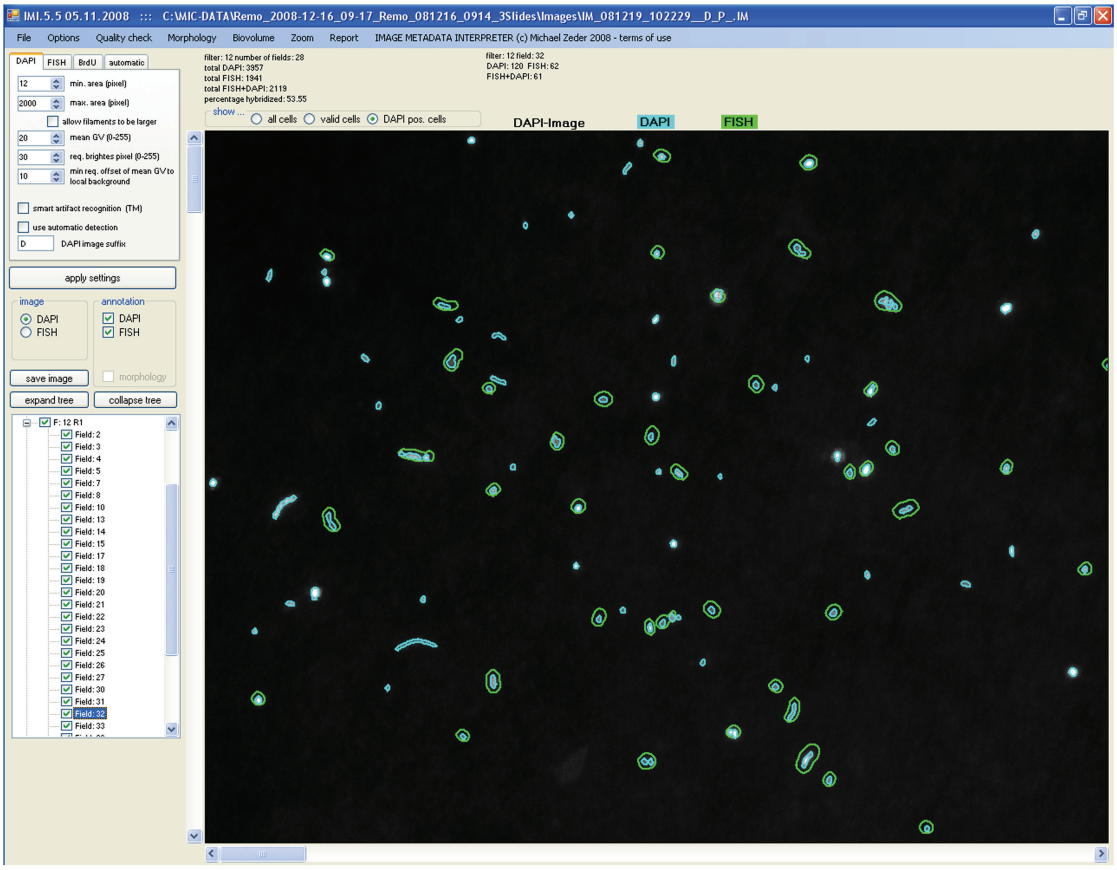

Fig. 8 Graphical user interface of the image metadata interpreter program.

5.2 Description of a Novel Algorithm for Biovolume Calculation

(To be extended into Manuscript 4)

Bacterial biovolumes are an important feature in aquatic microbial ecology. Recent studies have shown that conclusions about the composition of bacterial communities in aquatic systems may depend on whether the contribution of bacterial biomass to taxonomic groups is analyzed rather than their abundance (e.g. (Posch et al. 2009)). Fluorescence microscopy and image analysis represent suitable tools for the determination of bacterial biomass. However, the presently used methods to calculate bacterial biovolumes from digital images are biased by the models used to approximate the morphology of the cells. In this study the author developed a generic contour based algorithm to determine cell biovolumes that is not biased by the shape of a cell. Geometric models of commonly encountered bacterial morphotypes were

used to verify the algorithm and to compare its performance with the existing methods.

5.2.1 Description of the Problem

Multi parameter analysis of bacterial cells by automated high-throughput microscopy is a powerful approach to study microbial dynamics in ecosystems. Phylogenetic community assemblage and bacterial activity can be assessed on a single cell level by fluorescent staining techniques such as fluorescence in-situ hybridization (CARD-FISH) and microautoradiography (MAR). The evaluation is usually based upon cell counting and yields thus abundances of cells exhibiting specific features relative to total cell counts. However, mere counting does not take into account that bacteria exhibit a large range of cell sizes and morphologies (Young 2006), and it is a matter of discussion whether features should be related to cell numbers or biovolumes (Posch et al. 2009).

One argument for preferring cell counts to biovolumes as a reference is that cell counts can be retrieved faster, with less computational effort and much more accurate. Moreover, the automated cell counting by image analysis is increasingly becoming standard methodology nowadays (Pernthaler et al. 2003, Daims & Wagner 2007). However, in our opinion there are good reasons for the assessment of bacterial biovolumes in addition to cell counting: (i) if images of sufficient quality are acquired for counting, the prerequisite for biovolume calculation is already given, and (ii) biovolumes may represent another qualitative level of information with ecological importance (Psenner & Sommaruga 1992, Posch et al. 2007, Posch et al. 2009, Schattenhofer et al. 2009).

Calculation of biovolumes by image analysis is a long standing topic in literature and many methods have been proposed for this purpose (Bloem et al. 1995, Posch et al. 1997, Blackburn et al. 1998). Typically, simple geometrical models are used, assuming that bacterial shapes can be approximated with sufficient accuracy. These methods are based on the measurement of basic features such as area, perimeter, length and width. A more sophisticated algorithm has been proposed by Sieracki et al. (Sieracki et al. 1989). It is based on the contour and treats cells as solids of revolution, assuming a straight major axis. This assumption is valid for some classes of morphologies such as cocci and rods but not for others such as vibrioid and filamentous cells.

Therefore, an algorithm was developed that is free of unnecessary geometrical assumptions and requires only the contour of a microbial cell to estimate its biovolume. This algorithm is accurate and not affected by the cells morphology in contrast to the presently available algorithms. Thus, it is robust and suited to be integrated in fully automated image processing systems.

5.2.2 Conception of the Algorithm

The basic idea of the algorithm is that a microbial cell, independently of its morphology, can be cut into segments that can be approximated by half cylinders. In the two dimensional projection, as it is given by microscopic imaging, the cell contour, subsequently referred to as polygon, has to be cut into triangles. These triangles are subsequently used for the reconstruction of the half cylinders. The summation of the volumes of those volume elements finally results in the volume of the microbial cell.

The algorithm was implemented in VB.Net following an object oriented programming approach, packing the functionality in a separate class. The input for the algorithm to calculate the biovolume of an object consists of a list of the contour points (x,y-coordinates) of that particular object, in the form of a two dimensional array of the data type ‘double’. This input data has to be retrieved by image analysis either directly from the contour of an objects or indirectly via its fourier descriptors. The contour points have to be listed in adjacent order, anti-clockwise. In a first step, normal vectors are calculated for every point on the polygon considering the coordinates of the point and its two neighbouring points.

The algorithm segments a polygon with n corners into n-2 triangles. This is done in a recursive way, as the excision of a triangle from a polygon splits that particular polygon into two new polygons. Within the newly generated polygons, the same step is applied recursively, until all n-2 triangles have been defined.

Two cases are distinguished: (i) the new polygon is an end region of the entire contour or (ii) it is not. In the first case, the remaining polygon is consecutively divided into triangles, starting with the largest possible triangle. In the second case, an optimization function is used for finding the optimal triangle in a polygon (Fig. 9).

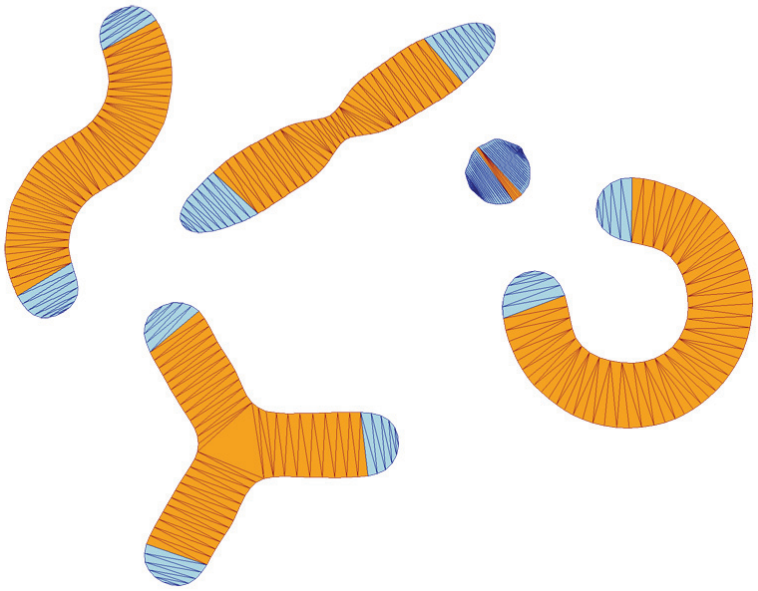

Fig. 9 Examples of five geometrical models subdivided in triangles by the algorithm. End regions are depicted in blue.

5.2.3 Verification of the Algorithm

For verification of the algorithm, we created 22 geometrical models of realistic bacterial morphotypes (Fig. 10) by computer aided design (CAD-tool ProEngineer Wildfire 4, PTC). Geometric formulas allow for the calculation of the true volume of an object from its cross-section area. The cross section is the projection of the object as it is given on a microscopic image. Cross section images have been generated and subjected to image analysis where object detection and measurement of basic features such as area, perimeter and Fourier descriptors was performed.

Three different algorithms described in the literature (Sieracki et al. 1989, Bloem et al. 1995, Blackburn et al. 1998) were compared with the described method to determine the volumes of the geometrical models, based on the cross section images and the measured features. As the true volume could be calculated for every model by measuring its area and applying the corresponding formula, the errors of the different methods could be quantified (Fig. 11).

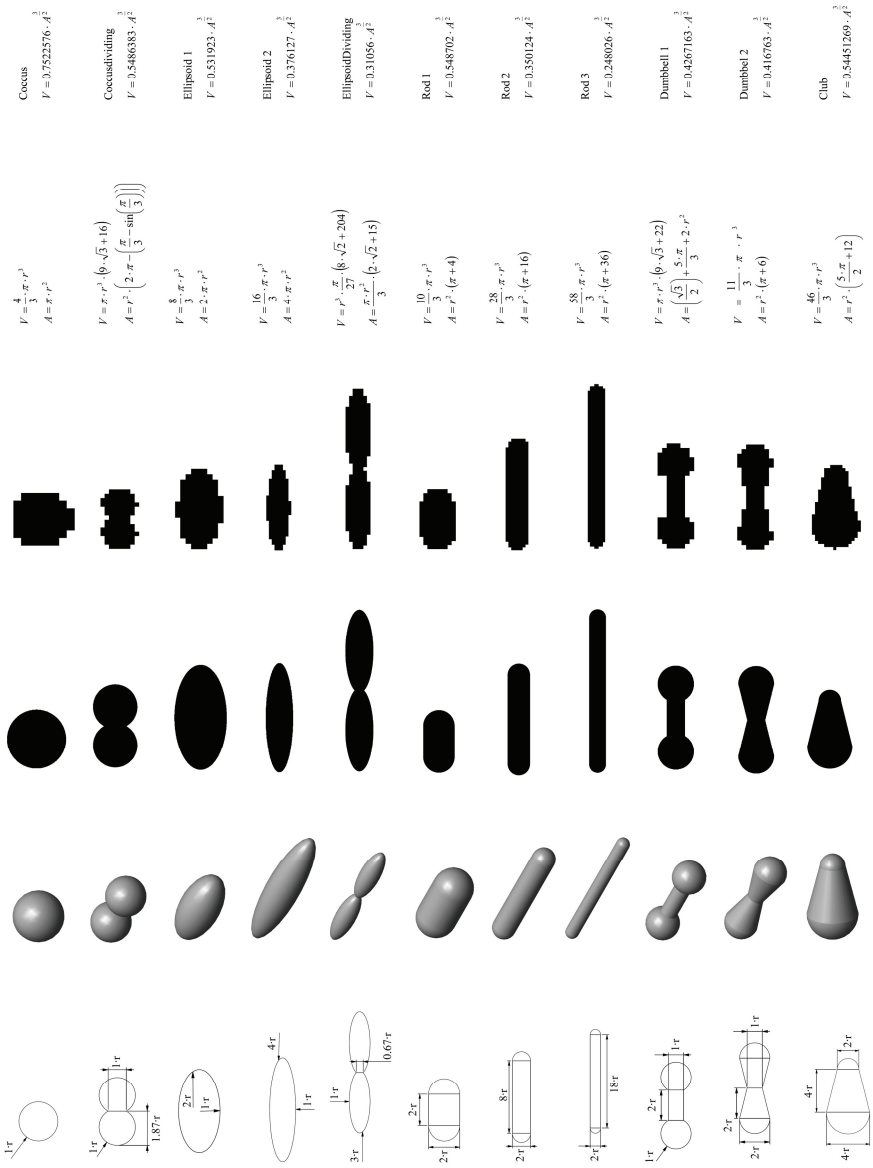

Fig. 10 Geometrical models of different bacterial morphologies. Formulas for volumes and areas are given.

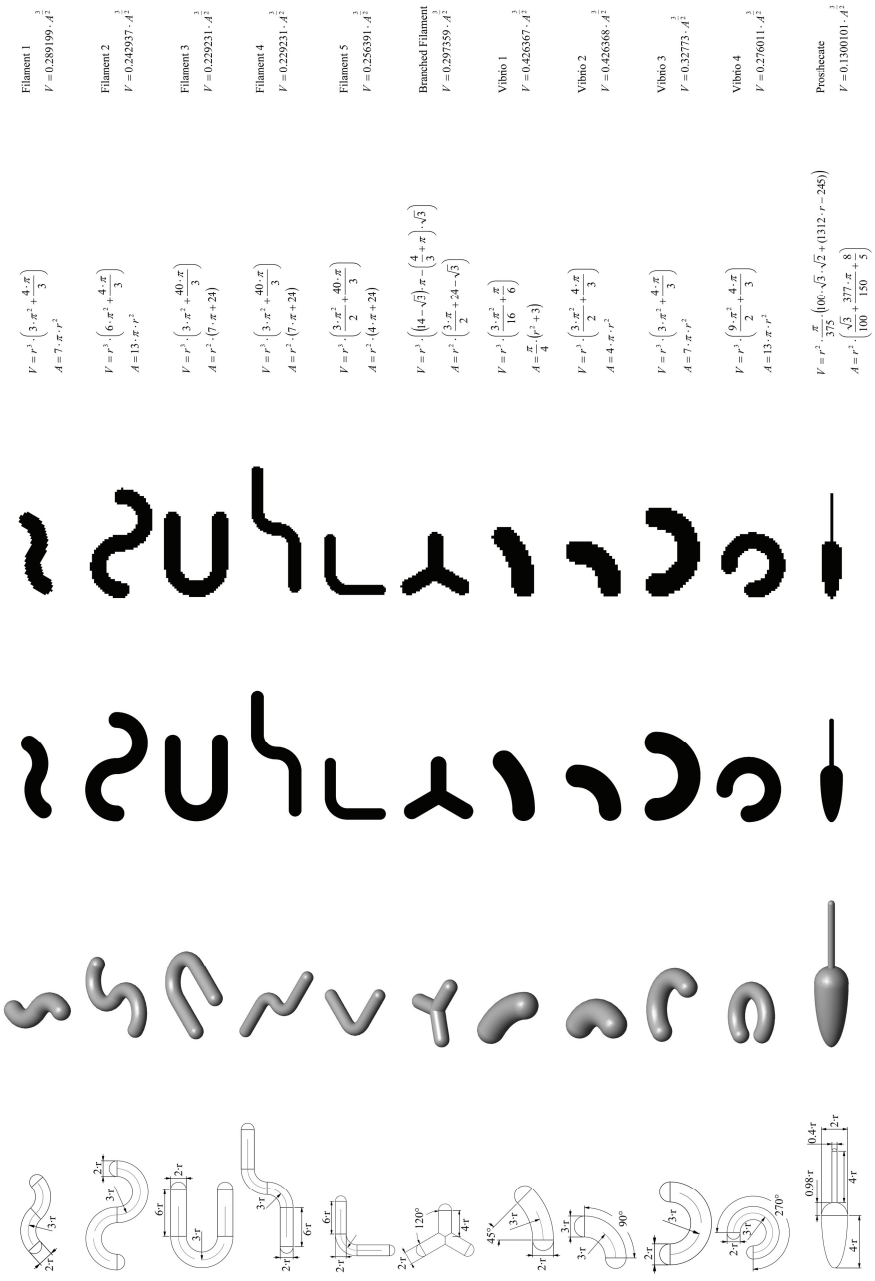

Fig. 10 continued. Geometrical models of different bacterial morphologies. Formulas for volumes and areas are given.

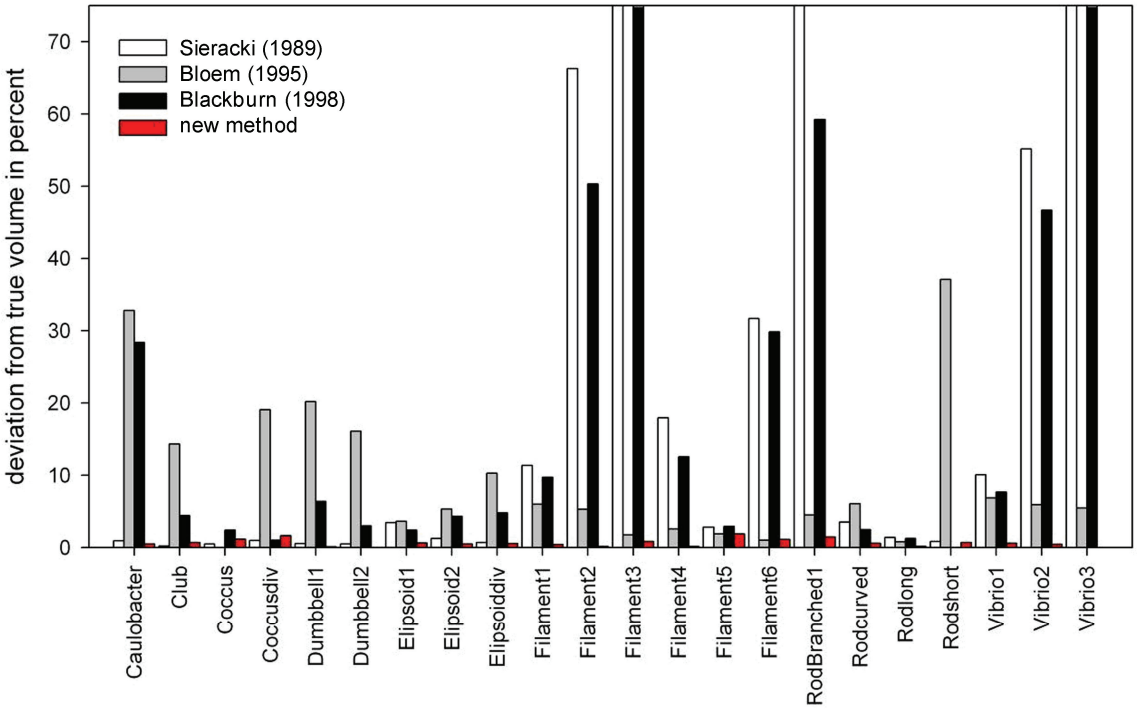

Fig. 11 Comparison of the errors of four methods for biovolume determination. Errors are depicted as absolute percentage of the deviation to the true volume for 22 different geometrical models. The errors of the here described method are shown as red bars.

The newly described algorithm was shown to be most accurate. The error in the calculation of the volume for the 22 different morphologies was constantly below 2%. The algorithm is thus largely unbiased by the morphology of cells in contrast to previously described algorithms and should be considered in studies that determine biovolumes of morphologically diverse communities.

6 Discussion

The introduction of computers in all fields of life sciences represented a series of far-reaching revolutions. In the 1980s, computers, at this time highly expensive and complicated, became available for a small circle of scientists. It required profound engineering skills to handle these machines but they nevertheless opened new perspectives. In aquatic microbiology for example, it allowed for next-level microscopy by digital image analysis (Bartels et al. 1972, Krambeck et al. 1981, Sieracki et al. 1985, Bjornsen 1986). Decades later, another revolution (or evolution) took place, as computers, now less expensive and far more powerful, became broadly available and user-friendly everyday equipment. A similar trend was observed for image analysis software, CCD cameras and motorized microscopes. However, the full potential of the computational power and sophisticated microscopic hardware that is available today is still widely unused by aquatic microbial ecologists. Limits are set by the functionality of 'ready-to-use' image analysis software. Since the field of microbial ecology does not represent a large, economically interesting market, companies are not particularly interested in them[4]. To overcome these limits, a certain degree of software engineering skills is required, and one has to leave the rather restrictive environment of commercial image analysis tools. However, some image analysis software offer an integrated development environment (e.g. AxioVision by Zeiss or the open source software ImageJ (Collins 2007)).

6.1 Advantages and Novel Features of the Developed Microscopic Screening Platform

The main advantage of the automated microscopic screening platform developed in this thesis is its intrinsic flexibility. It allows researchers for imaging different types of preparations, including polycarbonate membrane filters (filter pieces, whole filters, spots on filters) or direct spotting on conventional microscopic slides or multi-well slides. The coordinate list program (Fig. 6) allows for automated detection of preparations and up to eight slides (99 preparations) may be processed in one imaging run. The image acquisition program interface offers to flexibly adjust settings

[4] For biomedicine or cell biology, screening platforms are widely available. But, in contrast to the various available molecular biological kits, originally developed for cell biologists, they generally cannot be adopted by aquatic ecologists for their purposes.

to comply with several commonly applied staining protocols, including single staining to assess abundance, biomass and morphology, double staining for phylogenetic identification (FISH), and triple staining to investigate activity by means of substrate uptake (MAR-FISH) or growth measurement (BrdU-FISH). Moreover, it is possible to interrupt and change settings anytime during the image acquisition. The newly developed autofocus routine and the consequent acquisition of z-stacks greatly improved the overall image quality (Publication 1) and the newly developed automated image quality control tool eliminates the need of manually revision of images for quality after image acquisition (Manuscript 2). The evaluation of the images (e.g. cell counting or biomass and morphology determination) has been greatly accelerated by decoupling image processing from data analysis by the here introduced metadata concept. It allows for quasi real-time evaluation of image data at any computer, independently of commercial image analysis software.

6.2 The Value of High Throughput Analysis in Aquatic Ecology

The automated imaging platform described in this thesis is an example of how software development can substantially extend the potential of a commercially available microscopic system. It allowed us to conduct ecological studies that would have not been possible within this time frame before.

6.2.1 High Frequency Sampling

Publication 5 (Zeder et al. 2009) illustrates of how high frequency sampling in a short time period (i.e. a spring phytoplankton bloom) can provide profound knowledge about short-term successions of bacterial populations. Changes in the community structure take place within days and raise the need of sampling at the same frequency or even more often[5] in order to detect them. The processing of such large amounts of preparations is hardly feasible without an automated screening platform. Notably, Publication 5 involved assessment of the activity of distinct bacterial taxa by the BrdU incorporation approach, which results in triple fluorescently stained preparations. These are extremely difficult to evaluate by manual microscopy, as a

[5] In analogy to the Nyquist-Shannon sampling theorem (Wilkinson 1998), the frequency of biological sampling probably should be twice as high as the frequency of the observed event.

red fluorescent dye (Alexa 633, Invitrogen) had to be used (to avoid spectral overlaps), which is hardly visible by the human eye.

6.2.2 Ecophysiology: Multiple Substrates

Besides sampling density, the amount of replicates and parallel incubations of samples with different radio-labelled substrates is a limiting factor for the significance of ecophysiological studies. The number of MAR-FISH preparations (several hundred) processed in Publication 6 (Alonso et al. 2008) exceeds the typical amount of data in comparable publications by a factor of 5 – 10 (e.g. (Cottrell & Kirchman 2000)). This approach allowed to elucidate substrate preferences of distinct betaproteobacterial linages and to study their behaviour upon transfer to new environmental conditions.

6.2.3 Spatio–Temporal Studies and Monitoring

Long term studies, e.g. for monitoring purposes or the analysis of seasonal population changes described in Publication 7 (Salcher et al. 2008), result in enormous amount of samples and highly profit from an automated screening platform. Publication 7, featuring high-resolution seasonal and, importantly, vertical profiling, revealed that some betaproteobacteria only occur in the anoxic zone of the studied lake. Moreover, distinct betaproteobacterial populations showed a high affinity to amino acids wheras others – presumably methylotrophic – did not.

6.3 Model-Based Object-Oriented Image Analysis

Conventional image processing has been introduced in the 1960s and is generally based on mathematical processing of two-dimensional matrices derived from digital images. In most image analysis tools, image processing is done by sequentially applying filters or operations on an image, whereby the output of each operation is a new image. Subsequently, a binary image is created, in which objects are separated from the background and can be analyzed (e.g. sized and counted). However, in this respect, objects are defined as groups of connected pixels. If objects on a preparation overlap, there is no possibility for correct detection. This fact may be neglected for certain application, but not for others, such as the quantification of filamentous cyanobacteria described in Manuscript 3. The combination of object oriented programming (OOP) and image analysis allows for going beyond this

limitation. The first step of this approach, termed as ‘model based object oriented image analysis’ is to analyze the biological problem in a qualitative and quantitative way and the formulation of a model. The second step is the object oriented analysis of the model, and, finally, the third step is the implementation by means of OOP. This approach allowed for addressing two problems related to aquatic microbial ecology that cannot be resolved equally precise with conventional image analysis. Manuscript 3 discusses the correct detection of overlapping filaments on epifluorescence images, and Manuscript 4 describes a new algorithm for the calculation of bacterial biovolumes that is unbiased by cell morphologies.

6.4 Outlook

The concept of metadata generation and evaluation has proven to be an efficient way to analyze data resulting from high-throughput microscopy. First of all, it is significantly faster, as data in the transient memory (RAM) allows for quasi real-time analysis. Moreover, the program is able to run on every computer (having a Microsoft operation system) as it is not based on commercial image analysis software and does not require intensive computational power.

There is still a large potential of improving the metadata concept. Presently, the metadata consists of measurable cell features that are provided by conventional image analysis tools (e.g. area, perimeter, circularity and so on). Importantly, the contours of the cells have also to be saved for later online annotation. Depending on the size of the cells, the saving of the contour requires different amounts of memory. Another strategy that should be followed would be the use of Fourier descriptors for storing cell contours. They allow for the reconstruction of the contour of a cell at a sub pixel resolution and have been previously used to analyze shapes (Blackburn et al. 1998, Liu et al. 2001, Culverhouse et al. 2006, Neto et al. 2006, Pincus & Theriott 2007). Moreover, geometrical features can be directly deduced from them and do not need to be stored separately.

The next step in the development of the here described system would thus be to change the metadata structure. This also involves the adaptation of the image processing program and the metadata evaluation program. As the entire software has to be re-written, it would be of high advantage to develop both programs within VB.Net, because up to now, the image processing routine is bound to the commercial software AxioVision. This would imply the development of algorithms for cell

detection and Fourier descriptor retrieval within VB.Net. While this is presumably a difficult and highly time consuming project, it would allow providing both programs as free software and could thus be of high value for the community of microbial ecologists using single-cell analysis approaches.

6.5 Conclusion

During this Ph.D. thesis, an automated high-throughput imaging platform for the analysis of multiple stained preparations of aquatic bacteria was developed and applied. This system accelerates the evaluation of preparations by a factor of > 15 compared to manual microscopy. However, the automation of a time critical process simply shifts the bottleneck somewhere else[6]. Concurrently, some technical issues such as autofocusing and image quality control were addressed. In addition, new image analysis techniques in the context of ecology (i.e. filament quantification and biovolume estimation) were elaborated. The author hopes that this work contributes to the field of aquatic microbial ecology and that the described strategies and programs may be of use for other researchers.

[6] As Jeanne Hersch pointed out once: real scientists exactly know that they will never resolve all problems – not even their own, as the solution of a problem always bears new problems (Hersch 1976).

7 Publications & Manuscripts

Manuscript 4 is described in the ‘Methods and Results’ section.

7.1 Publication 1: Multi-Spot Live-Image Autofocusing for High-Throughput Microscopy of Fluorescently Stained Bacteria.

ORIGINAL ARTICLE

Cytometry
PART A
Journal of the International Society for Advancement of Cytometry

Multispot Live-Image Autofocusing for High-Throughput Microscopy of Fluorescently Stained Bacteria

M. Zeder, J. Pernthaler*

Department of Limnology, Institute of Plant Biology, University of Zürich, Kilchberg CH-8802, Switzerland

Received 4 May 2009; Revision Received 2 June 2009; Accepted 25 June 2009

*Correspondence to: J. Pernthaler, Department of Limnology, Institute of Plant Biology, University of Zürich, Seestrasse 187, Kilchberg CH-8802, Switzerland

Email: pernthaler@limnol.uzh.ch

Published online 00 Month 2009 in Wiley InterScience (www.interscience.wiley.com)

DOI: 10.1002/cyto.a.20770

• **Abstract**

Screening by automated high-throughput microscopy has become a valuable research tool. An essential component of such systems is the autonomous acquisition of focused images. Here we describe the implementation of a high-precision autofocus routine for imaging of fluorescently stained bacteria on a commercially available microscope. We integrated various concepts and strategies that together substantially enhance the performance of autonomous image acquisition. These are (i) nested focusing in bright-field and fluorescence illumination, (ii) autofocusing by continuous life-image acquisition during movement in *z*-direction rather than at distinct *z*-positions, (iii) assessment of the quality and topology of a field of view (FOV) by multispot focus measurements, and (iv) acquisition of *z*-stacks and application of an extended depth of field algorithm to compensate for FOV unevenness. The freely provided program and documented source code allow ready adaptation of the here presented approach to various platforms and scientific questions. © 2009 International Society for Advancement of Cytometry

• **Key terms**

autofocus; high-throughput microscopy; image analysis; microbial ecology

AUTOMATED microscopy has become an important screening instrument in many fields of research. High-throughput capabilities in image acquisition, image processing, and data evaluation have led to new types of experimental designs, e.g., genetic studies on multicellular organisms (1), pharmaceutical drug profiling (2,3), RNA interference studies (4), or investigation of microbial communities in environmental systems (5). Microscopic screening platforms are no longer restricted to selected customers with large research budgets, as many manufacturers now provide fully motorized microscopes with integrated software development environments. They have also become more user-friendly and extensive engineering and programming skills are no longer required to create specific applications. Image analysis techniques, routines and tools for object recognition, and measurements are widely available today, as well as powerful and inexpensive computer systems. However, only precisely focused images can provide optimal output in any image processing routine.

Autofocusing that precedes image acquisition is a crucial initial step in an automated workflow (6). Thus, the design and implementation of a precise, robust, and flexible autofocus routine is a critical issue and a potential pitfall in the development of autonomous imaging platforms, especially at high resolution, e.g., to investigate subcellular structures or bacteria. Deviations of a few hundred nanometers from the focal plane already significantly lower the image quality when using high numerical aperture (NA) objectives (7,8). There are two main implementations of autofocus functionality in commercially available light microscopes (hardware and software autofocus), and both require a motorized focus drive. Hardware autofocusing, based on light reflection on interfaces, requires additional optical and electronic components but offers fast and accurate focusing (9). Unfortunately these systems are also

ISAC
International Society for Advancement of Cytometry

expensive and complex. The more flexible and common software autofocusing relies on a CCD camera that acquires images at different *z*-positions and determines the most focused image via a focus algorithm.

Autofocusing has been widely discussed in the literature but mainly in the context of determining optimal focus algorithms (10–13). Many of these studies do not discuss the implementation of autofocus routines in screening applications. Moreover, they do not take into account the fact that biological preparations often exhibit areas that are of low quality where image acquisition will fail or yield nonevaluable images which may corrupt the data set. Microscopic fields of view (FOVs) may be empty, i.e., without objects of interest, contain large objects and artifacts, or may exhibit unevenness in z-direction, so that not all objects of interest are within the depth of focus. As time is a crucial factor in automated screening applications, it is important to recognize and discard such low-quality FOV as early as possible, preferably prior to image acquisition, i.e., during the autofocusing process.

Here we describe strategies that increase the performance of autonomous image acquisition, with emphasis on autofocusing. The specific biological context for the development of this autofocus was high-throughput cell quantification for studies on aquatic microbial ecology (14,15). However, the strategies described here are generally applicable to high-resolution imaging and the provided documented source code should thus also be valuable for other scientific questions.

Materials and Methods

Hardware, Software, and Integrated Development Environment

The autofocus routine was developed as an integral part of an automated high-throughput microscopy system to quantify the abundances and biovolumes of different bacteria in aquatic environments (16). The core of the system consists of an epifluorescence microscope (AxioImager.Z1; Carl Zeiss, Germany) equipped with a motorized stage for eight microscopic slides (step size, *x, y*: 200 nm, *z*: 10 nm). The epifluorescence illumination device Colibri (Carl Zeiss), featuring LED modules for 365, 470, and 590 nm excitation, was used in combination with a triple band filter set (Zeiss 62 HE) to image different fluorescent dyes. Additionally, a "neutral white" LED (emission: ~450–700 nm) was used at low intensity for bright-field autofocusing in a epi-illumination mode. Fluorescence and bright-field images were recorded with a CCD Camera (AxioCam MRm; Carl Zeiss) using a 63× objective (Plan-Apochromat, NA = 1.4). The camera delivered 12-bit grayscale images with a resolution of 1,388 × 1,040 pixels. The resolution of a live image was 692 × 520 pixels. The microscope was controlled by a personal computer and a software AxioVision 6.3 (Carl Zeiss). Automation of the image acquisition routine, including the autofocus, was performed by object-oriented programming in the Visual Basic for Application (VBA) module of AxioVision. The program code of the autofocus routine is available at http://www.kingdoms.ch under general public license.

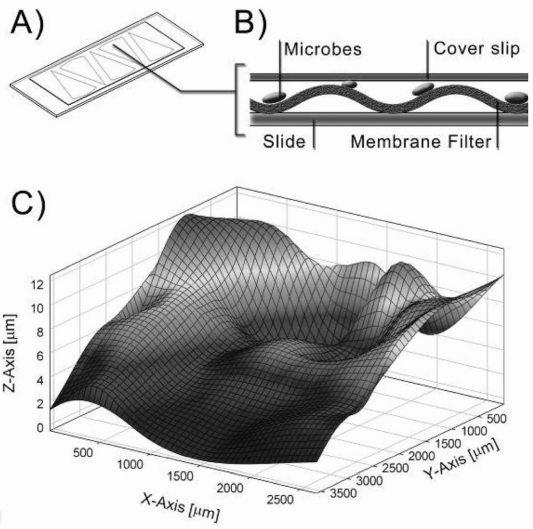

Figure 1. (**A**) Schematic representation of a microscopic preparation used in this study. Polycarbonate membrane filters with stained aquatic bacteria on top, cut into pieces, are placed on a microscopic slide and covered with a coverslip. (**B**) Schematic cross-section through the preparation. Unevenness of the supporting membrane filter is shown. (**C**) Topology of a 3 × 3 mm^2 section on a typical preparation; 64 locations in a rectangular pattern were subjected to the autofocus routine for determination of their *z*-positions.

Biological Samples

The biological preparations developed for this autofocus routine were multiple fluorescently stained bacteria from water samples of marine or freshwater systems, monodispersed on polycarbonate membranes (0.2 μm pore size) by filtration. The preparations were double stained by fluorescence in-situ hybridization (FISH) with rRNA-targeted oligonucleotide probes and by 4′,6-diamidino-2-phenylindole (DAPI) (17–19). The membrane filters were cut into sections, stained, and embedded on microscopic slides (Figs. 1A and 1b). The microbial cells were imaged using a 63× oil-immersion objective (Plan-Apochromat).

Nested Autofocus Strategy

Autofocusing was performed by continuous movement of the stage in *z*-direction and simultaneous data acquisition (6). Data acquisition was done on two independent devices, the CCD camera (live images) and the microscope stage (*z*-positions). As they deliver data at different rates, special emphasis had to be given to the mapping of the data from the two events. Briefly, the stage was moved downwards for a defined distance from an initial start *z*-position at a defined speed. While moving, data (camera live images and stage z-positions) were collected by two independent event handlers (Fig. 2A) and a timestamp was attached to each event. The collected data were stored transiently in the RAM of the computer. Data

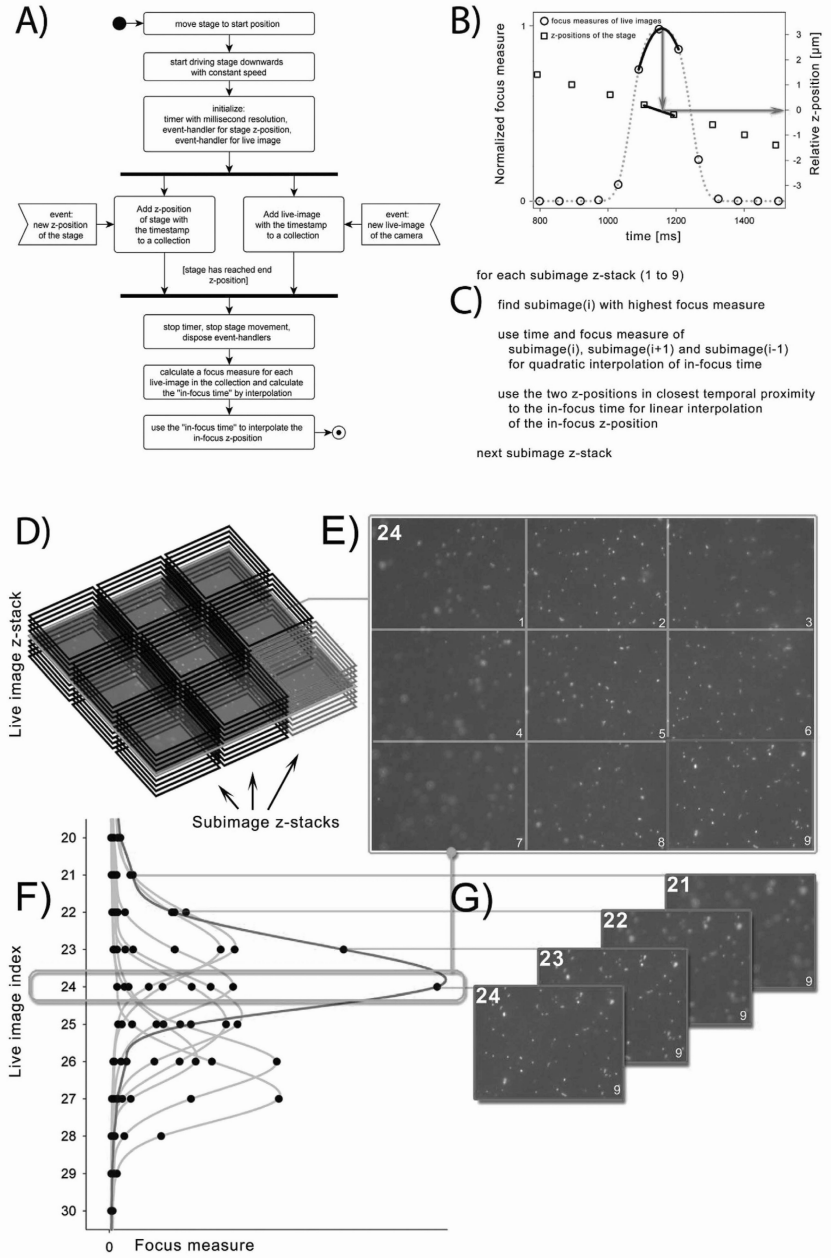

Figure 2. (**A**) Activity diagram describing the algorithm of the autofocus routine. (**B**) Representation of the measured parameters during the autofocus routine. Each circle represents the focus measure of a live image (or subimage, respectively) calculated by the weighted histogram sum (WHS) focus algorithm. The squares represent *z*-position measurements that are delivered by the stage event handler. Both, live-image and *z*-position events are plotted against time. Quadratic interpolation of the focus curve delivers the in-focus time for subsequent calculation of the in-focus *z*-position. (**C**) Pseudocode of the algorithm used to calculate the in-focus *z*-position from the measurements. (**D**) Schematic representation of a live-image collection from a typical FOV. Prior to the determination of the focus measure, each live image in the collection is divided into nine subimages resulting in nine *z*-stacks. (**E**) The live image with the index 24 (green frame) is shown as an example of an uneven FOV. (**F**) Representation of the nine focus curves. Each curve is derived from one of the subimage stacks. The abscissa of the graph indicates the live-image index. The index of the described image 24 is highlighted in green. (**G**) A sequence (Indices 18 to 26, red frames) of subimages of *z*-stack 9 is shown, where the subimage 24 is the most focused subimage. [Color figure can be viewed in the online issue, which is available at www.interscience.wiley.com.]

acquisition was stopped at the lower *z*-position by disposing the event handlers.

Autofocusing was performed twice on each FOV in a nested mode, as described previously (5,20). In the first run, focusing was performed at high speed (40 μm s^{-1}) over a large distance in bright-field illumination to determine the *z*-position of the membrane filter. A *z*-distance of 400 μm was covered on the first FOV on a new preparation, whereas subsequent bright-field focus runs on the same preparation were performed over a distance of 40 μm relative to the last in-focus *z*-position. In case of a focus error, bright-field refocusing was repeated over a distance of 400 μm. Fine focusing on cells was then performed in fluorescence illumination at a speed of 4 μm s^{-1}. The distance was 15 μm relative to the focused *z*-position of the membrane filter. After each run, the acquired data, i.e., the collection of live images and *z*-positions were evaluated and the live image collection was used to determine the time point of maximal sharpness. For this, a focus measure was calculated for each image in the collection (see below) and the maximum of the resulting curve was determined by a second-order polynomial interpolation (6). Subsequently, the *z*-position collection was used to obtain the *z*-position corresponding to that particular time point by linear interpolation (Fig. 2B).

Focus Algorithm

To measure the sharpness of each image in the live-image collection, a new histogram-based focus algorithm was developed, designated as weighted histogram sum (WHS). For each gray level i, ranging from 0 to 4,095 in a 12-bit image, the histogram h contains the number of pixels $h(i)$ of that particular gray level. Focused images in fluorescence illumination exhibit higher portions of pixels with bright gray levels (large i) than unfocussed images. However, the number of noninformative background pixels is still by far larger (>98%). To use the shift to brighter gray levels in the histogram as a focus measure without introducing a constant threshold, the histogram has to be weighted. This was done by multiplying the fifth root of the number of pixels of each gray level $h(i)$ by the fifth potency of its gray level i and subsequent division by 10^{15}. The sum of all transformed gray values was then used as a focus measure:

$$F_{\mathrm{WHS}} = \sum_{i=0}^{4,095} \left(h(i)^{\frac{1}{5}}\, i^{5}\, 10^{-15} \right). \qquad (1)$$

The choice of the fifth root and the fifth potency for nonlinear weighting resulted from empirical optimization trials (data not shown). A division by 10^{15} was done for data normalization. For performance comparison, two earlier described algorithms were additionally implemented, normalized variance (NV) (10,11) and Brenner gradient (BG) (21).

Multispot Autofocus

To determine the topology and inhomogeneity within an FOV, the focus algorithm was not applied to the entire image. Instead, every live image in the collection was divided into nine rectangular parts (Figs. 2D and 2E), and a focus measure was calculated for each of the resulting subimages. This resulted in nine *z*-stacks which can be represented as nine focus curves when plotting the focus measure against the live-image index (or the corresponding timestamp, respectively) (Fig. 2F). The nine in-focus *z*-positions of each of the nine subimage stacks were calculated as described earlier (Fig. 2C). Because the focus measure is based on the weighted histogram, it additionally served as an estimator for the presence of bright objects, i.e., bacterial cells. Thereby, subimages containing few or no cells could be readily detected by applying a threshold. The overall in-focus *z*-position was then calculated as the average of the focus positions of the cell-containing subimages only. As the camera and the stage of the microscope are two independent, nonreal-time devices, an empirically determined constant offset had to be added to the calculated *z*-position for precise adjustment. Unevenness within an FOV was quantified as the difference between the maximal and the minimal in-focus *z*-position of the nine subimages.

Based on the above described measurements, the routine featured several aborting criteria, error detection, and feedback routines, e.g., recognition of empty FOV or extremely uneven FOV. More details are documented in the available source code.

Measurement of Sample Topology

The topology of a typical preparation was assessed by performing bright-field autofocus runs in a rectangular 8 × 8 grid pattern. The distances between the measurements accounted for 501 and 370 μm in x and y directions, respectively. The determination was repeated three times using the same coordinates.

Autofocus Reproducibility and Comparison of Focus algorithms

Sixteen FOVs were arbitrarily chosen from a typical FISH preparation. On each FOV, a microscopist determined the in-focus position of the bacterial cells (DAPI, UV excitation) manually for 16 times, using the camera image on a computer screen. Subsequently, the autofocus routine was run using the three above described algorithms in sequence. The sequence was performed 16 times for each FOV.

Extended Depth of Field Imaging

The limited depth of field in fluorescence microscopy due to the usage of high NA objectives was extended by the acquisition of image stacks in *z*-direction and the subsequent application of a wavelet-based extended depth of field (EDF) algorithm (22). *z*-Stacks were acquired in an interval of 0.4 μm. The EDF functionality was provided by the commercially available AxioVision module "Extended Focus." *z*-Stacks processed by the EDF algorithm resulted in a single image where every object in the image was present in its most focused state within the input *z*-stack.

Generation of an Image Test Set

To assess the quality of a FOV during the autofocusing process and the effect of *z*-stacking and EDF imaging, a test set of images was generated on a set of typical samples from Lake Zürich. Forty-four preparations of FISH and DAPI-stained bacteria were imaged using the autofocusing routine described here. The system was set to automatically acquire 45 FOV per preparation in a systematic uniform random sampling scheme. On each FOV, a nested autofocus as described earlier was run. The unevenness of each FOV was measured during fluorescence autofocusing. Then, a *z*-stack of 11 images was acquired at UV excitation with a *z*-distance of 0.4 μm between the images. From this stack, EDF images were calculated with different numbers (3, 5, 7, 9, and 11) of stack images symmetrically around the central image. Each FOV was thus represented by six images with different depths of field ranges (termed EDF3, EDF5, EDF7, EDF9, and EDF11) and the non-EDF central image, subsequently termed EDF1.

All FOV were manually assigned to four different quality categories, according to whether the images were of sufficient quality to be subjected to subsequent cell counting by image analysis: (i) High quality (HQ): FOVs where the single image (EDF1) was of sufficient quality to be evaluated. (ii) Medium quality (MQ): FOVs where the EDF1 image was not of sufficient quality to be evaluated but the EDF7 was. (iii) Low quality (LQ): FOVs where the unevenness was so pronounced that the EDF7 image was not of sufficient quality to be analyzed further. (iv) Artifacts (AR): FOVs that contained artifacts (e.g., large debris particles) were thus not suitable for cell counting.

Cell Counting

Cell counting on images was performed by image analysis using a custom-made automated routine developed with VBA in AxioVision. Briefly, binary images were created using a dynamic thresholding procedure provided by AxioVision and objects within a certain range of size and brightness were counted.

Results

Determination of Filter Topology

To assess the topology of a typical FISH preparation, i.e., the evenness of the supporting polycarbonate membrane filter on a larger scale in the range of millimeters (Fig. 1B), *z*-positions on 64 FOVs were determined (Fig. 1C). The mean horizontal distance between FOVs was 486 μm. The maximal difference in *z*-direction in the topology of the membrane filter within the analyzed area of 9.1 mm^2 was 12.5 μm. The average maximal deviation of replicated measurements per FOV was 0.7 μm. The average *z*-displacement between neighboring FOVs accounted to 1.92 $\pm$ 1.50 μm (min: 0.05 μm; max: 6.37 μm).

Performance of the Autofocus Routine

The precision and performance of the autofocus routine were compared with a those of a microscopist, and the newly developed focus algorithm (WHS) was compared with two previously described ones. The deviations in *z*-direction of single focus events to the overall mean are depicted in Figure 3. The precision of the three algorithms did not significantly differ (one-way ANOVA, post-hoc tests by Tukey, and Scheffé method) but significantly outperformed the microscopist. In terms of computation time of the three implemented algorithms, WHS was about five times faster than BG and four times faster than NV.

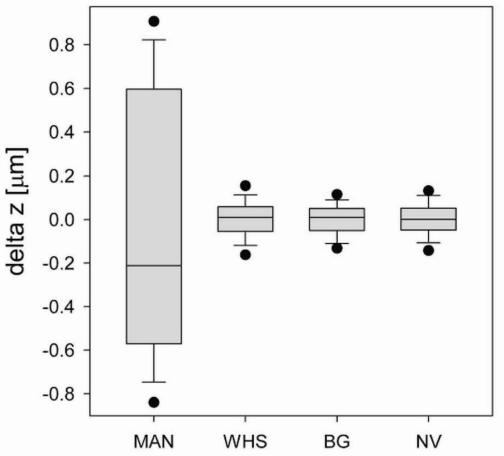

Figure 3. Performance and reproducibility of the autofocus routine; manual focusing (Man) was compared with three algorithms: weighted histogram sum (WHS), Brenner gradient (BG), and normalized variance (NV). Each box represents 256 measurements.

Acquisition of the Image Test Set

The autofocus routine aborted 83 of the 1,980 FOVs because focus criteria were not met, because of either FOV emptiness or FOV unevenness of >10 μm. The remaining 1,897 FOVs were successfully imaged and manually assigned to four different quality classes resulting in 829 HQ, 894 MQ, and 141 LQ FOVs. Thirty-three FOVs contained artifacts, mainly large planktonic organisms (algae).

Quality Assessment of a FOV During the Autofocus Procedure

The unevenness of each FOV category is depicted in Figure 4A. Statistical analyses (one-way ANOVA, post-hoc tests by Tukey, and Scheffé method) revealed that the categories HQ and MQ FOVs were significantly different from all other categories in terms of FOV unevenness. LQ and AR FOVs exhibited larger unevenness than both HQ and MQ.

Effect of *z*-Stacking and EDF Imaging on Bacterial Cell Counts

Cell counts were performed only on the HQ and MQ FOVs. Within each FOV, the number of cells detected in the EDF11 image was compared with cell numbers on EDF images with different depths of field (EDF1, EDF3, EDF5, EDF7, and

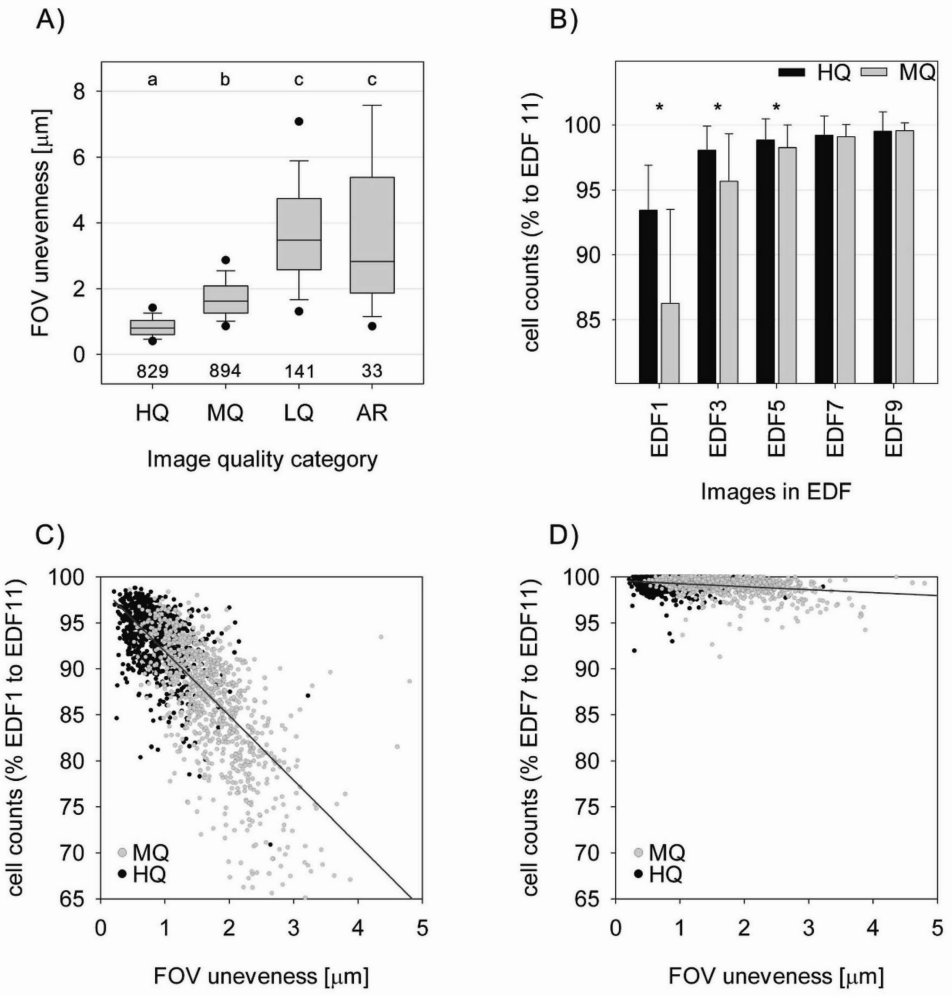

Figure 4. (**A**) Image quality in relation to unevenness of the FOV. Automatically acquired images were manually assigned to four categories according to the image quality and plotted against their unevenness. Numbers below box plots represent the number of images per category. Small letters above box plots indicate groups of significantly different means determined by ANOVA. (**B**) Relative cell counts in the categories HQ and MQ are depicted for different amount of stack images used in EDF. Values are calculated as percentages of EDF1, EDF3, EDF5, EDF7, and EDF9 to EDF11. Cell counts in EDF1, EDF3, and EDF5 are significantly different (ANOVA, indicated by asterisks). (**C**, **D**) Relative cell counts of EDF1 (EDF7, respectively) to EDF11 images of the categories HQ (black dots) and MQ (gray dots) are plotted against their unevenness. Red lines represent linear regressions.

EDF9) (Fig. 4B). A total number of 724,037 cells were counted on 1,723 EDF11 images. *z*-Stacking and EDF increased cell counts both in the HQ and MQ categories. This effect was more pronounced in the MQ category, as these FOVs exhibited higher unevenness (Fig. 4A). HQ and MQ did not significantly differ in cell counts in the EDF7 and EDF9 images.

The relative cell counts per image versus the FOV unevenness of EDF1 and EDF7 images are depicted as scatter plots in Figures 4C and 4D. In the nonstacked images (Fig. 4C), relative cell counts were strongly correlated with the unevenness of the FOV. By contrast, the stacking of seven images and subsequent EDF substantially decreased the influence of FOV unevenness (Fig. 4D).

Discussion

Depending on the nature of the sample, autofocusing can be challenging. The application of high-resolution objectives, e.g., to image bacteria or subcellular structures of eukaryotes, results in small depth of fields in the submicrometer range. Frequently, preparations exhibit large inhomogeneity, e.g., in terms of uneven surface structure that can displace the focal

position of the objects of interest between FOVs by several micrometers (Fig. 1C). This requires autofocusing over a large distance at each FOV. Precise autofocusing depends on the sampling of focus information in high spatial resolution and the required time thus depends on the distance within which autofocusing is performed. An autofocus routine for autonomous image acquisition systems should thus be able to search for a focal plain across a large absolute *z*-range (e.g., to find the focus of the first FOV on a preparation) but it should then flexibly adapt this range depending on the last good focus position (for subsequent FOVs). As the distance with measurable focus information is much smaller in fluorescence compared with bright-field illumination (5,20), fast autofocusing can be performed over a large range to localize the focal plane of the supporting material, e.g., a filter membrane. Subsequent fine focusing in fluorescence illumination over a short range accurately locates objects of interest. As a side effect, photobleaching of fluorescently stained objects can be reduced by shorter focusing time in fluorescence.

Another strategy to increase the performance of focusing is to continuously move the stage in *z*-direction and to evaluate all the live camera images as a source of focus information instead of sampling at distinct *z*-positions. This offers the highest possible temporal resolution as it eliminates the need of repositioning the stage between image acquisitions. The possibility to dynamically set the driving speed and *z*-distance allows adjusting the spatial sampling resolution, thus providing greater overall flexibility. However, assigning live images to *z*-position is not trivial. Two processes, live image acquisition and movement in *z*-direction, run synchronously on two independent devices (camera and stage) that deliver information at different rates. The frame rate of the camera is not constant and provides output every 20 to 100 ms depending on the type of camera, illumination mode, and other factors. The stage, on the other hand, delivers *z*-positions at a constant frequency, e.g., every 100 ms. Thus, a direct assignment of the live images to their corresponding *z*-positions is not possible. We therefore used a timer with millisecond resolution to map all events to time (Fig. 2) and subsequently calculate the focus position. Recently, selective sampling in *z*-direction based on dynamic extremum search (23) or model-based curve fitting (24) has been proposed to decrease focusing time. However, these methods require strictly unimodal focus curves or distinct focus functions, limiting their flexibility, e.g., with respect to implementing different focus algorithms, and they are not compatible with the concept of multispot autofocusing.

A general problem of autonomous microscopy is the uncertainty of finding objects of interest on a particular FOV. If no objects, e.g., fluorescently stained bacteria, are present on an FOV because of their inhomogeneous distribution, or if an FOV features large unspecifically stained particles, autofocusing in fluorescence will not succeed. Prediction of empty fields has been demonstrated previously (6), but topological unevenness within an FOV also leads to unsuccessful imaging. Here we demonstrate that an autofocus routine can be used to determine more specific quality parameters, e.g., the unevenness within a FOV, which is closely linked to the quality of the resulting image (Fig. 4A). Focus information can be measured on multiple spots within an FOV by division of the live image into subimages. This allows to quantify unevenness and to assess the quality of a FOV while focusing. Such a quality assessment prior to actual image acquisition is advantageous for several reasons, e.g., it reduces the total time of imaging and of postacquisition image quality control by immediately discarding low-quality FOV.

A limited FOV unevenness that would nevertheless lead to significant loss in measurement precision can be compensated by the acquisition of *z*-stacks and the application of an EDF algorithm (Figs. 4C and 4D). Moreover, we observed that stacking and EDF also increased the image quality on high-quality FOV and led to higher cell detection rates, albeit to a lesser extent than in medium-quality FOV (Fig. 4B). If high measurement precision is required, we thus suggest to always acquire image stacks and perform EDF. On our samples, using a 63× objective, stacks of seven images (covering a range of 2.4 μm) represented an optimal compromise between acquisition speed and data quality.

The choice of autofocus algorithm provides another means of obtaining additional FOV quality information. Many algorithms aim for image contrast, entropy, or spatial frequency content (12,24,25), whereas the WHS algorithm introduced here specifically targets brightness: the maxima of the focus curves of the subimages correlate to the overall brightness of the subimage (Fig. 2F). This yields a rough estimator for the presence of fluorescent objects, and FOVs containing few or no cells can thus be discarded prior to image acquisition. Additionally, FOVs containing too many cells or bright artifacts can also be recognized and excluded by appropriate thresholding. The precision and reproducibility of the WHS algorithm were not significantly different to NV and BG (Fig. 3) which have been recommended in other studies (10,23–25) even though WHS is computationally less intensive. Interestingly, all three algorithms significantly outperformed a microscopist, probably because humans do not always focus on the same part of slightly uneven FOVs. For nonfluorescent objects in other illumination modes (e.g., bright-field imaging), other focus algorithms are more appropriate. Presently, the three mentioned algorithms are implemented by default in our routine. Because the documented source code is freely available (http://www.kingdoms.ch), more algorithms can be readily added. Furthermore, the system has the potential to be extended with more specific image-processing steps on the live-image level, such as early-stage object detection and measurement.

In conclusion, we combined several strategies to enhance the overall performance of autofocusing. Moreover, we showed that autofocusing has the potential of delivering more information than the mere in-focus position and that it can be used to assess the quality of a FOV prior to image acquisition. Because of its intrinsic flexibility we are confident that the strategies described here can be readily adapted for different wide-field microscopy-based screening systems in other fields of research, and for other kinds of samples, e.g., biofilms, eukaryotic cells, tissue preparations.

Acknowledgments

The authors gratefully acknowledge Evelyn Hofer for technical expertise and Michaela Salcher for providing biological samples.

Literature Cited

1. Chung KH, Crane MM, Lu H. Automated on-chip rapid microscopy, phenotyping and sorting of*C. elegans*. Nat Methods 2008;5:637–643.
2. Perlman ZE, Slack MD, Feng Y, Mitchison TJ, Wu LF, Altschuler SJ. Multidimensional drug profiling by automated microscopy. Science 2004;306:1194–1198.
3. Loo LH, Wu LF, Altschuler SJ. Image-based multivariate profiling of drug responses from single cells. Nat Methods 2007;4:445–453.
4. Wheeler DB, Carpenter AE, Sabatini DM. Cell microarrays and RNA interference chip away at gene function. Nat Genet 2005;37:S25–S30.
5. Pernthaler J, Pernthaler A, Amann R. Automated enumeration of groups of marine picoplankton after fluorescence in situ hybridization. Appl Environ Microbiol 2003;69:2631–2637.
6. Geusebroek JM, Cornelissen F, Smeulders AWM, Geerts H. Robust autofocusing in microscopy. Cytometry 2000;39:1–9.
7. Brock TD. How sensitive is the light-microscope for observations on microorganisms in natural habitats. Microb Ecol 1984;10:297–300.
8. Ortyn WE, Perry DJ, Venkatachalam V, Liang LC, Hall BE, Frost K, Basiji DA. Extended depth of field imaging for high speed cell analysis. Cytometry Part A 2007;71A:215–231.
9. Liron Y, Paran Y, Zatorsky NG, Geiger B, Kam Z. Laser autofocusing system for high-resolution cell biological imaging. J Microsc 2006;221:145–151.
10. Groen FCA, Young IT, Ligthart G. A comparison of different focus functions for use in autofocus algorithms. Cytometry 1985;6:81–91.
11. Yeo TTE, Ong SH, Jayasooriah, Sinniah R. Autofocusing for tissue microscopy. Image Vis Comput 1993;11:629–639.
12. Firestone L, Cook K, Culp K, Talsania N, Preston K. Comparison of autofocus methods for automated microscopy. Cytometry 1991;12:195–206.
13. Price JH, Gough DA. Comparison of phase-contrast and fluorescence digital autofocus for scanning microscopy. Cytometry 1994;16:283–297.
14. Salcher MM, Pernthaler J, Zeder M, Psenner R, Posch T. Spatio-temporal niche separation of planktonic betaproteobacteria in an oligo-mesotrophic lake. Environ Microbiol 2008;10:2074–2086.
15. Alonso C, Zeder M, Piccini C, Conde D, Pernthaler J. Ecophysiological differences of betaproteobacterial populations in two hydrochemically distinct compartments of a subtropical lagoon. Environ Microbiol 2008.
16. Schattenhofer M, Fuchs BM, Amann R, Zubkov MV, Tarran GA, Pernthaler J. Latitudinal distribution of prokaryotic picoplankton populations in the Atlantic Ocean. Environ Microbiol 2009;11.
17. Amann RI, Ludwig W, Schleifer KH. Phylogenetic Identification and in-situ detection of individual microbial-cells without cultivation. Microbiol Rev 1995;59:143–169.
18. Pernthaler A, Pernthaler J, Amann R. Fluorescence in situ hybridization and catalyzed reporter deposition for the identification of marine bacteria. Appl Environ Microbiol 2002;68:3094–3101.
19. Porter KG, Feig YS. the use of DAPI for identifying and counting aquatic microflora. Limnol Oceanogr 1980;25:943–948.
20. Boddeke F, van Vliet L, Netten H, Young I. Autofocusing in microscopy based on the OTF and sampling. Bioimaging 1994;2:193–203.
21. Brenner JF, Dew BS, Horton JB, King T, Neurath PW, Selles WD. An automated microscope for cytologic research a preliminary evaluation. J Histochem Cytochem 1976;24:100–111.
22. Forster B, Van de Ville D, Berent J, Sage D, Unser M. Complex wavelets for extended depth-of-field: A new method for the fusion of multichannel microscopy images. Microsc Res Tech 2004;65:33–42.
23. Liu XY, Wang WH, Sun Y. Dynamic evaluation of autofocusing for automated microscopic analysis of blood smear and pap smear. J Microsc 2007;227:15–23.
24. Yazdanfar S, Kenny KB, Tasimi K, Corwin AD, Dixon EL, Filkins RJ. Simple and robust image-based autofocusing for digital microscopy. Opt Express 2008;16:8670–8677.
25. Sun Y, Duthaler S, Nelson BJ. Autofocusing in computer microscopy: Selecting the optimal focus algorithm. Microsc Res Tech 2004;65:139–149.

7.2 Publication 2: Automated Quality Assessment of Autonomously Acquired Microscopic Images of Bacteria by Artificial Neural Network Analysis.

Automated quality assessment of autonomously acquired microscopic images of fluorescently stained bacteria

Zeder M., Kohler, E., Pernthaler J.*

Department of Limnology, Institute of Plant Biology, University of Zürich, Seestrasse 187, CH-8802 Kilchberg, Switzerland (http://www.limnology.ch)

Running head: automated image quality assessment

* corresponding author:
Limnological Station, Institute of Plant Biology
Seestrasse 187, CH-8802 Kilchberg
Phone: +41 (0)44 716 1211; fax.: +41 (0)44 716 1225
Email: pernthaler@limnol.uzh.ch

Abstract:

Quality assessment of autonomously acquired microscopic images is an important issue in high-throughput imaging systems. For example, the presence of low quality images (≥ 10%) in a dataset significantly influences the counting precision of fluorescently stained bacterial cells. We present an approach based on an artificial neural network (ANN) to assess the quality of such images. Spatially invariant estimators were extracted as ANN input data from subdivided images by low level image processing. Different ANN designs were compared and > 400 ANNs were trained and tested on a set of 25000 manually classified images. The optimal ANN featured a correct identification rate of 94% (3% false positives, 3% false negatives) and could process about 10 images per second. We compared its performance with the image quality assessment by different humans and discuss the difficulties in assigning images to the correct quality class. The computer program and the documented source code (VB.Net) are provided under general public licence.

48 ***Introduction:***

49

50 High throughput imaging has become a widely applied methodology in scientific
51 research, e.g. for quantification of viral infection or phenotyping (1,2). In aquatic microbial
52 ecology, motorized epifluorescence microscopes and image analysis systems are used to
53 evaluate preparations of multiple fluorescently stained bacteria in a fully automated
54 manner (3,4). The possibility of screening large numbers of samples greatly enhanced the
55 scope of ecological studies, e.g., by allowing for larger spatial and temporal resolution in
56 sampling (5-7). However, producing large amounts of image data raises new challenges in
57 quality control, image processing and data evaluation (1).

58 Autonomous image acquisition from samples of environmental bacteria is prone to
59 produce a certain degree of images that are non-evaluable. On the one hand, the
60 preparations subjected to autonomous imaging -often without prior manual inspection-
61 may be of low quality for various reasons. Commonly encountered problems are fields of
62 view (FOVs) with no cells, too high cell densities or an inhomogeneous distribution of cells.
63 Preparations may feature high background or a low signal to noise ratio due to problems
64 with the staining procedure or contain artifacts such as large algae that impair successful
65 imaging of bacteria. Another source for low quality images can be the topological
66 unevenness of some FOVs, especially when high magnification objectives are used. This
67 may affect both, an entire preparation or only small areas thereof. On the other hand,
68 failures in the automated image acquisition procedure, e.g. inappropriate exposure times
69 or autofocus errors may lead to low quality images even from flawless preparations.

70 It seems important that such low quality images should not be further analyzed,
71 because they decrease accuracy and reproducibility of cell counting routines and may thus
72 lead to unpredictable results. It is thus necessary to inspect autonomously acquired
73 images and to remove low quality images from the data set. As autonomous image
74 acquisition yields large numbers of images within a short time period (i.e. thousands within
75 a few hours) the manual quality control of image data is a time consuming and tedious
76 activity and automation of this process would be highly advantageous.

77 Even though in most cases it is easy for a human observer to decide whether an
78 image is of high (HQ), medium (MQ) or low quality (LQ), automation is not trivial. It is

generally difficult to find reliable, measurable parameters to assess image quality. For one, an entire image has to be classified as LQ if only a minor part of that particular image is unusable. Moreover, there are several categories of low quality images (Fig. 1) and even human observers may face difficulties to clearly define them.

However, as humans are obviously able to rapidly assess the quality of an image without the need of pre-defined quality measures or categories, the application of artificial intelligence seems to be a promising approach to address this problem. Artificial neural networks (ANNs) are mathematical models inspired by the structure and behavior of animal neurons (8-10). They consist of interconnected layers of artificial neurons and learn from training data sets to recognize complex patterns. ANNs have been successfully used to address a variety of scientific problems, e.g. face recognition (11), protein phosphorylation site prediction (12), tumor diagnosis (13), or the classification of bacterial morphotypes (14). ANN analysis has also found application in industrial quality control, e.g. in machine vision based grading of apples (15) or cherries (16).

We developed a computer program that performs automated or semi-automated quality control of autonomously acquired microscopic images of fluorescently stained bacteria. The program includes an image viewer functionality and allows for manual and automated sorting of images. Automation was achieved by low level image analysis and the implementation of a custom trained ANN. The algorithms for image processing are described in detail, and the program and the documented source code (VB.NET) are provided under general public license.

Materials and Methods

Biological samples, microscopic system and images

The preparations subjected to autonomous imaging were produced in studies of bacterioplankton ecology in freshwater or marine ecosystems (5-7). Briefly, aquatic bacteria were filtered onto polycarbonate membrane filters and fluorescently stained. On all preparations, 4',6-diamidino-2-phenylindole (DAPI) was used to stain nucleic acids in bacterial cells (17). Specific phylogenetic staining was performed by fluorescence in-situ hybridization (FISH) (18,19). On some of the preparations, microautoradiography (MAR) was additionally performed for assessment of bacterial activity (20). Automated image quality assessment was exclusively performed on the images of DAPI stained cells (primary image).

Autonomous image acquisition was performed on a high-throughput imaging platform based on a motorized microscope (AxioImager Z.1, Zeiss, Germany). Functionality for autonomous imaging was implemented via the Visual Basic for Applications module within AxioVision (Zeiss, Germany) (M. Zeder, unpubl.). Imaging was carried out using a CCD camera (AxioCam Mrm, 12 bit grayscale, 1388 x 1040 px, Zeiss, Germany), a 63 x Plan-Apochromat (NA: 1.4) objective, and a LED epifluorescence illumination device (Colibri, Zeiss, Germany) with four LEDs (365 nm, 450-700 nm, 470 nm, and 590 nm) in combination with a multi filter set (filter set 62 HE, Zeiss, Germany). Silver grains in the MAR preparations were imaged in bright field illumination.

Images were stored in the JPG format (grayscale, 8 bit). A fixed number of FOVs were imaged for every preparation, and the file naming was defined as follows: variant A: XX_YY_Z.JPG, or variant B: XXXYYYZ.JPG, where XX or XXX denotes the number of the preparation, YY or YYY the number of FOVs on that particular preparation, and Z represents the fluorescence channel (D: DAPI, P: FISH-Probe, T: MAR). The image quality assessment program is able to handle both naming variants.

Image test set

For training and testing of the ANN underlying the automated image quality

assessment, 25000 DAPI images were randomly chosen from the roughly 250000 image sets acquired in 2008 by different scientists at our department. The 25000 images were manually assigned to three different quality categories. The HQ category contained perfect images whereas the LQ category contained images that should not be subjected to further image analysis. The remaining images were assigned to the MQ category. Training subsets consisting of 33, 366 and 2200 randomly chosen images of each category were created. The images from each category were mixed in a regular systematic manner in the training set (HQ1, MQ1, LQ1, HQ2, MQ2 ... etc.). A validation subset with the same number of images was created accordingly.

Image processing, feature extraction and ANN design

Image processing for quality assessment was realized in VB.NET using direct memory access to efficiently retrieve pixel intensities of an image and transferring them into a two-dimensional array for further calculations. In order to address quality issues related to FOV unevenness or inhomogenous image quality, the image was subdivided into 9 or 16 rectangular parts referred to as subimages (SI). For evaluation purposes, the routine was also tested without image subdivision. Each image or SI was subsequently processed to extract three features for input to the ANN (Fig. 2). These features were the mean gray value (MGV), a cell density measure (CDM) and a background inhomogeneity measure (BGI).

The MGV was calculated as the sum of all pixel intensities *i(x,y)* in a SI divided by the number of pixels in that particular SI:

$$MGV = \frac{1}{x_{\max}\, y_{\max}} \sum_x \sum_y \left(i(x,y)\right), \qquad (1)$$

where x_{max} and y_{max} were the number of pixels in *x* and *y* direction, respectively.

CDM and BGI were calculated using every second pixel scan line in *x* direction in order to increase processing speed. These features are similar to the focus algorithm described by Brenner et al. (21) but differ in that they apply a threshold (T = 20) for assessing large (CDM) and small (BGI) pixel intensity gradients. CDM was calculated as

$$CDM = \sum_x \sum_y (\Delta - 2 \cdot T)^2, \qquad (2)$$

where Δ is equal to $|i(x,y)-i(x+2,y)|$ if this term is > 2 T, else Δ is 2 T.

BGI was calculated as:

$$BGI = \sum_x \sum_y (\Delta - T)^2 , \quad (3)$$

where Δ is equal to $|i(x,y)-i(x+2,y)|$ if this term is > T and < 2 T, else Δ is T.

Prior to input to the ANN, the values of each feature from the subimages were normalized and sorted in ascending order to create a position invariant input (Fig. 2). Normalized values V_{Norm} were calculated from the values V as follows:

$$V_{Norm} = 0.8 \cdot \min(V, V_{\max}) / V_{\max} + 0.1 , \quad (4)$$

where V_{max} was 255 for MGV and 5×10^6 for CDM and BGI, respectively.

The ANN was implemented in VB.NET as a feed-forward network with three layers, an input, a hidden and an output layer. A sigmoid activation function was used. The number of neurons in the input and the hidden layer was varied to determine optimal performance. There were three neurons in the output layer, one for HQ, MQ and LQ, respectively. The back propagation of error method was used to train the net. The ANN was trained to yield output values of 0.9 for a positive result and 0.1 for a negative result.

ANN training and testing

Different combinations of numbers of hidden neurons, training cycles, degrees of image subdivision and numbers of images in the training set were used to create a multitude of ANNs. The numbers of training cycles were 50, 100, 500, 1000, 5000, 10000, and 20000. The number of hidden neurons was chosen according to the number of input values (i.e. input nodes) that were dependent on the degree of image subdivision. ANNs for the analysis of entire images (no subdivision, 3 input nodes) were trained with 5, 10, 15, and 20 hidden nodes. ANNs for image subdivision into 9 SI (27 input nodes) were trained with 30, 50, 70, and 90 hidden nodes and ANNs for image subdivision into 16 SI (48 input nodes) were trained with 60, 80, 100, and 140 hidden nodes. All ANN variants were trained in triplicates. The resulting ANNs were subsequently tested against (i) the corresponding training subset, (ii) a validation subset consisting of 2200 images per quality category that were not present in the training subset and (iii) the entire set consisting of

25000 images (data not shown). The ANN with the highest correct identification rate was finally implemented in the newly developed program (see below).

Performance comparison of humans and the optimal ANN

The performance of six scientists was compared to that of the ANN. 250 randomly chosen images were assigned to the three categories HQ, MQ, LQ both by humans and the ANN. The classification by the scientists was repeated after several weeks to assess its reproducibility. The assignments were compared pairwise among the six scientists and to the ANN. In addition, the time required for classification was also considered. The image set is available for download (http://www.technobiology.ch).

Influence of low quality images on counting precision

In order to assess the influence of the presence of LQ images within an image set on the counting precision, six preparations of DAPI stained bacteria were imaged with the above described instrumentation. From each preparation, 60 HQ and 60 LQ images were used to create image sets containing different portions of LQ images. For this, different numbers of LQ images were added to the core set of 60 HQ images to obtain sets with 0, 10, 20, 30, 40, and 50% LQ images. The image sets were subjected to an automated cell counting routine (M. Zeder, unpubl.). Mean cell counts on the image sets were statistically analyzed by one way ANOVA to assess the level of acceptable LQ images in a set. In addition, the mean coefficients of variation (CV) in sets with different portions of LQ images were also compared statistically.

Programming strategy, ANN implementation, and program description

The program, subsequently termed “Automated Image Quality Control” (AIQC), was developed in Visual Basic .NET (Microsoft) using an object oriented programming approach. The workflow is as follows: the program checks a user defined directory, for the presence of .JPG images with file names complying to either variant A or B. Images with equal indices for preparation and FOV but different suffices are grouped as single image sets. Image sets with different indices for FOV but equal indices for preparation are

grouped as single preparations. The preparations are depicted in a graphical user interface as bars which represent the number of images (or image sets) available from a particular preparation. The user is then able to browse preparations, image sets and images by keyboard commands. Image sets can be selected and manually sorted into a different directory. The implemented default ANN allows for automated detection of either LQ or of MQ and LQ images. In order to extend the ANN functionality to other kinds of images than the default ANN was trained for, it is possible to create, train and save novel ANNs based on user-specific classification of images. The program can be run exclusively by command line arguments to facilitate its integration into an automated workflow.

The program and the documented source code are available under general public license at http://www.technobiology.ch.

Results

ANN optimization

Altogether, 420 ANNs with different combinations of parameters were created to find the optimal configuration. The categories HQ and MQ were merged into a single category 'good' to obtain dichotomous data. The percentage of correct classification was determined for both the training and the validation set (Fig. 3) by division of the number of correctly identified images by the sum of all images.

Training iterations and hidden neuron numbers. All ANN variations (Fig. 3 A-E) were trained with different numbers of training iterations, ranging from 50 to 20000. The correct identification rate on the training set increased steadily with the number of training iterations (Fig. 3 A-E, left panel side). However, on the validation set, there was an optimum reached (Fig. 3 A-E, right panel side) at 500 to 1000 iterations. All ANN variations featured four different hidden neuron variants. In general, higher numbers of hidden neurons lead to slightly higher correct identification rates, but at the expense of longer computation times.

Degree of image subdivision. The ANNs based on images without subdivision yielded a maximal correct identification rate of 82.1% (Fig. 3 A) on the validation set. Subdivision into 16 SI lead to a maximum of 91.1% (Fig. 3 B). The overall maximum was achieved by subdivision into 9 SI and accounted for 93.7% of correct identification (Fig. 3 E).

Training set size. In order to assess the influence of the training set size on the performance of the resulting ANNs, three different set sizes were tested (Fig. 3 C-E). By using 33 images per category (HQ, MQ, LQ) a correct identification rate of 80.4% was achieved. 336 images per category yielded 92.2% of correct identification. The overall maximum of 93.7% was achieved with 2200 images per quality category.

Optimal configuration. Considering the correct identification rate and the rate of false positive and false negative identifications of all tested variants, the ANN based on nine SI, 90 hidden neurons and 1000 training iterations on a set of 2200 images per category was found to be optimal. The best of the three replicate ANNs was implemented in the AIQC program. The overall correct identification rate of this ANN on the entire set of manually classified images (n = 25000) was 94.0%.

Performance comparison of humans and the ANN

Consensus among different humans. Pairwise comparisons of image classification by humans (n = 6) revealed a mean consensus of 90.5 ± 4.2% (min = 81.6%; max = 97.6%).

Reproducibility of humans. When humans classified the same set twice, they agreed with themselves on 92.3 ± 2.5% (min = 88.4%; max = 95.6%) of the images.

Consensus of humans and the ANN. Pairwise comparison of classification between humans and the ANN showed a mean consensus of 88.5 ± 2.7% (min = 82.8%; max = 90.8%). Statistical analysis (one way ANOVA; Post-hoc test by Tukey's method) revealed that none of the three above mentioned means was significantly different.

Agreement of the ANN on the human consensus set. A consensus set of images where all six humans agreed was compared to the ANN's decision. 78% of all images were identically classified by all humans. 96.4% of the images from this consensus set were equally classified by the ANN.

Classification speed. Humans classified 0.85 ± 0.11 images per second whereas the AIQC program processed about 10 images per second on a state of the art personal computer.

Influence of quality control on counting precision

The presence of LQ images in a set lead to significant increase of the coefficient of variation of cell counts from a single preparation (Fig. 4) already when 10% of the images in the respective set were LQ. The mean of cell counts on a preparation was more robust against the presence of LQ images and significant differences were only observed at proportions of 30% (n = 4) to 40% (n = 2) (one way ANOVA; Post-hoc test by Tukey's method). The application of the ANN to the image data set with 50% LQ images correctly removed the majority of LQ images, so that the resulting mean cell counts as well as CVs were not significantly different from the original set of HQ images only.

Discussion

Image quality control is an important issue in automated imaging platforms (1). Low quality images need to be removed from data-sets prior to image analysis, because they decrease the counting precision and accuracy, as experimentally shown for bacterial cell counts (Fig. 4). It should be noted that these results are conservative error estimates, as the effects of LQ images on data derived from double or triple staining might be considerably more drastic. Automated removal of low quality images is thus of high advantage. On one hand, it significantly accelerates the quality control process. On the other hand, decisions are more objective and reproducible, as illustrated by the comparatively low reproducibility of human assessment.

The investigation of aquatic habitats with different characteristics (e.g., productivity) will result in microscopic preparations with a large heterogeneity of image properties such as staining quality, background, cell densities and morphologies. Automated differentiation between HQ and LQ images is thus not trivial, as quality is highly context dependant and no clear and simple rules exists that could be implemented in a classification system such as a linear decision tree. In this work we present a computer program that allows for automated quality control of microscopic images of fluorescently stained aquatic bacteria from a variety of samples. The availability of a large amount of image data and the human ability to rapidly assess image quality suggested the implementation of a trainable system, i.e., an ANN.

ANN input data. The input data for an ANN are of crucial importance. The information retrieved from the image should not be too specific and should be invariant to rotation and position. Moreover, it should allow recognizing a LQ image if only a small part of the image is of low quality (Fig. 1 F). The strategy of dividing an image into separately analyzed SI can to be a powerful approach for identifying FOV unevenness during autofocusing (22). Image subdivision into 9 parts also significantly improved the correct identification rate in image quality control, compared to the analysis of entire images (Fig. 3). However, subdivision into 16 parts did not result in further improvement. A possible explanation could be that higher degrees of subdivision increase the number of input values, thereby rendering the learning process more complex, and the input values *per se* are less meaningful, as they represent smaller image areas. Alternatively, there might be an optimal relationship between the size of the SI and the image features of interest (in our case, fluorescently stained bacteria).

In order to assess the quality of a SI, three features were extracted: the mean gray level intensity (MGV), a measure for cell density (CDM) and a measure for background inhomogeneity (BGI). On the whole image level, the parameter MGV is sensitive to some types of unfocussed images or too long exposure times (Fig. 1, H and E). Moreover, the presence of single large bright objects (Fig. 1 G) can be detected by comparing the MGVs on the 9 SI. However, this parameter is not able to, e.g., detect empty fields, because cells, even though they feature high gray level intensities (approx. 100 to 255) compared to the background (approx. 20 to 40), only cover a small part of the total image area. Thus, most of the image pixels represent background (> 98%) and the presence or absence of cells cannot be deduced by the MGV parameter. Therefore, the presence of cells was assessed by the CDM feature which is a custom modification of the Brenner Gradient algorithm (21). It quantifies gray level gradients by measuring the squared difference of the intensity of a pixel and its neighbor two pixel ahead on a scan line. Fluorescent objects typically feature large gradients along their contour. As an indicator for cells we thus introduced a threshold in order to exclusively detect strong gradients. On the whole image level, this allows a reliable distinction between empty images and images containing cells, Moreover, the inhomogeneity of the distribution of cells within the image can be assessed by comparing CDM values on the individual SI.

For the counting and sizing of cells, the mere presence of fluorescence signals from objects is not sufficient, as they must be well focused, too. While it is easy to specify the in-

focus image of cells in a z-stack of images (e.g. during autofocusing), it is much more demanding to derive focus information exclusively from a single image (1). This is even more difficult if it has to be specified *a priori* before actual object detection, i.e. without knowledge of the geometrical and densitometrical properties of the objects. Small objects in the sub-micrometer range, such as many aquatic bacteria, exhibit a halo when they are imaged out of focus, because the image of a point source of light is a three-dimensional diffraction pattern (23). The intensity of the halo is lower than the fluorescence intensity of the object itself. These weak gray level intensity gradients in close proximity to fluorescent objects are thus characteristic for unfocussed images. We, therefore, modified the CDM parameter by applying another threshold to exclusively measure weak gradients, rendering this new parameter (BGI) sensitive to the halo pattern. A linear combination of two parameters, e.g. their difference, gives a rough measure for the 'focussedness' of objects on an image (Fig. 5), allowing for detection of unfocussed or partially unfocussed images (Fig. 1 F, Fig. 2) by ANN analysis. A similar approach, but relying on prior cell detection and subsequent analysis of the pixel intensities around the cell boundaries has recently been described for successful detection of unfocussed cells (1).

ANN Training. Comparison of different sizes of training sets showed that larger training sets enhance the performance of the ANN (Fig. 3 B, J, L), but also that the gain is greatest when increasing the training set size from 33 to 366 images per quality category. Moreover, equal numbers of images per category and regular mixing of those appeared to be an important issue for successful training (data not shown).

Several variants of feed forward back propagation ANN were trained. The two main variables were the number of training iterations and the number of hidden neurons, and the former was found to be of greater importance. The effect of overtraining was observed after more than 1000 iterations: the rate of correct identification still increased on the training set whereas the correct identification rate on the validation set cumulated on 500 – 1000 iterations and subsequently decreased (Fig. 3 E).

Overall ANN and human performance. The ANN optimization resulted in a maximal performance of 94% of correctly classified images. However, the correct identification rate is based on a training set that had been manually classified by a human expert. Comparison of the classification performance of different humans showed that the same set of images (n = 250) was differently classified by different humans, with a mean pairwise agreement of about 91%. If humans classified the same set twice, the

reproducibility was slightly but not significantly higher (92%), reflecting the fact that there is a fraction of images that cannot be unambiguously assigned to either category even by the same individual. The pairwise agreement of the ANN to the humans was not statistically significantly different from the pairwise agreement between humans. We, therefore, conclude that the ANN can be trained with high precision to a specific training set. This is moreover supported by the finding that 96% of the images from the core set (i.e. all the images that were identically classified by six humans) were also classified likewise by the ANN. As it is obviously very difficult to assign a certain percentage of images (around five to ten percent) to the 'correct' quality class, we must assume some inconsistency in any human-made training set. Thus, we cannot expect the ANN to behave more precise than the human ability for correct assignment.

Altogether, the ANN approach for an automated quality assessment of microscopic images of stained bacteria proved to be successful, both with respect to correct identification rate and to classification speed. The program offers the possibility to implement differently trained ANNs in order to classify other types of images than described here. The authors are therefore confident that the program and the underlying strategies can be applied for quality control in other image based screening platforms.

Acknowledgements

The authors gratefully acknowledge Kathrin Felder for critical manuscript revision. Ester Eckert, Michaela Salcher and Markus Steinkellner are acknowledged for participating in the comparison study.

References

1. Matula P, Kumar A, Worz I, Erfle H, Bartenschlager R, Eils R, Rohr K. Single-Cell-Based Image Analysis of High-Throughput Cell Array Screens for Quantification of Viral Infection. Cytometry Part A 2009;75A(4):309-318.

2. Chung KH, Crane MM, Lu H. Automated on-chip rapid microscopy, phenotyping and sorting of C. elegans. Nature Methods 2008;5(7):637-643.

3. Pernthaler J, Pernthaler A, Amann R. Automated enumeration of groups of marine picoplankton after fluorescence in situ hybridization. Applied and Environmental Microbiology 2003;69(5):2631-2637.

4. Daims H, Wagner M. Quantification of uncultured microorganisms by fluorescence microscopy and digital image analysis. Applied Microbiology and Biotechnology 2007;75(2):237-248.

5. Alonso C, Zeder M, Piccini C, Conde D, Pernthaler J. Ecophysiological differences of betaproteobacterial populations in two hydrochemically distinct compartments of a subtropical lagoon. Environ Microbiol 2008.

6. Salcher MM, Pernthaler J, Zeder M, Psenner R, Posch T. Spatio-temporal niche separation of planktonic Betaproteobacteria in an oligo-mesotrophic lake. Environmental Microbiology 2008;10(8):2074-2086.

7. Zeder M, Peter S, Shabarova T, Pernthaler J. A small population of planktonic Flavobacteria with disproportionally high growth during the spring phytoplankton bloom in a prealpine lake. Environmental Microbiology 2009:*in press*.

8. Basheer IA, Hajmeer M. Artificial neural networks: fundamentals, computing, design, and application. Journal of Microbiological Methods 2000;43(1):3-31.

9. Maier HR, Dandy GC. Neural networks for the prediction and forecasting of water resources variables: a review of modelling issues and applications. Environmental Modelling & Software 2000;15(1):101-124.

10. Rumelhart DE, Hinton GE, Williams RJ. Learning Representations by Back-Propagating Errors. Nature 1986;323(6088):533-536.

11. Rowley HA, Baluja S, Kanade T. Neural network-based face detection. Ieee Transactions on Pattern Analysis and Machine Intelligence 1998;20(1):23-38.

12. Blom N, Gammeltoft S, Brunak S. Sequence and structure-based prediction of eukaryotic protein phosphorylation sites. Journal of Molecular Biology 1999;294(5):1351-1362.

13. Khan J, Wei JS, Ringner M, Saal LH, Ladanyi M, Westermann F, Berthold F, Schwab M, Antonescu CR, Peterson C and others. Classification and diagnostic prediction of cancers using gene expression profiling and artificial neural networks. Nature Medicine 2001;7(6):673-679.

14. Blackburn N, Hagstrom A, Wikner J, Cuadros-Hansson R, Bjornsen PK. Rapid determination of bacterial abundance, biovolume, morphology, and growth by neural network-based image analysis. Applied and Environmental Microbiology 1998;64(9):3246-3255.

15. Unay D, Gosselin B. Artificial neural network-based segmentation and apple grading by machine vision. 2005 International Conference on Image Processing (ICIP), Vols 1-5 2005:1773-1776.

16. Guyer D, Yang XK. Use of genetic artificial neural networks and spectral imaging for defect detection on cherries. Computers and Electronics in Agriculture 2000;29(3):179-194.

17. Porter KG, Feig YS. The Use of Dapi for Identifying and Counting Aquatic Microflora. Limnology and Oceanography 1980;25(5):943-948.

18. Amann RI, Ludwig W, Schleifer KH. Phylogenetic Identification and in-Situ Detection of Individual Microbial-Cells without Cultivation. Microbiological Reviews 1995;59(1):143-169.

19. Pernthaler A, Pernthaler J, Amann R. Fluorescence in situ hybridization and catalyzed reporter deposition for the identification of marine bacteria. Applied and Environmental Microbiology 2002;68(6):3094-3101.

20. Alonso C, Pernthaler J. Incorporation of glucose under anoxic conditions by bacterioplankton from coastal North Sea surface waters. Applied and Environmental Microbiology 2005;71(4):1709-1716.

21. Brenner JF, Dew BS, Horton JB, King T, Neurath PW, Selles WD. An automated microscope for cytologic research a preliminary evaluation. J Histochem Cytochem 1976;24(1):100-11.

22. Zeder M, Pernthaler J. Multi-spot live-image autofocusing for high-throughput microscopy of fluorescently stained bacteria. Cytometry A 2009:*in press*.

23. Hecht E. Optics. San Francisco: Addison Wesley; 2002.

Legends to Figures

Figure 1:

Examples of microscopic images of fluorescently stained bacterial cells on membrane filters exhibiting different qualities (A: high quality [HQ]; B,C: medium quality [MQ]; D-I: low quality [LQ]). A: homogenously distributed bacterial cells. B: image with optically dense spots as produced by microautoradiography. C: Inhomogeneously distributed bacterial cells. D: Too high density of stained objects. E: High unspecific fluorescent background. F: Uneven preparation, the image is only partly in focus. G: biological artifact, a large blue-green algal cell (*Planktothrix rubescens*). H: Unfocused image. I: Image focused on an interface but not on bacterial cells.

Figure 2:

Schematic representation of the image processing workflow: Subdivision of the image into nine parts and determination of three features (MGV, BGI, CDM) per SI. ANN input is generated by normalization and sorting of the measured features. The ANN consists of 27 input (Nr. 1-9 for MGV, nr. 10-18 for BGI, and nr. 19-27 for CDM values), 90 hidden and 3 output neurons. The ANN output for the depicted image is maximal on the LQ output neuron (0.910) and the image is thus correctly identified as LQ image.

Figure 3:

Performance of different ANN configurations. For differently configured ANNs, the correct identification rate (A-E) on both, training (T) and validation (V) set is plotted against increasing training iterations. In F, false positive and false negative identification rate on the validation set is plotted against the number of training iterations. Each data point represents a triplicate of the same ANN configuration (Error bars show standard deviation of the triplicates). The hidden neurons number (symbols), the degree of image subdivision (SI: 0, 9, 16) and the training set size (33, 336, 2200 images per quality category) was varied.

Figure 4:

Precision of cell counting in relation to the fraction of LQ images in an image set. A: Mean cell counts per image of image sets with different portions of LQ images of one preparation (60 HQ images plus 0 – 60 LQ images). B: Coefficients of Variation of cell counts of 6 image sets with different portions of LQ images. Asterisks above boxes indicate significantly different means (ANOVA, Post-hoc test by Tukey's method) from the image sets containing no LQ images (white box).

Figure 5:

Changes of the image quality measures (CDM and BGI parameter) along a z-stack of 20 images. Sections of the images 6 to 15 are depicted on the right. Normalized measures of CDM and BGI on every image are shown as full and dashed lines, respectively. The gray area on the plot resembles the difference of BGI and CDM.

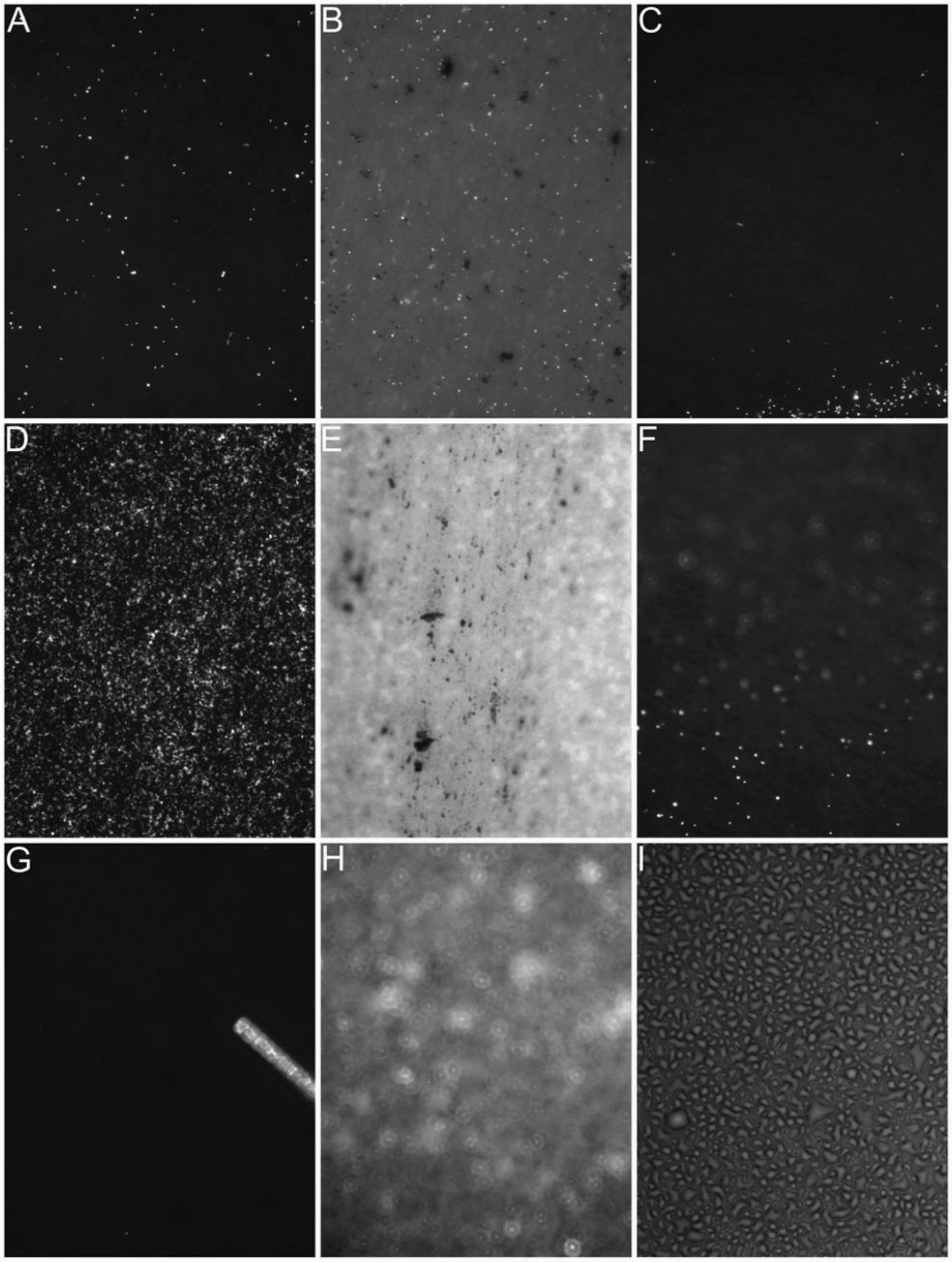

Zeder et al, Figure 1

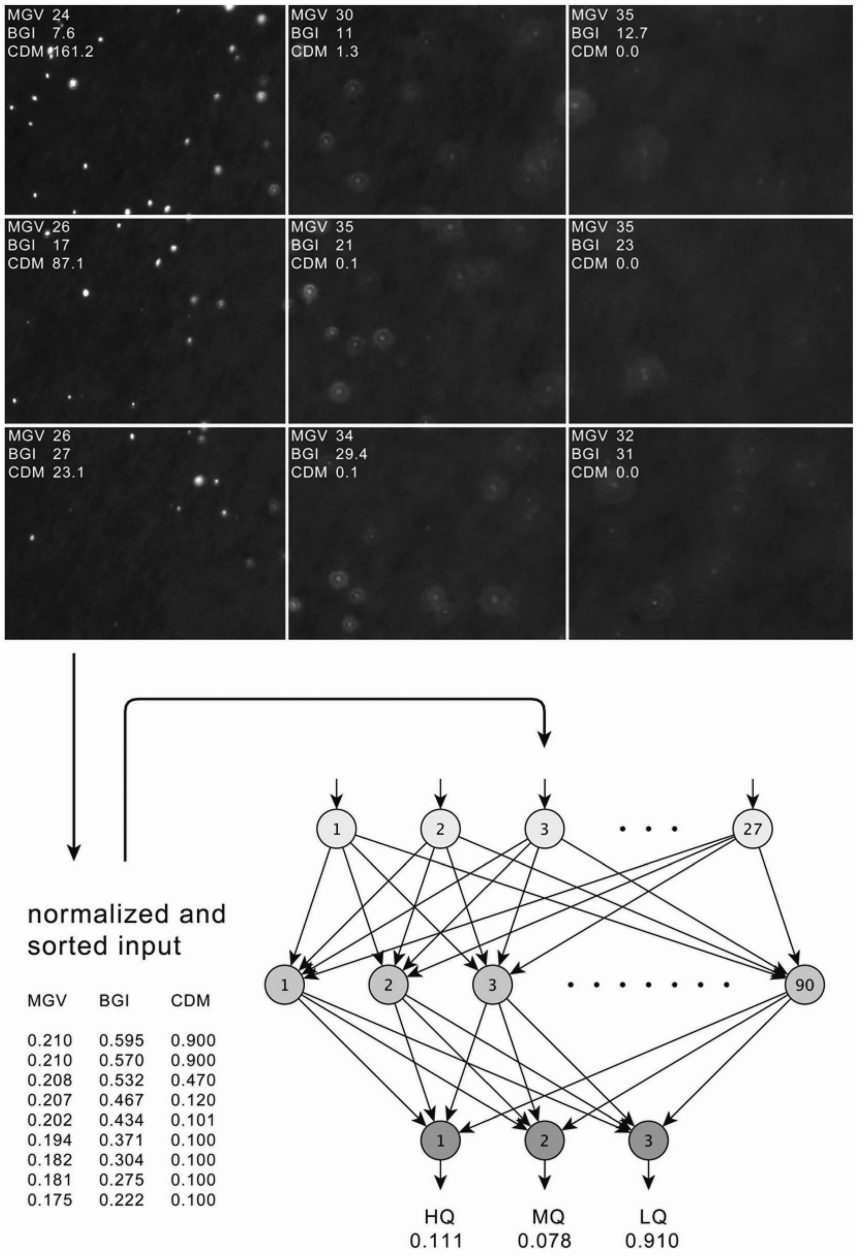

Zeder et al, Figure 2

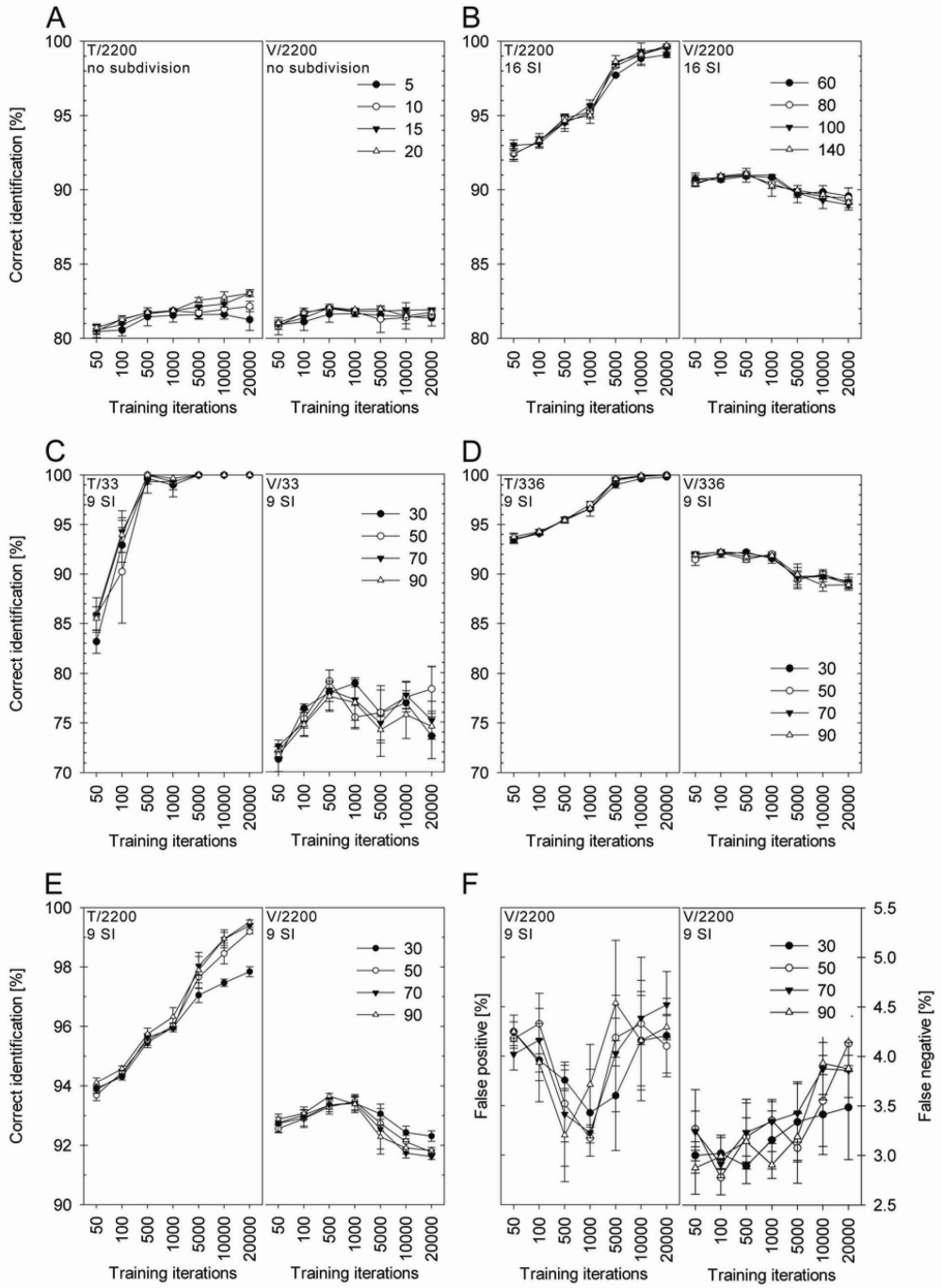

Zeder et al, Figure 3

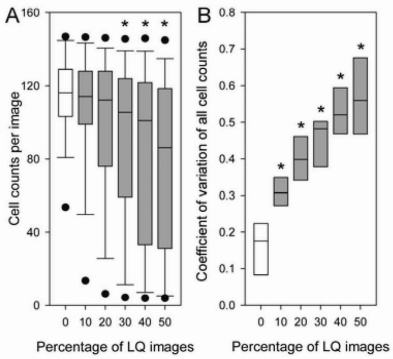

Zeder et al, Figure 4

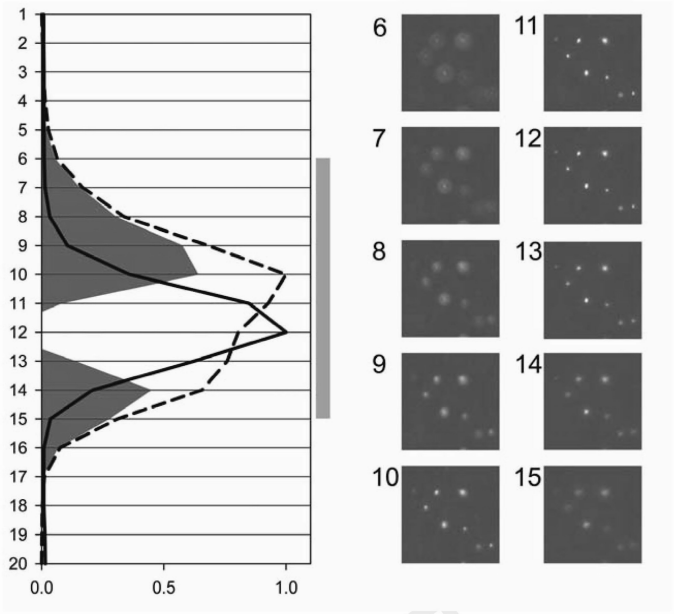

Zeder et al, Figure 5

7.3 Manuscript 3: Automated Quantification and Sizing of Unbranched Filamentous Cyanobacteria by Model Based Object Oriented Image Analysis.

Automated quantification and sizing of unbranched filamentous cyanobacteria by model based object oriented image analysis

Zeder M.[1], Van den Wyngaert S.[2], Felder K.[3], Pernthaler J.[1*]

[1] Department of Limnology, Institute of Plant Biology, University of Zürich, Seestrasse 187, CH-8802 Kilchberg, Switzerland (http://www.limnology.ch)

[2] Eawag, Swiss Federal Institute of Aquatic Science and Technology, 8600 Dübendorf, Switzerland

[3] Institute of Veterinary Bacteriology, University of Zürich, Winterthurerstrasse 270 CH-8057 Zürich

Running headline: automated filament quantification

* corresponding author
Prof. Dr. Jakob Pernthaler
Limnological Station, Institute of Plant Biology
Seestrasse 187, CH-8802 Kilchberg
Phone: +41 (0)44 716 1211; fax.: +41 (0)44 716 1225
Email: pernthaler@limnol.uzh.ch

To be submitted to: applied and environmental microbiology

Abstract

The quantification and sizing of filamentous cyanobacteria in environmental samples or cultures is often performed by manual or semi-automated microscopic analysis and thus a time consuming process. Automation by conventional image analysis is difficult as filaments may exhibit large variation in length and patchy auto fluorescence. Moreover, individual filaments frequently cross each other on microscopic preparations, as can be deduced by modelling. This study presents a novel approach based on object oriented image analysis to simultaneously retrieve (a) filament number, (b) individual filament lengths, and (c) cumulative filament length of unbranched morphotypes on fluorescence microscopic images in a fully automated high-throughput manner. Special emphasis was given to the problem of correct detection of overlapping objects by image analysis. The method was validated on a dataset of *Planktothrix rubescens* from field samples and compared with manual measurements by filament tracing, the line intercept method, and the Utermöhl counting approach. The described computer program features batch processing of .JPG images and annotation of detected filaments, requires no user interaction and is freely available.

Introduction

Automated quantification and sizing of single cells by microscopy and image analysis is a routinely applied technique to determine microbial biomass (2, 6, 17). In contrast, the fully automated quantification and length measurement of filamentous organisms is considerably more difficult to achieve and not yet satisfactorily solved in all details, even though there is a strong demand for in microbial ecology as well as in drinking water quality control (5). The filamentous cyanobacterium *Planktothrix rubescens* is a prominent example in this context. It is known to produce a variety of potent toxins (3, 4, 11, 12, 14) threatening animal and human health. It is also known to occur in large populations and its ability to form blooms renders this organism highly relevant in terms of public health and drinking water control (8, 9, 13, 20). Not surprisingly, the monitoring of filamentous cyanobacteria is a standard task in many laboratories. Cyanobacterial biomass is often taken as an estimator for toxin concentration, as its determination is less costly than a direct determination. Abundance and biomass determination is routinely performed by manual microscopy using either the Utermöhl sedimentation method (Utermöhl 1958) or by filtration of samples on track-etch membrane filters. These methods imply manual microscopy and are thus labor intensive and time consuming. A major improvement in filament quantification arose with the availability of CCD cameras and image analysis software in microscopy. Several automated or semi-automated methods have been proposed to measure total filament length, either indirectly (e.g. the line-intercept method) (15, 16) or directly by filament detection via image analysis on either fluorescence (10, 19) or bright field (1) images. However, the filamentous nature of *Planktothrix rubescens* (i.e. its remarkable length to width ratio) raises severe problems for processing by conventional image analysis. *Planktothrix* filaments exhibit a width of around 5 – 8 µm (7, 20) whereas their lengths are in a range from less than 50 to more than 2500 µm. If length measurements of individual filaments is performed, filaments have to be entirely located within a field of view (FOV), demanding for large areas to be imaged. Larger FOV areas may be achieved by choosing lower magnifying objectives, but on the cost of fluorescence intensity, and resolution that is both important for efficient imaging. A second problem results from the fact that filamentous organisms often overlap on a microscopic preparation. Overlapping objects in a two dimensional image, generated by wide field microscopy, cannot be correctly separated by

conventional image analysis that is based upon thresholding and binarization: two overlapping objects result in a single object. While the effect on the abundance determination in an automated procedure is obvious, the error of length measurement strongly depends on the applied method. These problems have been discussed in great detail by Walsby (19) but no automated solution has yet been proposed.

The aim of this work was to develop a computer program that (a) counts, and (b) measures the length of individual filaments, as well as (c) determines the cumulative lengths of filaments on images generated by epifluorescence microscopy. We moreover specifically addressed the problem of overlapping filaments and described a strategy to recognize and correctly count them. The probability of a filament being located only partially within the FOV and thus not measurable and the probability of filament overlaps were also assessed theoretically by a Monte Carlo simulation approach. The performance of the algorithm was subsequently tested against measurement of filaments on images by manual filament tracing, the line-intercept (15) and the Utermöhl methods.

106 ## Materials and Methods

107 ### *Monte Carlo simulation*

108 To estimate the number of filaments on a membrane filter being partially out of a
109 FOV, depending on filament length and FOV size, as well as the number of filaments
110 overlapping on a FOV as a function of filament density and filament length, a Monte
111 Carlo simulation was performed. The simulation was written in VB.Net, featuring a
112 graphical user interface. The simulation assumes filaments beeing straight lines and
113 uses a random number generator to create and position filaments on a FOV.
114

115 ### *Microscopy system and software development environment*

116 Image acquisition was performed on a motorized microscope (AxioImager Z.1, Zeiss,
117 Germany) using a CCD camera (AxioCam Mrm, 12 bit grayscale, 1388 × 1040 px,
118 Zeiss, Germany), a 10 × EC Plan-Neofluar (NA: 0.3) objective, and a LED
119 epifluorescence illumination device (Colibri, Zeiss, Germany) with four LEDs (365
120 nm, 450-700 nm, 470 nm, and 590 nm) in combination with a multi filter cube (filter
121 set 62 HE, Zeiss, Germany). For the extension of FOV size, multiple single adjacent
122 images were acquired and assembled automatically using the MosaiX module of the
123 AxioVision software (Zeiss, Germany). The composite image consisted of 11 × 15
124 single images and covered an area of approximately 1 cm^2 (~ 15000 × 15000 px;
125 0.645 µm px^{-1}). Images were stored in the JPG format (grayscale, 8 bit). For an
126 internal validation, smaller images of the size of 5000 × 5000 px were acquired.
127 The filament counting and sizing program as well as the Monte Carlo simulation were
128 developed in Microsoft Visual Basic .Net (VB.Net). Both programs are available for
129 free (http://www.technobiology.ch).
130

131 ### *Program and algorithm description*

132 **The Fixel concept.** The pixel (picture element) depicts the smallest element of an in
133 image in conventional image processing. Therefore, objects to be measured are
134 represented as groups of connected pixels. As a consequence, overlapping objects,
135 i.e. objects sharing the same pixels are detected as one single object. As filaments
136 are expected to frequently overlap, as a function of their density and length (Fig. 1A),

a new concept had to be introduced to correctly handle overlapping objects (for examples see the left panel of Figure 2). We followed a model based object oriented image analysis approach. The model assumptions were as follows: (a) Filaments appear on the image as bright objects on dark background; (b) Filaments exhibit a width of approximately 10 px; (c) Filaments are not branched. The basic objects in the algorithm are 'filaments' and 'fixels', with filaments consisting of multiple fixels. The term fixel was chosen in analogy to pixel to denote the smallest element of a filament. A fixel is a rectangular structure that covers a small part of a filament and has the same orientation as the filament at that particular location.

In a first step of the analysis, the image, derived from epifluorescence microscopy, is loaded and transferred into a two-dimensional pixel array. The background of the image is estimated by taking the mean pixel intensities of the first scan line in x-direction, assuming that most of the pixels present are background. Subsequently the array is processed by a kernel to detect all fixels on the image.

Fixel detection: The primary kernel for fixel detection is shown in Figure 3 A. It is no kernel in the classical sense in that it only analyses a subset of selected pixels in close proximity to a centre pixel. The gray level intensities of these pixles are compared to three empirically determined thresholds (T1 = 16, T2 = 13, T3 = 10) and yield a positive result if all the intensities are above the background-corrected threshold. If a potential fixel is detected, its orientation is determined. A cross-like structure consisting of two orthogonal transect lines (A, B) trough the centre pixel is used to sum up pixel intensities. This structure is rotated in steps of 22.5°, and the difference of the sum of the two transect lines is analyzed (Fig. 3 B). If one of the lines is parallel to the filament and the other one is perpendicular to the filament, the difference of their integrated intensities is maximal (Fig. 3 C). If the orientation is confirmed, a rectangular field with the same orientation is moved along a line perpendicular to the fixel's orientation to locally optimize the precise location of the fixel by maximizing the sum of the gray level intensities within the rectangle. Finally, the fixel location is set and the corresponding area is locked in order not to place another fixel within this area (Fig. 3 D). All detected fixels on the image are stored in a list.

Assignment of neighbouring fixels. After the detection of all fixels and their orientations on the image, filaments are reconstructed by connecting neighbouring fixels. In addition to its orientation and spatial position on the image, a fixel also

features two sides that can link connected to a neighbouring fixel. Figure 3 E illustrates all possible fixel orientations and Fig. 3 F shows detected fixels on two crossing filaments. For every fixel, two lists of suitable neighbours are generated, one for each side of the fixel. Potential neighbours have to be within a defined distance interval (6 to 70 px) and the difference in orientation must not exceed 45°. From all potential neighbours of a fixel, the best neighbour on each side is selected by an empirical optimization function, considering distance, orientation and gray level intensity profile between fixels (Fig. 3 G). Three cases are possible: (i) a fixel may have no neighbours and will not be considered for filament assembly; (ii) a fixel may have two neighbours and can be a part of a filament, or (iii) a fixel may have one neighbour only and can be a starting point for filament assembly.

Filament assembly. Starting from the ends, filaments are assembled by joining each fixel with its best-scoring neighbour on the other side in a recursive way. As there are twice as many 'end fixels' than filaments, too many filaments are assembled. As filament assembly from the two different ends does not necessarily has to result in the same filament, (e.g. in the case of ambiguous crossings) a score for each filament assembly is generated and the better-scoring version of the filament is maintained (Fig. 3 H).

Iteration of neighbour assignment and filament assembly. After this procedure of neighbour detection and filament assembly, there may still be unassigned fixels remaining. Therefore up to four iterations of neighbour detection and filament assembly are performed, and fixels already assigned to filaments are removed from the fixel list after each iteration.

Filament annotation and length measurement. In order to allow for manual verification of the filament detection, an annotated image is created for each analyzed image, where all detected fixels and filaments are imprinted and enumerated. Filament length measurement is performed by addition of the distances between the fixels of a filament. As the end regions are systematically underestimated by this method, an empirically determined value (24 px) was added to each filament as determined from correlation analysis (see results). Finally a report is generated as a text file comprising the length of the individual filaments.

Image set for internal validation

Seven representative images (5000 × 5000 px , approx. 0.1 cm^2) containing *Planktothrix* filaments on polycarbonate membrane filters were analyzed (method see below). Manual filament measurement by means of tracing single filaments within AxioVision was performed by four researches independently. The results were compared between the researchers, and with the output of the automated routine. Additionally, the images were evaluated by the line-intercept method according to Nedoma *et al*. (15), using 16 horizontal test bars of the length of 5000 px each. For assessing the rate of correct recognition and assembly of parallel or overlapping filaments, the annotated images generated by the program were manually compared to the original images. In order to verify the accuracy of length measurement of individual filaments, a total amount of 100 filaments that were correctly detected by the program and by all four researchers were selected. For each filament, the means of the four replicate human length measurements were compared to the automated measurement. The seven images are available online at http://www.technobiology.ch.

Sampling and evaluation of joint dataset with an external laboratory

A depth profile (0, 1, 2.5, 5, 7.5, 10, 12.5, 15, 20, 30, 40, 80, 120, and 135 m) was sampled on Lake Zurich (sampling location: Thalwil) on July 9, 2008 in the context of a routine sampling by the water supply company of Zurich (WVZ). Samples (50 ml) were fixed with paraformaldehyde (2% final concentration). Volumes between 1.5 and 12 ml, depending on the filament density, were filtered onto polycarbonate membrane filters (25 mm diameter, 5 um pore size, Sterico). Filters were imaged as described above to produce large composite images (~ 15000 × 15000 px = 1 cm^2) using the green light fluorescence illumination to detect the autoflurescence of *Planktothrix rubescens*. From the depth of maximal *Planktothrix* abundance, four replicate preparations were produced. Images were then analyzed by the here described program as well as measured by manual tracing of filaments and drawing of poly-lines using AxioVision. Additionally, the samples were independently analyzed by the WVZ using the Utermöhl method (25 ml per sample, analyzed area = 1 cm^2; measurement of 20 – 30 individual filaments for the determination of the average length).

Result

Monte Carlo simulation

The importance to image large FOV areas to correctly measure the length of individual filaments as well as the need for a method to handle overlapping filaments was confirmed by a computational simulation using the Monte Carlo method. Figure 1 A predicts the number of expected filament crossings as a function of filament density and filament length. On the internal validation set of seven images, a number of 44 intersects was counted. By performing the simulation, with the input of the average filament density (192 filaments on 0.7 cm^2) and the average filament length measured on the seven images of 487 µm, 36 intersections are suggested.

Internal validation

A high correlation was found between manual and automated measurement of both, filament numbers (linear regression, $r^2 = 0.9591$, $P = 0.001$) and cumulative filament length (linear regression, $r^2 = 0.9946$, $P < 0.001$) for the seven images (Fig. 4 A, B). In addition, the automated measurement of the cumulative length was more accurate than the previously described line-intercept method (linear regression of manual measurements and line intercept estimates, $r^2 = 0.7433$, $P = 0.0216$).

The four replicates of manual determinations exhibited only small variations in filament counts (CV = 0.02) and the automated estimation of the filament number was slightly higher than the manually determined values. However, the means of manual replicates and the automated counting were not statistically significantly different from one another (one-way ANOVA, post-hoc test by Tukey's method).

The numbers of incorrectly handled events in the case of parallel and overlapping filaments by automated filament detection as well as of frequently observed artefacts such as air bubbles below the cover slip or premature filament breaks are shown in Table 1. Most importantly, overlapping events were handled correctly in > 85% of the cases. The example image sections depicted in Figure 2 are derived from the seven images and illustrate some of the listed artefacts.

To prove the ability of our method to accurately measure the length of individual filaments independent of length or curvature, 100 filaments on the seven images where compared individually (Fig. 4 C). A high linear correlation was found between the automated and manual length determination ($r^2 = 0.9997$) and the slope of the

268 regression was nearly 1 (Fig. 4 C). The observed offset of 14.6 µm results from the
269 fact that the centre of the first and last fixel of a filament is not at the ends of the
270 filament. Thus, a mean amount of 12 px per filament end has to be added for
271 correction (as already described in the 'Methods' section).
272

273 ***External validation***

274 For an external validation of the method, a joint sampling was conducted on the July
275 9, 2008 in collaboration with the WVZ. The here described automated method,
276 manual filament tracing on microscopic images by a technician and the
277 independently validated and certified analysis using the Utermöhl approach by the
278 WVZ were used to estimate filament concentrations as well as cumulative filament
279 lengths in the water samples from the depth profile (Fig. 5).
280 A large variation of filament concentrations along the depth profile was observed.
281 Almost no filaments were present in the upper half of the epilimnion (< 7.5 m) and in
282 the hypolimnion (> 40 m). By contrast, the metalimnion featured a pronounced peak
283 below the maximum of oxygen concentration at a depth of 15 m with a density of
284 approx. 400 filaments per ml (Fig 5 A). The cumulative filament length showed a
285 similar distribution and featured a maximal value of roughly 2 m l^{-1} at 15 m depth (Fig.
286 5 B). The observed pattern goes in perfect accordance with previous observations
287 (21) confirming the ability of *Planktothrix* to form dense layers in the thermocline and
288 eventually being responsible for a steep oxygen gradient within their layer (Fig. 5 C).
289 The three different methods for both, filament density and cumulative length
290 determination behaved similarly and no statistical difference was observed, with the
291 exception of one measurement with the Utermöhl approach at the depth of 20 m,
292 right below the maximal filament concentration. Statistical analysis to compare the
293 methods was performed by of linear regression. Automated and manual filament
294 measurement on images showed high correlation for both, filament numbers (r^2 =
295 1.000, $P < 0.0001$) and cumulative filament length (r^2 = 1.000, $P < 0.0001$). In the
296 four replicate preparations the manual measurement yielded coefficients of variations
297 of 0.07 for number and 0.08 for cumulative length, whereas the CVs of the
298 automated method were 0.10 and 0.11, respectively.

299 The comparison of the automated method and the Utermöhl approach after exclusion
300 of the data point from 20 m depth also yielded a high correlation for filament number
301 (r^2 = 0.9995, P < 0.0001) and cumulative length (r^2 = 0.9998, P < 0.0001).
302
303
304

Discussion

We present a model based, object oriented image analysis approach for the detection and sizing of individual filamentous cyanobacteria on fluorescence microscopic images. A central problem in the context of measuring filament length distributions emerges from the enormous length of filaments, both in terms of absolute size as well as in length variation within a sample. The determination of the length of a single filament is possible only if that particular filament lies completely within the observed field of view (FOV). The probability of a filament being partially out of a FOV is a function of filament length and FOV size, as shown by Monte Carlo simulation (Fig. 1 B). This result implies that large FOV areas need to be observed (approx. one cm^2 for *Planktothrix rubescens*) in order to avoid an underestimation of the mean filament length. This can be realized by stitching single FOVs to large composite images as described in this study. The processing of such large images requires a powerful computer, preferably deployed with a 64 bit operation system and 4 GB RAM. Still, even in such large images, only approx. 75% of 2000 µm filaments are correctly represented. Thus it might be advisable to apply a mathematical correction when measuring filament length distributions in detail, based on the here shown simulation results.

Filamentous organisms are difficult to analyze by conventional image processing, as they overlap frequently (Fig 1 A). The extent of overlap events on an image can be predicted as a function of filament length and filament density, as shown in a comparison of a computational simulation with actual frequencies of overlaps. Overlap events may be decreased by reducing the filament density, but on the cost of analyzing lower numbers of individuals per sample, thus reducing the significance of the measurement. For reliable quantification, and particularly if the mean length or the length distribution of filaments is of interest, a large amount of individuals have to be measured and overlapping cannot be avoided. Overlapping objects cannot be correctly handled by conventional image analysis and therefore, we decided for a model based, object oriented image analysis approach, explicitly designed for the purpose of analyzing non-branched, overlapping filaments. It does not primarily detect individual filaments as a whole, but small elements of filaments (fixels). These are then iteratively assembled to reconstruct entire filaments by applying a probabilistic model (i.e. they are linked with their most likely neighbours). Our method

is robust to several critical issues related to detection of filaments by image analysis, such as patchy fluorescent signals (1) or the frequently observed shifting artefacts when stitching individual FOVs into a large composite image (Fig. 2 C).

The automated image analysis method was compared to the ‘gold standard’, i.e. manual filament tracing on images by experienced researchers. Comparing the results of manual analysis by four individuals showed that there were only small variations between evaluations, both in filament counts and in cumulative length measurements. Despite its accuracy and robustness to artefacts, the manual method is highly time consuming and tedious (i.e. several hours per composite image).

A faster approach based on manual image analysis, but limited to retrieve the cumulative length only, is given by the line-intercept method (15). Although this method has the potential to be performed in a fully automated manner, it was less precise than our automated method if compared to manual measurements (Fig. 4 A). This may be due to the fact that the line-intercept method is dependant on a homogenous random distribution of filaments on an image, as a consequence of the underlying statistical model. It is unclear whether this assumption on filtered preparations is legitimate, as filtration is prone to artefacts such as higher cell densities at the border zones of preparations. Notably, our method does not relay on a homogenous random distribution of filaments.

A comparison of our approach with the Utermöhl approach also showed a tight correlation. The only exception was the data point at 20 m depth (Fig. 5 A, B). *Planktothrix* filaments are able to produce gas vesicles (18) to adjust their buoyancy. The depth layer of 20 m is below the preferred depth of *Planktothrix* and possibly filaments in 20 m might try to increase their buoyancy to ascend to 15 m where the light conditions are more preferable. Filaments containing high amounts of gas vesicles may compromise the Utermöhl approach as it is based on sedimentation (O. Köster (WVZ), personal communication).

Besides this discrepancy it seems that the variation emerging from the sample preparation, as shown by four replicates from the water sample of 15 m, was much higher than the variation between manual and automated analysis by either approach. Still, also our automated method sometimes produces artefacts as summarized in Table 1 and Figure 2 E-G. They emerge from either wrong assembly of fixels or the detection of image artefacts such as air bubbles. On the internal validation set, 86% of the overlap events and 55% of the parallel running filaments

were handled correctly. These rates could be increased by further optimization of the program code (e.g. fine adjustment of the probability weighting for fixel assembly). However, as the program produces annotated output images, possible artefacts are readily identifiable.

Finally, the automated image analysis is significantly faster than manual image analysis. While the manual tracing of filaments on a 15000 × 15000 px image takes up to several hours, depending on the filament density, the automated analysis is performed within a few minutes.

Altogether, we described a fast, accurate and revisable method for the high-throughput quantification of filamentous cyanobacteria by fluorescence microscopy and image analysis. The easy to use program is freely available and may be useful in basic research as well as in monitoring applications.

Acknowledgments

The authors thank Judith Blom, Oliver Köster, Rainer Kurmayer, Thomas Posch and Ferdinand Schanz for valuable comments, and Angela Mechsner for additional manual filament measurement. S. van den Wyngaert was supported by the project SNF 31003A-11765. The water supply company of Zurich (WVZ) is highly acknowledged for the joint sampling and the provision of data. The first author wishes to thank Anthony Walsby for the introduction into image analysis and the motivation for working on *Planktothrix* quantification.

References

1. **Almesjo, L., and C. Rolff.** 2007. Automated measurements of filamentous cyanobacteria by digital image analysis. Limnology and Oceanography-Methods **5:**217-224.
2. **Blackburn, N., A. Hagstrom, J. Wikner, R. Cuadros-Hansson, and P. K. Bjornsen.** 1998. Rapid determination of bacterial abundance, biovolume, morphology, and growth by neural network-based image analysis. Applied and Environmental Microbiology **64:**3246-3255.
3. **Blom, J. F., B. Bister, D. Bischoff, G. Nicholson, G. Jung, R. D. Sussmuth, and F. Juttner.** 2003. Oscillapeptin J, a new grazer toxin of the freshwater cyanobacterium Planktothrix rubescens. Journal of Natural Products **66:**431-434.
4. **Blom, J. F., J. A. Robinson, and F. Juttner.** 2001. High grazer toxicity of [D-Asp(3) (E)-Dhb(7)]microcystin-RR of Planktothrix rubescens as compared to different microcystins. Toxicon **39:**1923-1932.
5. **Chorus, I., I. R. Falconer, H. J. Salas, and J. Bartram.** 2000. Health risks caused by freshwater cyanobacteria in recreational waters. Journal of Toxicology and Environmental Health-Part B-Critical Reviews **3:**323-347.
6. **Daims, H., and M. Wagner.** 2007. Quantification of uncultured microorganisms by fluorescence microscopy and digital image analysis. Applied Microbiology and Biotechnology **75:**237-248.
7. **Davis, P., J. Beard, and A. Walsby.** 2003. Variation in filament width and gas vesicles of red and green isolates of Planktothrix spp. Archiv für Hydrobiologie, Supplementband, Algological studies **146**.
8. **Ernst, B., B. Hitzfeld, and D. Dietrich.** 2001. Presence of Planktothrix sp and cyanobacterial toxins in Lake Ammersee, Germany and their impact on whitefish (Coregonus lavaretus L.). Environmental Toxicology **16:**483-488.
9. **Ernst, B., S. J. Hoeger, E. O'Brien, and D. R. Dietrich.** 2009. Abundance and toxicity of Planktothrix rubescens in the pre-alpine Lake Ammersee, Germany. Harmful Algae **8:**329-342.
10. **Ernst, B., S. Neser, E. O'Brien, S. J. Hoeger, and D. R. Dietrich.** 2006. Determination of the filamentous cyanobacteria Planktothrix rubescens in environmental water samples using an image processing system. Harmful Algae **5:**281-289.
11. **Fastner, J., M. Erhard, W. W. Carmichael, F. Sun, K. L. Rinehart, H. Ronicke, and I. Chorus.** 1999. Characterization and diversity of microcystins in natural blooms and strains of the genera Microcystis and Planktothrix from German freshwaters. Archiv Fur Hydrobiologie **145:**147-163.
12. **Fastner, J., U. Neumann, B. Wirsing, J. Weckesser, C. Wiedner, B. Nixdorf, and I. Chorus.** 1999. Microcystins (hepatotoxic heptapeptides) in German fresh water bodies. Environmental Toxicology **14:**13-22.
13. **Hoeger, S. J., B. C. Hitzfeld, and D. R. Dietrich.** 2005. Occurrence and elimination of cyanobacterial toxins in drinking water treatment plants. Toxicology and Applied Pharmacology **203:**231-242.
14. **Kurmayer, R., and M. Gumpenberger.** 2006. Diversity of microcystin genotypes among populations of the filamentous cyanobacteria Planktothrix rubescens and Planktothrix agardhii. Molecular Ecology **15:**3849-3861.

15. **Nedoma, J., J. Vrba, T. Hanzl, and L. Nedbalova.** 2001. Quantification of pelagic filamentous microorganisms in aquatic environments using the line-intercept method. Fems Microbiology Ecology **38:**81-85.
16. **Olson, F.** 1950. Quantitative Estimates of Filamentous Algae. Transactions of the American Microscopical Society **69**.
17. **Pernthaler, J., A. Pernthaler, and R. Amann.** 2003. Automated enumeration of groups of marine picoplankton after fluorescence in situ hybridization. Applied and Environmental Microbiology **69:**2631-2637.
18. **Walsby, A. E.** 1994. Gas Vesicles. Microbiological Reviews **58:**94-144.
19. **Walsby, A. E., and A. Avery.** 1996. Measurement of filamentous cyanobacteria by image analysis. Journal of Microbiological Methods **26:**11-20.
20. **Walsby, A. E., A. Avery, and F. Schanz.** 1998. The critical pressures of gas vesicles in Planktothrix rubescens in relation to the depth of winter mixing in Lake Zurich, Switzerland. Journal of Plankton Research **20:**1357-1375.
21. **Walsby, A. E., and F. Schanz.** 2002. Light-dependent growth rate determines changes in the population of Planktothrix rubescens over the annual cycle in Lake Zurich, Switzerland. New Phytologist **154:**671-687.

Legends to Figures and Tables

Table 1

Data on the internal validation set of 7 images. Manual and automated counts are given and typical issues such as overlaps, parallel filaments, air bubbles and filament breaks on images were quantified. The number before the dash indicates the count of incorrectly handled events, the number behind the dash resembles the total amount.

Figure 1

Monte Carlo simulation: A: The number of intersections of filaments was simulated as a function of the filament density (filaments cm^{-2}) on a field of view (FOV) and the filament length. B: The proportion of filaments of a given length being entirely within a FOV of a given length was simulated. As an example, on a one cm^2 FOV, approx. 75% of the 2 mm long filaments are expected to be entirely within the FOV.

Figure 2

Sections from typical fluorescent microscopic images of *Planktothrix rubescens*. The left column depicts the original image, the right column shows the annotated image automatically produced by the program for validation purposes. Detected filaments are shown as coloured overlay and are enumerated. Detected fixels appear as gray squares, end-fixels as red squares, respectively. A: A typical short filament that was correctly recognized. B: A filament exhibiting a patchy fluorescent signal. C: Two crossing filaments that are correctly recognized. Additionally a horizontal shift is visible, depicting a stitching artefact. D: Two parallel filaments. E: Two parallel filaments crossed by a third filament. The filaments were wrongly assembled by the program. F: Two crossing filaments, whereas one filament exhibits a break, depicting an artefact of the method. G: A filament laying in close proximity to an air bubble. The air bubble is recognized as a filament by the program.

Figure 3

Concept of the program illustrated on a sample image section. A: The image is processed by a circular kernel to detect filamentous structures (fixel) by applying three brightness thresholds. B: Possible fixels are checked for featuring high gray level intensity on the filament and low gray level intensity on their sides. A cross like structure (red and blue line) is rotated on the location and gray level profiles are measured. C: The orientation of a fixel is determined by comparing orthogonal gray level profiles. D: Once a fixel is set, its area is locked in order not to set other fixels within. E: All possible orientations a fixel may feature. F: Detected fixels on two crossing filaments. G: Filament assembly based on allocating possible neighbours to each fixel. Defined criteria have to be met. In this example, possible neighbours for fixel #1 evaluated. #2 - #8 are in range but #8 is outside the 90° angle of both ends of #1. #6 and #7 differ too much in their orientation from #1. #2 - #5 are thus the only valid neighbours. The best neighbours on both ends are #2 and #4 as they are closest. H: Assembled fixels.

Figure 4

Comparison of the different methods on the internal validation set of 7 images. A: Measurement of cumulative filament length by manual filament tracing, the automated method and the line-intercept method. Lines on the bars of the manual measurement depict the standard deviation of four replicates. B: Filament numbers were quantified by manual counting and by the automated method. Lines on the bars of the manual measurement depict the standard deviation of four replicates. C: Hundred selected filaments of different length from the 7 images were individually measured manually and automated. A linear regression was calculated.

Figure 5

Comparison of different methods (automated, manual filament tracing and the Utermöhl method) for the evaluation of samples from a depth profile on Lake Zürich on the 9. July 2008. A: Filament abundance along the depth profile. B: Measurement of the cumulative length along the depth profile. The lines on the bars for automated and manual measurements at the depth of 15 m depict the standard deviations from four experimental replicates. On panel A and B, the depths are not originally scaled

in contrast to panel C but as categories for better visibility of the bars. C: The cumulative length (gray area) along the depth gradient is shown in context of the parameters temperature and oxygen.

Figures and tables

Table 1

Image	Human counts	Automated counts	Overlaps & touching	Parallel filaments	Air bubbles	Premature breaks
1	25.8 ± 1.5	27	1/5	0/0	1	0
2	18.5 ± 0.5	23	1/3	0/0	3	2
3	27.5 ± 1.5	27	0/1	0/1	0	0
4	44.0 ± 0.0	44	1/10	2/3	0	0
5	36.8 ± 0.4	40	3/8	1/3	0	2
6	21.8 ± 0.4	21	0/2	1/1	0	0
7	17.5 ± 1.1	18	0/5	1/2	0	1
Total	191.8 ± 3.6	200	6/44	5/11	4	5

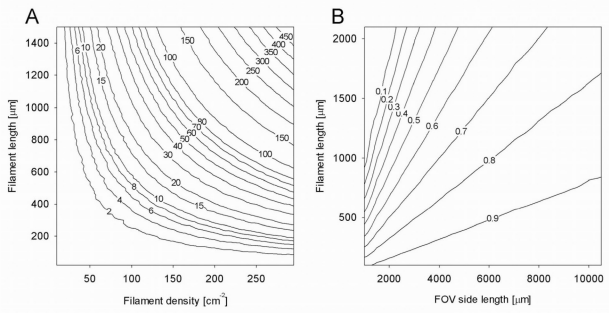

Figure 1

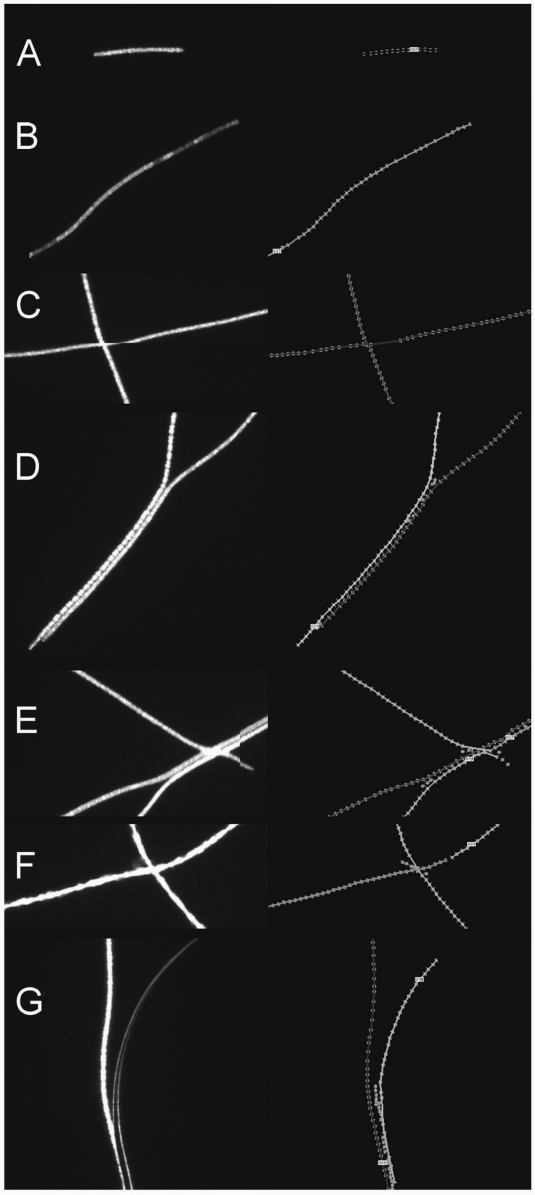

Figure 2

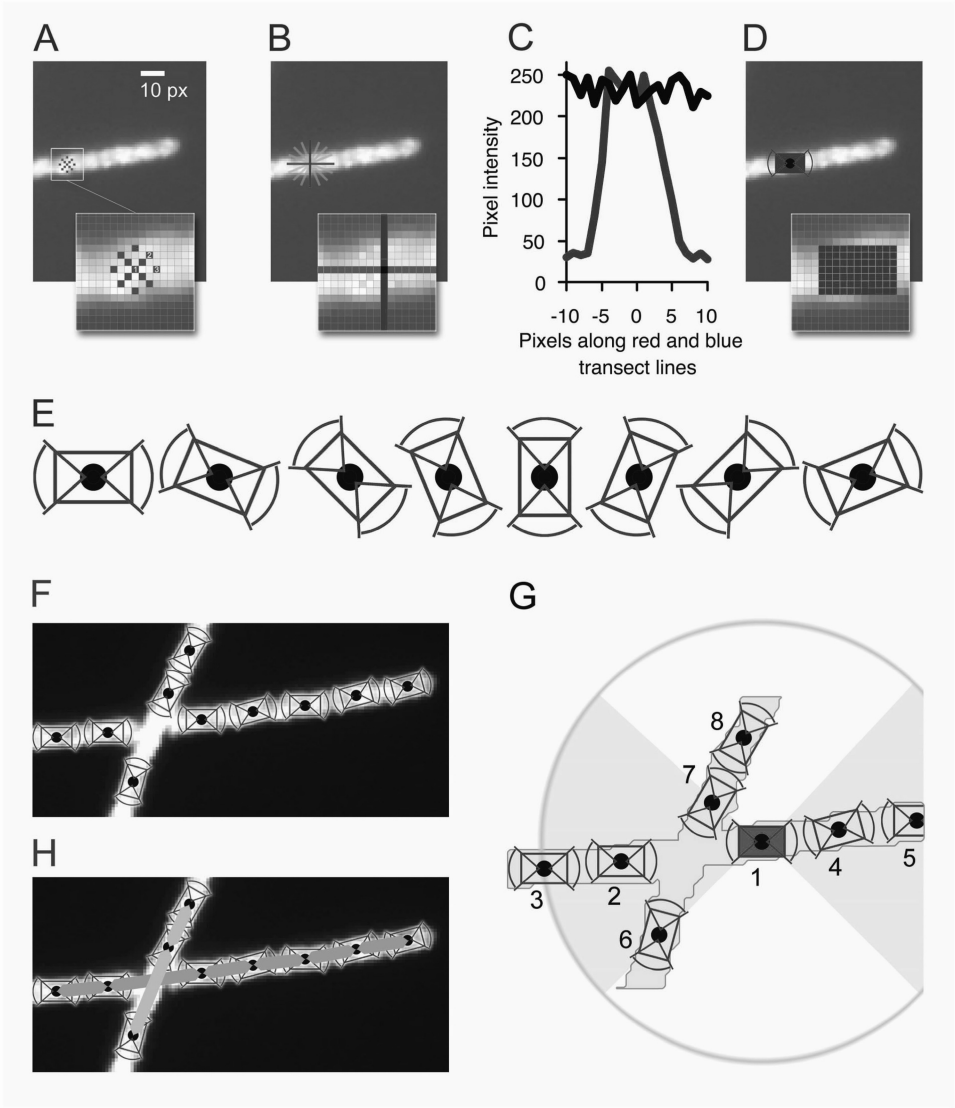
A
10 px
B
C
250
200
150
100
50
0
Pixel intensity
-10 -5 0 5 10
Pixels along red and blue
transect lines
D
E
F
G
8
7
1
4
5
3
2
6
H

Figure 3

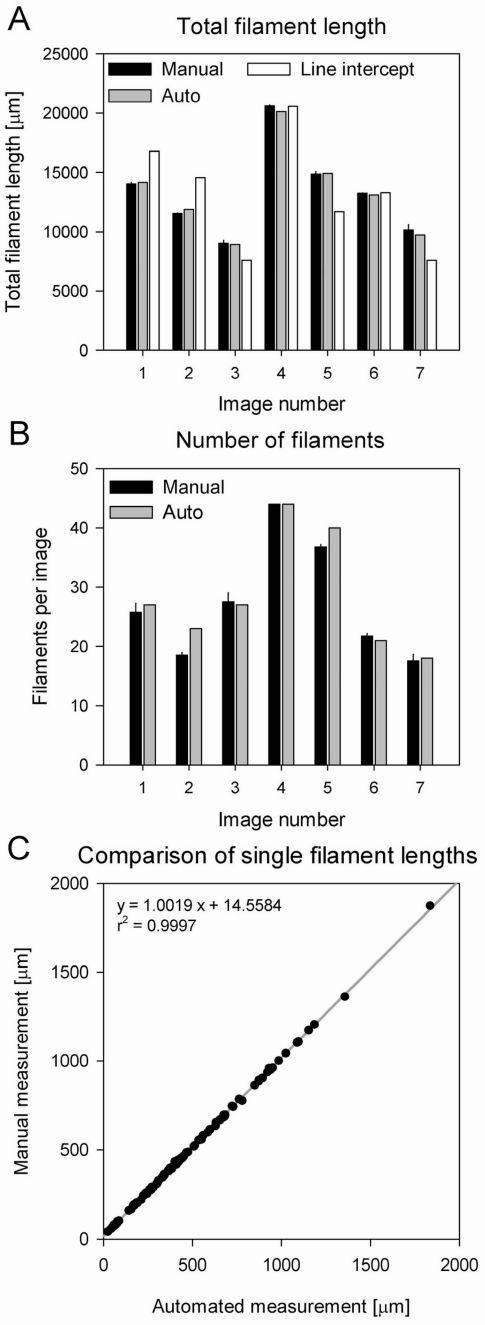
A
Total filament length
Manual
Line intercept
Auto
Total filament length [µm]
25000
20000
15000
10000
5000
0
1
2
3
4
5
6
7
Image number
B
Number of filaments
Manual
Auto
Filaments per image
50
40
30
20
10
0
1
2
3
4
5
6
7
Image number
C
Comparison of single filament lengths
y = 1.0019 x + 14.5584
r2 = 0.9997
Manual measurement [µm]
2000
1500
1000
500
0
0
500
1000
1500
2000
Automated measurement [µm]

Figure 4

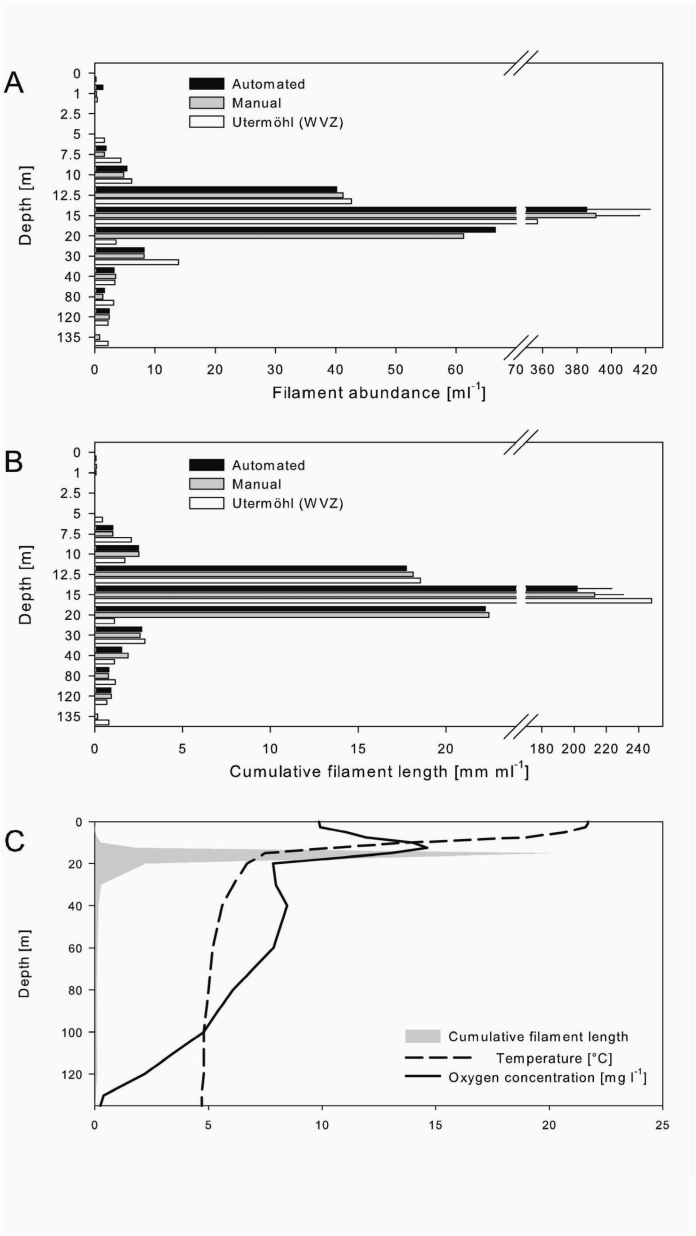
A
Automated
Manual
Utermöhl (WVZ)
Depth [m]
0
1
2.5
5
7.5
10
12.5
15
20
30
40
80
120
135
0 10 20 30 40 50 60 70 360 380 400 420
Filament abundance [ml-1]
B
Automated
Manual
Utermöhl (WVZ)
Depth [m]
0 5 10 15 20 180 200 220 240
Cumulative filament length [mm ml-1]
C
Depth [m]
0
20
40
60
80
100
120
0 5 10 15 20 25
Cumulative filament length
Temperature [°C]
Oxygen concentration [mg l-1]

Figure 5

7.4 Publication 5: A Small Population of Planktonic Flavobacteria *with Disproportionally high Growth during the Spring Phytoplankton Bloom in a Prealpine Lake.*

Environmental Microbiology (2009) doi:10.1111/j.1462-2920.2009.01994.x

A small population of planktonic *Flavobacteria* with disproportionally high growth during the spring phytoplankton bloom in a prealpine lake

Michael Zeder, Simone Peter, Tatiana Shabarova and Jakob Pernthaler*
Limnological Station Kilchberg, University of Zurich, Zurich, Switzerland.

Summary

Bacterioplankton growth in temperate Lake Zurich (Switzerland) was studied during the spring phytoplankton bloom by *in situ* techniques and short-term dilution bioassays. A peak of chlorophyll *a* (Chl *a*) concentrations was followed by a rise of bacterial cell numbers and leucine assimilation rates, of the proportions of cells incorporating 5-bromo-2-deoxyuridine (BrdU), and of community net growth rates in dilution cultures. Incorporation of BrdU was low in *Betaproteobacteria* (2 ± 1%), indicating that these bacteria did not incorporate the tracer. Pronounced growth of *Betaproteobacteria* in the enrichments was only observed after the decline of the phytoplankton bloom. An initial peak in the proportions of BrdU-positive *Actinobacteria* (30%) preceded a distinct rise of their cell numbers during the period of the Chl *a* maximum. *Cytophaga–Flavobacteria* (CF) changed little in numbers, but featured high proportions of BrdU-positive cells (28 ± 12%). Moreover, CF represented > 90% of all newly formed cells in dilution cultures before and during the phytoplankton bloom. One phylogenetic lineage of cultivable *Flavobacteria* (FLAV2) represented a small (0.5–1%) but highly active population in lake plankton. The growth rates of FLAV2 in dilution cultures doubled during the period of the Chl *a* maximum, indicating stimulation by phytoplankton exudates. Thus, CF, and specifically *Flavobacteria*, appeared to be substantially more important for carbon transfer in Lake Zurich spring bacterioplankton than was suggested by their standing stocks. The high *in situ* growth potential of these bacteria might have been counterbalanced by top-down control.

Received 15 November, 2008; accepted 4 June, 2009. *For correspondence. E-mail pernthaler@limnol.uzh.ch; Tel. (+41) 44 716 1210; Fax (+41) 44 716 1225.

Introduction

Phytoplankton communities in temperate lakes undergo predictable seasonal transitions (Sommer *et al.*, 1986). The first bloom of algal biomass during spring time is typically triggered by the interplay of increasing solar irradiation levels and the onset of thermal stratification (Bleiker and Schanz, 1997), and it is eventually terminated by the grazing pressure of herbivorous zooplankton. The primary algal colonizers of the spring water column (small diatoms and flagellates) share common ecophysiological features, i.e. they compensate for increasing predation by achieving high growth rates despite low ambient temperatures (Sommer, 1981).

The abundances and biomasses of heterotrophic bacterioplankton in lakes usually show less annual fluctuations than the phytoplankton. This is thought to be a consequence of the tight coupling between bacteria and their protistan consumers, or between bacteria and viral lysis respectively (Weinbauer, 2004; Pernthaler, 2005). Even so, bacterioplankton numbers increase during the spring period at least by a factor of two, typically with a small temporal delay to the primary producers (Simon *et al.*, 1998). Unlike the phytoplankton, the pelagic bacterial assemblages are typically not suppressed to their pre-bloom abundances during early summer, likely due to the complex cascading trophic interactions within aquatic food webs (Zöllner *et al.*, 2003).

Little is known about the ecological attributes of bacterial taxa that occur during the period of the spring phytoplankton maximum in temperate lakes. Cultivation-independent approaches allow for the quantitative analysis of the dynamics of freshwater bacterioplankton populations (Pernthaler *et al.*, 1998; Eiler and Bertilsson, 2007). However, a determination of changes in cell (or rRNA gene copy) numbers may not be sufficient to unambiguously identify those bacterial taxa that are most strongly favoured by ambient growth conditions. Both protistan grazing and viral lysis tend to disproportionally affect the most rapidly growing microbial populations

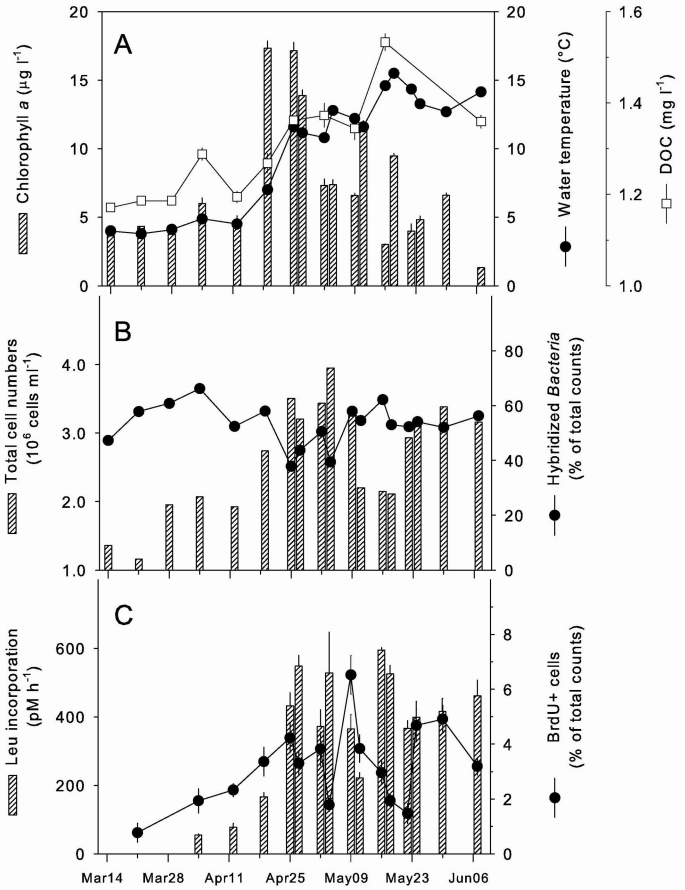

Fig. 1. A. Temperature, concentrations of chlorophyll *a* and dissolved organic carbon (DOC).
B. Total microbial cell number (DAPI staining) and fraction of hybridized *Bacteria* (probe EUB I-III).
C. Incorporation rates of [^{3}H]-leucine and proportions of BrdU-positive DAPI-stained microbial cells in Lake Zurich during the investigation period.
Error bars in this and all subsequent graphs represent one standard error of the mean values of triplicate determinations.

(Sherr *et al.*, 1992; Weinbauer, 2004). Thus, it is possible that small and/or apparently stable populations of highly active bacterial taxa might nevertheless be responsible for a considerable fraction of carbon transfer to higher trophic levels (Simek *et al.*, 2005).

Several strategies allow linking the changes in the standing stocks of bacterioplankton populations with their growth activity. For one, growing cells in lake water may be distinguished from inactive ones by pulse labelling techniques (Warnecke *et al.*, 2005; Salcher *et al.*, 2008). The typically short incubation times required to probe for particular activities allow evaluating physiological properties of populations at close to *in situ* conditions. Second, the *in situ* growth potential of microbes can also be assessed by short-term dilution cultures (Elser *et al.*, 1995). The reduction of predation mortality in these assays typically induces a profound shift of community composition: those genotypes are favoured that might be most proficient in utilizing the available resources but that are at the same time disproportionally affected by grazing (Beardsley *et al.*, 2003). Dilution enrichments can therefore provide valuable additional information about the growth strategies of different microbial taxa (Burkert *et al.*, 2003).

We investigated the dynamics and growth state of bacterioplankton taxa during the spring phytoplankton bloom in the mesotrophic Lake Zurich. Samples were collected at high temporal resolution to adequately map the development of physicochemical and biological parameters during this dynamic period of plankton succession. Microbial growth was assayed by the two complementary approaches outlined above. In addition, the *in situ* population dynamics and growth potential of cultivable bacteria from a readily enriched phylogenetic group were assessed.

Results

Physicochemical changes during phytoplankton bloom

Water temperatures at the sampling depth (2.5 m) rose from 3.3 to 15.5°C during the study period (Fig. 1A). A

distinct spring phytoplankton bloom was observed in the epilimnion of Lake Zurich during the second half of April 2006 (Fig. 1A). Chlorophyll *a* (Chl *a*) concentrations in 2.5 m depth ranged between 3.7 and 17.3 $\mu g\ l^{-1}$, with maximal values between 19 and 27 April. The algal community during that period was dominated by phytoflagellates (*Rhodomonas* sp., *Cryptomonas* sp., *Erkenia* sp.) and diatoms (*Cyclotella* sp., *Asterionella* sp.), and a pronounced maximum of the mixotrophic flagellate *Dinobryon* sp. (> 3000 ml^{-1}) was observed at the beginning of May. In parallel, the concentrations of dissolved phosphorus dropped from 10 to 4 $\mu g\ l^{-1}$ during April (source: water monitoring programme of Water Supply Zurich). The concentrations of dissolved organic carbon (DOC) increased during and after the bloom, from 1.2 $mg\ l^{-1}$ in the pre-bloom period to 1.5 $mg\ l^{-1}$ thereafter (Fig. 1A). Dissolved organic carbon on average represented 72% (± 9%) of total organic carbon (TOC), and the lowest DOC : TOC ratios (0.53–0.59) were observed during peak values of Chl *a*. Oxygen saturation followed the development of Chl *a*, ranging from 90% to 150% (data not shown).

Bacterial abundance and bulk activity

Total microbial cell numbers ranged between 1.5 and 2.0×10^6 cells ml^{-1} prior to the peak of Chl *a* concentrations, and reached approximately twice these values thereafter (Fig. 1B). An intermediate drop of total cell counts was observed for a 1-week period in mid-May. The incorporation rates of radiolabelled leucine increased by approximately one order of magnitude over the study period (Fig. 1C). The temporal pattern of leucine incorporation rates closely reflected the changes in cell abundances during the actual phytoplankton bloom period (4 April–11 May, linear regression, $r^2 = 0.80$, $n = 9$), whereas the two parameters were clearly uncoupled during the subsequent minimum of cell numbers.

The proportions of 5-bromo-2-deoxyuridine (BrdU)-incorporating [BrdU-positive (BrdU+)] cells (Fig. 1C) were determined from three parallel incubations per sampling time point and from five separate preparations per incubation. Only a small fraction of total (DAPI-stained) cells visibly incorporated BrdU into their DNA, corresponding to a range of $0.1–2.3 \times 10^5$ BrdU+ cells ml^{-1} (mean, 1.0×10^5 cells ml^{-1}). The fractions and total numbers of BrdU+ cells steadily increased until the peak of Chl *a* concentrations but became distinctly more variable thereafter. While this general pattern was also observed for total abundances and leucine incorporation rates, no significant correlation was observed between either parameter and the proportions of BrdU+ cells over the course of the investigation.

Contribution of phylogenetic groups to total and BrdU+ cells

On average, only 53% of DAPI-stained cells could be detected by fluorescence *in situ* hybridization (FISH) in combination with catalysed reporter deposition (CARD) and using a probe targeted to *Bacteria* (Fig. 1B). The sum of the three studied groups represented 68% (± 8%) of all hybridized *Bacteria* at four consecutive sampling time points during the decline of the phytoplankton bloom (25 April–4 May), but only 33% (± 14%) of *Bacteria* before and after this period. *Betaproteobacteria* accounted for 3% (7 June) to 11% (16 May) of cell counts (i.e. 6–22% of hybridized *Bacteria*). Slightly higher relative proportions and abundances of *Betaproteobacteria* were observed during and after the phytoplankton bloom (Fig. 2). Microbes affiliated with the *Cytophaga–Flavobacteria* lineage (CF) of *Bacteroidetes* showed a trend similar to

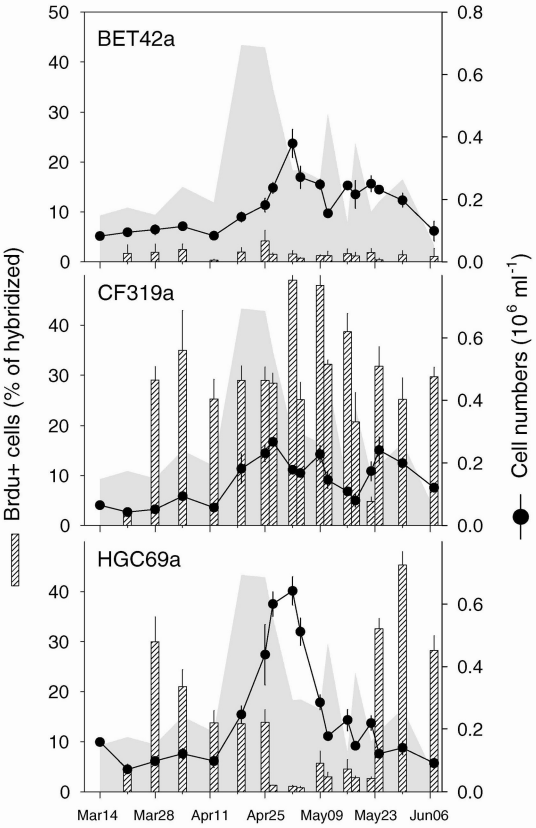

Fig. 2. Cell numbers and proportions of BrdU-positive *Betaproteobacteria* (probe BET42a), *Cytophaga–Flavobacteria* (probe CF319a) and *Actinobacteria* (probe HGC69a) during the spring phytoplankton bloom period 2006. Chlorophyll *a* concentrations (from Fig. 1A, shaded area) are depicted for reference.

Betaproteobacteria in terms of both relative proportions and absolute counts (Fig. 2). In contrast, a distinct peak of actinobacterial abundances was observed that followed the period of the Chl *a* maximum with a delay of 1 week (Fig. 2). During that period *Actinobacteria* represented > 40% of all hybridized *Bacteria* (*c.* 20% of total cell counts), whereas they reached approximately half this value at the other sampling time points.

Bacteria hybridized by the three probes represented 62% (± 18%) of all BrdU+ cells, and the combined contribution of the three groups to active cells was significantly higher than to all hybridized *Bacteria* (paired Student's *t*-test, $P < 0.05$). This was mainly due to microbes affiliated with CF and *Actinobacteria* (Fig. 2), whereas only low fractions of *Betaproteobacteria* were found to incorporate the halogenated compound into their DNA (Fig. 2). Remarkable temporal dynamics of the fractions of BrdU+ actinobacterial cells were observed: two maxima of 30% and > 40% of active cells at the beginning and ending of the investigation period could be distinguished. In contrast, only a minor fraction of *Actinobacteria* visibly incorporated BrdU for a period of 4 weeks following the phytoplankton bloom period. CF hybridized by probe CF319a on average featured significantly higher proportions of BrdU+ cells than the other two studied groups over the study period (one-way ANOVA, $P < 0.05$). The highest fractions of active cells within this lineage (approximately 50%) were found in the immediate aftermath of the phytoplankton bloom period (Fig. 2).

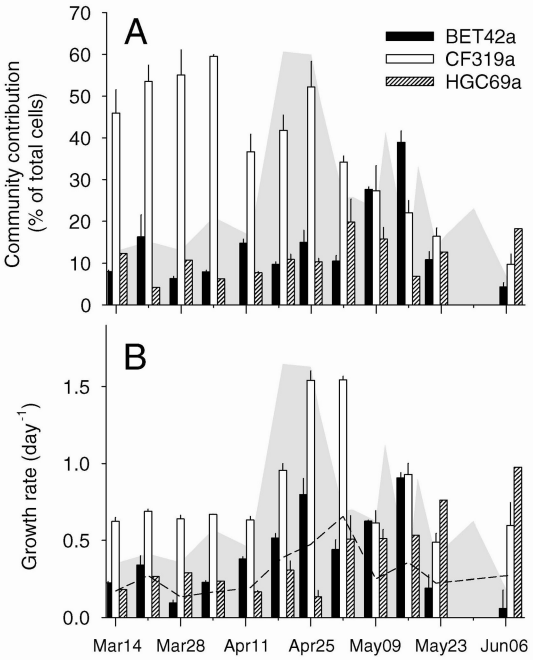

Fig. 3. A. Proportions of *Betaproteobacteria* (probe BET42a), *Cytophaga–Flavobacteria* (probe CF319a) and *Actinobacteria* (probe HGC69a) in weekly dilution bioassay after approximately one doubling of total cell numbers.
B. Estimated growth rates of the three groups in the enrichments, as compared with the overall community growth rate (broken line). Chlorophyll *a* concentrations (shaded area) are depicted for reference.

Dilution enrichments

Bacteria targeted by the three FISH probes on average represented 63% (range, 32–74%) of all DAPI-stained cells after 48–120 h of enrichment, or > 90% of hybridized *Bacteria*. The average enrichment factors of CF, *Betaproteobacteria* and *Actinobacteria* over the whole investigation period (i.e. the ratio between their abundances at the beginning and ending of the dilution enrichments) were 26 (range, 5–81), 6 (2–11) and 4 (2–11) respectively. During the first month of the investigation CF represented approximately half of the microbial assemblage at the end-points of the dilution cultures or 90% of all newly formed cells (Fig. 3A). Their relative abundances in the enriched assemblages remained high until the onset of the phytoplankton bloom and continuously decreased thereafter; to about twice the proportions of CF in environmental samples on the last sampling date. *Betaproteobacteria* were not conspicuously enriched before and during the period of the Chl *a* maximum or at the end of the investigation period. However, these bacteria represented 50–80% of the newly formed cells (30–40% of final abundances) in two subsequent dilution bioassays in May. *Actinobacteria* never formed more than 20% of cells in the enrichments.

The lowest overall growth rates of the experimental assemblage in the dilution cultures were observed prior to the phytoplankton bloom at water temperatures < 5°C (Figs 1 and 3B). However, the community growth rates were not linearly related to the continuous increase in temperature, but rather peaked during and after the Chl *a* maximum. This was paralleled by a distinct maximum of the growth rates of CF between 25 April and 3 May (Fig. 3B). The growth of CF was significantly more rapid than the community average also at all other sampling time points. *Betaproteobacteria* exhibited the highest growth rates between mid-April and mid-May, whereas *Actinobacteria* significantly exceeded the average community growth in the dilution cultures only at the end of the investigation period.

No differences in the proportions of bacteria hybridized with probe CF319a were observed after 48 h of incubation of unmanipulated lake water performed in spring 2007 (initial and final concentrations: 7–8% of DAPI-stained cells). In contrast, CF319a-positive cells almost doubled

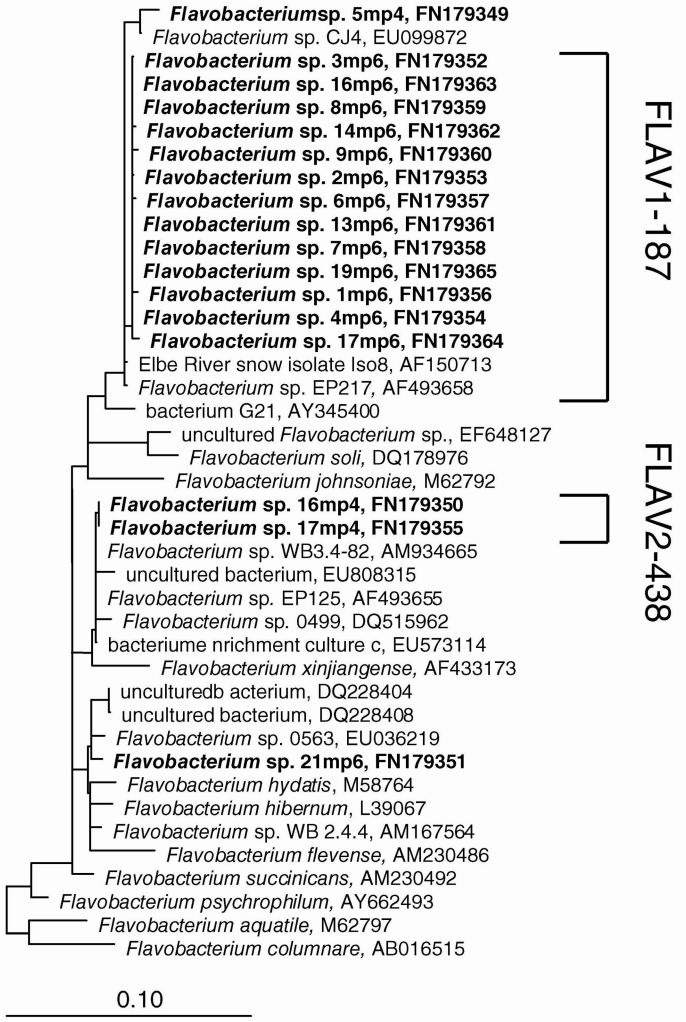

Fig. 4. Phylogenetic affiliation of flavobacterial isolates obtained from dilution enrichments in spring 2007 (in bold face). The depicted tree is based on Maximum Likelihood (ML) analysis of 650 flavobacterial sequences, and multifurcations indicating discrepancies between ML and other analyses (Maximum Parsimony, Neighbour Joining). Brackets indicate sequence types targeted by probes FLAV1-187 and FLAV2-438 respectively.

(to 14%) in 1:10 dilutions with 0.1 μm pre-filtered water. The total bacterial cell numbers in the unmanipulated samples increased by < 20% over the incubation period, whereas they changed by more than twofold in the dilution treatment.

Bacterial isolates, design of new FISH probes

Twenty of 86 obtained isolates were affiliated with the *Flavobacteria*. These strains could be clustered into three separate phylogenetic lineages (Fig. 4). The first lineage harboured a set of almost identical sequence types and one strain (5mp4) with only 98% sequence identity with the other isolates. The second group was formed by two isolates (strains 16mp4, 17mp4) which only differed by one base position and that formed a monophyletic lineage together with a psychrophilic strain and with isolates from riverine biofilms (99% sequence identity). One isolate (21mp6) could not clearly be grouped with a specific sequence type. It displayed around 97% of sequence similarity to the other strains. Specific FISH probes were designed for two phylogenetic clades of *Flavobacteria* that harboured isolates and tested on pure cultures from these groups. Probe FLAV1-187 (5′-AAT AAT CTA CTC ATG CGA AT-3′) detects the set of highly similar sequences from the FLAV1 clade as well as two isolates from riverine aggregates or biofilms. Probe FLAV2-438 (5′-GAA CTG TTT CTT CCT GTA CAA-3′) is targeted to the two isolates 16mp4 and 17mp4. Stringent hybridization conditions for CARD-FISH according to the protocol by Pernthaler and colleagues (2004) were obtained at 50% and 45% of

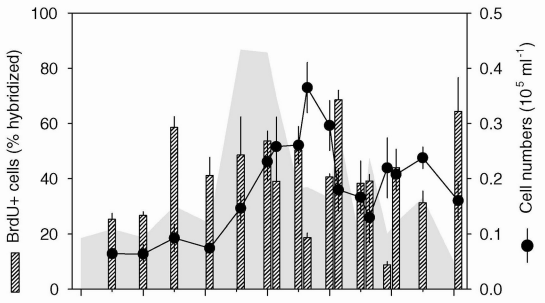

Fig. 5. Cell numbers and proportions of BrdU-positive cells of *Flavobacteria* targeted by probe FLAV2-438 in Lake Zurich during the spring phytoplankton bloom period 2006.

formamide in the hybridization buffer for probes FLAV1-187 and FLAV2-438 respectively.

FLAV1 and FLAV2 bacteria in environmental samples and enrichments

The concentrations of bacteria targeted by probe FLAV1 were below the detection limit by our FISH quantification technique at all sampling time points both in the environmental samples and in the dilution cultures (< 0.25% of total counts, data not shown). Cells detected by probe FLAV2-438 represented a small but quantifiable population in Lake Zurich (0.7 ± 0.1% of total counts). The cell numbers of FLAV2 bacteria varied by a factor of approximately 6 over the study period, and a distinct maximum of this population was observed subsequent to the phytoplankton bloom (Fig. 5). Typically, high proportions of FLAV2 bacteria were found to incorporated BrdU (mean 41%, range 9–69%), at instances even exceeding the fractions of BrdU+ cells within the CF lineage.

Bacteria hybridized by probe FLAV2-438 produced substantial populations in the dilution cultures, in particular at the first two sampling time points and in the period of the Chl *a* maximum (19 and 25 April) (Fig. 6). During the phytoplankton bloom FLAV2 bacteria enriched by a factor of > 100 within 48 h and represented > 40% of all newly formed cells (> 50% of newly formed CF). The growth rates of FLAV2 bacteria in the dilution cultures always exceeded the community average by a factor of 4–6. Moreover, these bacteria approximately doubled their growth rates during and immediately after the phytoplankton bloom in comparison with the rest of the study period (Fig. 6).

Discussion

Community level activity

The proportions of hybridized *Bacteria* in all DAPI stained cells were rather low (Fig. 1B), as has also been reported from other lakes (Allgaier and Grossart, 2006). This suggests either that a large fraction of DAPI-stained objects from the pelagic zone of Lake Zurich were not viable or of non-bacterial origin (Zweifel and Hagström, 1995) or that some microbes were not targeted by the FISH probe EUB I-III. The presence of non-viable cells or cell fragments would imply that the low fractions of BrdU+ cells of all DAPI-stainable objects (Fig. 1C) might in fact have underestimated the real proportion of growing cells in the microbial assemblages. In any case, the method probably only detects microbial growth above a certain threshold (Pernthaler and Pernthaler, 2005), as is the case for similar approaches (Sherr *et al.*, 1999). In addition, some bacteria might not be able to incorporate BrdU at all (Urbach *et al.*, 1999). Thus, while cells without BrdU incorporation generally should not be regarded as dead or dormant, many of them likely grow substantially more slowly than BrdU+ bacteria. A small subset of highly active cells within a generally slowly growing microbial assemblage would also agree with the low overall community growth rate estimates observed in the dilution bioassays (on average 0.3 day^{-1}, Fig. 3).

Dilution culture bioassays are a traditional means of assessing the growth rates of planktonic algae (Landry and Hassett, 1982). High dilution reduces microconsumer grazing and permits a closer determination of bacterial gross growth rates (Elser *et al.*, 1995). Moreover, dilution cultures provide a means of growing microbes under the substrate and nutrient concentrations of the original samples for several generations (Sterner, 1994) without introducing unintended bottom-up limitations (Posch *et al.*, 2007). Ambient substrate concentrations might in fact also be artificially augmented in dilution treatments, e.g. by the destruction of phytoplankton cells during filtration and/or preparation of the diluent (Ferguson *et al.*, 1984). However, particle removal by tangential flow filtration does not measurably increase the ambient

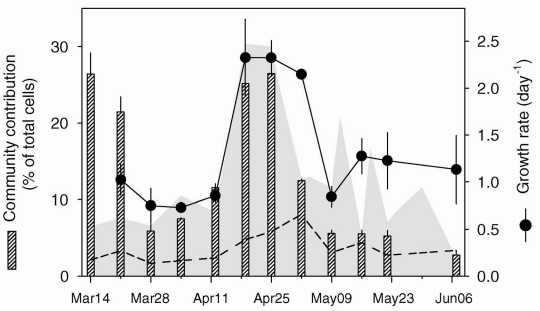

Fig. 6. Proportions of FLAV2 bacteria and estimated growth rates in dilution bioassays. Chlorophyll *a* concentrations (shaded area) and the average community growth rate (broken line) are depicted for reference.

concentrations of dissolved assimilable organic carbon in lake water filtrates (Jüttner *et al*., 1997).

Growth behaviour of different phylogenetic groups

The low fractions of BrdU+ cells in *Betaproteobacteria* appear to suggest that these bacteria reproduced more slowly than the two other studied groups (Fig. 2). In view of their increasing abundances in lake water (Fig. 2) and their high growth rates during the later phase of the experimental incubations (Fig. 3), it is more likely that some freshwater *Betaproteobacteria* might not be able to assimilate BrdU. In contrast, the high fractions of BrdU incorporating cells within *Actinobacteria* and CF (Fig. 2) constitute plausible evidence for the autochthonous growth of these bacterial groups in lake water (Warnecke *et al*., 2005).

Some members of the CF lineage in freshwater plankton appear to readily respond to changes in growth conditions (Simek *et al*., 2005; Salcher *et al*., 2007; Bertoni *et al*., 2008). Thus, the observation of high CF growth rates in our dilution cultures by itself does not represent unambiguous evidence that these bacteria were also active in the environment. However, at the same time high fractions of BrdU+ CF cells were also present *in situ* (Figs 2 and 3). In view of these complementary lines of evidence we may conclude that some genotypes affiliated with CF were a highly active component of the spring bacterioplankton assemblage. While CF have been associated with phytoplankton blooms in marine habitats before (Simon *et al*., 1999; Riemann *et al*., 2000), no evidence has so far been produced for a similar ecological function in freshwaters.

Actinobacteria differed from CF both in their temporal dynamics and growth behaviour (Figs 2 and 3). Maximal abundances of *Actinobacteria* during spring or early summer have also been reported from other lakes with different limnological characteristics (Allgaier and Grossart, 2006). Freshwater representatives of this lineage are substantially less sensitive to predation by bacterivorous protists than other bacteria (Hahn *et al*., 2003; Jezbera *et al*., 2006). This might explain why *Actinobacteria* featured such a pronounced increase in population size whereas the equally active CF did not. The bimodal patterns of BrdU incorporation (Fig. 2) and the inverse relationship between the fraction of BrdU+ cells and total actinobacterial abundances suggest a succession of different genotypes from the bloom to the post-bloom period. This hypothesis should be followed up in future investigations at higher phylogenetic resolution. Moreover, there was a striking contrast between the high proportions of BrdU+ *Actinobacteria* in lake water prior to the Chl *a* maximum and their apparent failure to grow in dilution bioassays. Thus, different activity assays may need to be combined in order to reach reliable ecophysiological conclusions, and the absence of evidence for growth by one particular approach may not automatically be evidence for non-growth. So far, enrichment of *Actinobacteria* after experimental manipulation of lake water has only been achieved at high protistan predation (Hornak *et al*., 2005; Simek *et al*., 2005).

Cultivable Flavobacteria in spring bacterioplankton

Flavobacteria are a rather poorly studied component of limnic bacterioplankton. Sequence types affiliated with *Flavobacteria* have been obtained from a variety of lakes with contrasting limnological characteristics during various seasons, including phytoplankton bloom events (Eiler and Bertilsson, 2007). High rRNA gene copy numbers of bacteria from this phylogenetic lineage were found in the spring and summer plankton of several eutrophic lakes during periods of high bacterial production (Eiler and Bertilsson, 2007), suggesting that *Flavobacteria* may be particularly successful if resources are plenty. In addition, many freshwater representatives of this lineage appear to be readily cultivable, e.g. more than 40 putative novel phylospecies of *Flavobacteria* have recently been isolated from a hardwater creek (Cousin *et al*., 2008).

In our study, the phylogenetic lineage that harboured most isolated strains of *Flavobacteria* (FLAV1, Fig. 4) could only be detected in extremely low numbers in environmental samples, and no enrichment of these bacteria was observed in dilution cultures. It is possible that members of FLAV1 isolated in 2007 were not present in the spring bacterioplankton in 2006. Alternatively, these bacteria may not be predominantly planktonic but rather originate from the particle-associated aquatic microflora. Strains that are phylogenetically closely related to our FLAV1 isolates (Fig. 4) have been obtained from riverine organic aggregates (Böckelmann *et al*., 2000) and river biofilms. So far, we have not investigated if bacteria from the FLAV1 lineage were also abundant on lake snow particles in Lake Zurich. The 16 isolates within the FLAV1 clade displayed high sequence identity between each other of approximately 99%. Interestingly, several strains featured base ambiguities in regions corresponding to bases 95, 455–478, 590–593 and 646–651 in *Escherichia coli* 16S rRNA numbering (Brosius *et al*., 1981). This is probably due to sequence variability between different rRNA operons that might be erroneously interpreted as microdiversity by cultivation-independent approaches.

In contrast, the presence of bacteria from the FLAV2 lineage with high proportions of BrdU+ cells (Fig. 5) suggests that these bacteria were an actively growing component of the spring bacterioplankton assemblage in Lake Zurich. Preliminary FISH analysis of samples from the two subsequent years moreover indicates that these bacteria

might in fact form annually recurrent population (J. Pernthaler, unpubl. data). The rapid enrichment of FLAV2 in dilution cultures (Fig. 6) illustrates that they were well adapted to grow in lake water at ambient substrate concentrations, i.e. that they could successfully pursue an entirely planktonic lifestyle.

The growth rates of FLAV2 bacteria in the dilution cultures were distinctly higher for the period of the phytoplankton maximum than during the rest of the study period (Fig. 6). This stimulation might be due to the short-term availability of specific algal exudates (Hama and Yanagi, 2001) that were particularly favourable for some members of FLAV2. The composition of labile organic substrates in lake water can be temporally highly variable, e.g. carbohydrates may be released in pulses that last for a few hours only (Meon and Juttner, 1999). The high growth rates of FLAV2 in the dilution cultures during and after the maximum of Chl *a* concentrations (Fig. 6) moreover appeared to mirror their population increase in the environment during that period (Fig. 5). However, the net increase in FLAV2 cell numbers during the period of the Chl *a* maximum (11 April to 3 May) was much smaller than suggested by their rapid growth in the bioassays. Following the logic of the dilution assay approach (Landry and Hassett, 1982) this discrepancy could be an indication for strong top-down control (Beardsley *et al*., 2003) of FLAV2 (e.g. by the abundant mixotrophic chrysophyte *Dinobryon*). Such an interpretation is also supported by the lack of growth of *Flavobacteriaceae* in incubations of unmanipulated lake water in spring 2007. Mixo- and heterotrophic flagellates are known to strongly affect bacterioplankton assemblages in temperate lakes during the spring period (Pernthaler *et al*., 1996; Comte *et al*., 2006). Size-selective grazing on FLAV2 (and CF in general) due to size (Simek and Chrzanowski, 1992) is indicated by their larger mean cell volumes (0.07 ± 0.014 and $0.071 \pm 0.027\ \mu m^3$ respectively), which significantly exceeded those of *Actinobacteria* ($0.041 \pm 0.011\ \mu m^3$) or of the total community ($0.044 \pm 0.007\ \mu m^3$) (one-way ANOVA, $P < 0.01$). In fact, a selective elimination of freshwater CF by flagellate predation has been previously demonstrated via direct analysis of protistan food vacuole content (Jezbera *et al*., 2006). Thus, the high growth rates of FLAV2 in dilution cultures during periods of stable *in situ* cell numbers (i.e. before and after the maximum of Chl *a*, Fig. 6) suggest that this bacterial population was turned over at least once per day by predation.

Experimental procedures

Sampling, physicochemical parameters, Chl a

Surface water samples were collected weekly from Lake Zurich (47°18′14″N, 8°34′14″E) from the middle of March to the beginning of June 2006 and twice a week during 4 weeks that represented the actual phytoplankton bloom period (25 April–24 May). Water was collected with a 5 l Friedinger water sampler at 2.5 m depth (the typical zone of the maximal algal densities during spring in Lake Zurich) and filled in 1 l glass bottles pre-washed with hydrochloric acid. Water temperature, conductivity and oxygen concentrations were monitored along a depth profile of the photic zone (0–20 m) with a multiparameter probe at the time of sampling (model 6600 *Yellow Springs* Instruments). Chlorophyll *a* concentrations were determined fluorometrically (model F-2000, Hitachi) after acetone extraction (Schanz, 1982). Total organic carbon was determined in triplicates from unfiltered water samples on a TOC 5000 analyser (Shimadzu). Dissolved organic carbon was measured following hollow fibre tangential flow filtration with a particle exclusion size of 0.1 (Hydac International). Subsamples (20 ml) for the analysis of total bacterial abundances and community composition were fixed for 1–24 h with buffered paraformaldehyde (PFA, final concentration, 2%).

Bulk incorporation of leucine

The uptake of tritiated leucine was determined starting on April 4 until the end of the study period. Five millilitres of samples were incubated in triplicates (plus one pre-fixed control) with [^{3}H]-leucine (Amersham, final concentration, 20 nM) for 2 h at *in situ* temperature in the dark. Incubations were stopped by addition of formaldehyde solution (2% final concentration). After 1 h of fixation the water was filtered on cellulose-ester filters (Sartorius, diameter, 25 mm, pore size, 0.22 μm). Filters were dissolved and macromolecules were extracted as described (Kirchman *et al*., 1985). After addition of scintillation cocktail (UltimaGold, Perkin-Elmer) the amount of assimilated radiolabelled substrate was estimated by scintillation counting (Tri-Carb 3170 TR, Perkin-Elmer). Measurements were corrected for quench (external standard method), and by subtraction of counts from the prefixed controls.

Total microbial abundances and community composition

Total bacterial abundances in lake water samples and in experimental enrichments were determined by epifluorescence microscopy after filtration of subsamples (2 ml) on black membrane filters and staining with 4′,6-diamidino-2-phenylindole (DAPI) (Porter and Feig, 1980). The proportions of different microbial taxa in lake water and dilution enrichments were determined by FISH with horseradish peroxidase-labelled oligonucleotide probes (purchased from Biomers Inc, www.biomers.net) on filter sections as described before (Pernthaler *et al*., 2004). Signal amplification was performed with tyramides custom labelled with the fluorochrome Alexa488 (Invitrogen). FISH probes were used that target bacteria affiliated with *Betaproteobacteria* (BET42a), *Actinobacteria* (HGC69a), and with the *Cytophaga–Flavobacteria* sublineage of *Bacteroidetes* (CF319a) (Amann *et al*., 1995). In addition, two new specific probes were designed and tested by hybridization on isolates at increasing levels of stringency (i.e. increasing formamide concentrations in the hybridization buffer). These probes are targeted to two phylogenetic lineages of isolates that were

obtained from additional dilution enrichments conducted in 2007 (see below).

Proportions of cells with DNA de novo *synthesis*

The proportions of cells with visible DNA *de novo* synthesis were determined from 21 March until the end of the study period. Triplicate lake water samples (200 ml) were incubated in 250 ml glass bottles with BrdU (20 μM) and thymidine (33 nM) at *in situ* temperature in the dark (Pernthaler and Pernthaler, 2005). After 2 h of incubation subsamples (20 ml) were fixed with PFA for 1 h at room temperature. One additional treatment pre-fixed with PFA (20 ml) served as negative control. Portions of 2–7 ml from all replicates were filtered onto polycarbonate membrane filters (type GTTP, Millipore, diameter, 47 mm, pore size, 0.2 μm). Preparations were stored at −20°C until further processing.

The incorporation of BrdU into *de novo* synthesized DNA in whole cells was visualized cytochemically using a BrdU-specific horseradish peroxidase-labelled antibody FAB fragment (Roche) followed by CARD signal amplification (Pernthaler and Pernthaler, 2005). BrdU detection was subsequently combined with cell identification by CARD-FISH (Pernthaler and Pernthaler, 2005). In order to avoid a spectral overlap of fluorochromes between the FISH and BrdU stainings, CARD detection of BrdU-conferred HRP was performed with tyramides labelled with Alexa633 (Invitrogen).

Epifluorescence microscopy

The evaluations of CARD-FISH staining and BrdU incorporation experiments were performed on an integrated automated high-throughput screening platform based on motorized epifluorescence microscopy and image analysis (M. Zeder, unpublished). The core of the system consisted of a conventional epifluorescence microscope (AxioImager.Z1, Carl Zeiss) equipped with a motorized stage for eight microscopic slides. The epifluorescence illumination device (Colibri, Carl Zeiss) included LED modules for 365, 470 and 590 nm excitation. A triple filter set (62 HE) was used in combination with the Colibri system to image three different fluorescent dyes (DAPI, Alexa488, Alexa633), thus eliminating the need of changing filter blocks between different excitation wavelengths. Fluorescence images were recorded with a CCD Camera (AxioCam MRm, Carl Zeiss) using a 63× objective (Plan-Apochromat). The microscope was controlled by a computer (CPU: Intel Core2Duo 3 GHz; RAM: 3 GB) running Windows XP Professional (Microsoft) and the software AxioVision 6.3 (Carl Zeiss). Automation of the image acquisition and evaluation workflow was realized by object-oriented programming either in the Visual Basic for Application module in AxioVision or in Visual Basic.NET (Microsoft). Between 1000 and 4000 DAPI-stained objects were counted per preparation.

The sizes of cells hybridized with different probes were estimated at three time points and in four replicate preparations per time point. Images for cell sizing were acquired at higher magnification than for cell counting, using a 100× Plan Neofluar objective (Carl Zeiss). Cell volumes were inferred from the projected cell areas and perimeters of their DAPI-stained images according to a previously described geometric model (Posch *et al.*, 1997).

Dilution experiments

The growth response of lake bacteria to a relief of top-down control was assessed weekly in dilution cultures. Bacteria-free lake water was prepared by hollow fibre filtration (pore size, 0.1 μm) (Hydac International). Fifty millilitres of lake water samples were added to 450 ml of filtrate and incubated at *in situ* temperature (range, 3.3–14.1°C) in the dark in 1 l glass bottles. Incubations were conducted in triplicates for 120 h before the phytoplankton bloom period (14 March–9 April) and for periods of 48–72 h thereafter. The variable incubation times were chosen to obtain final cell numbers that were approximately twice as high as at the beginning of the experiments (as assessed by daily counting). The enrichments were stopped by fixation of subsamples (20–50 ml) with 1% PFA.

The apparent growth rates of the total microbial assemblage and of different FISH-defined populations in the dilution cultures were estimated from the differences between their cell numbers at the start and end points of the enrichments, assuming exponential cell increase and neglecting a potential growth delay after transfer (lag phase). The presented estimates thus represent conservative approximations of actual growth rates.

In order to test for intrinsic changes of *Flavobacteriacea* during bottle incubations, additional lake water was collected on 27 March 2007. A 1:10 dilution culture was prepared as described above and compared with a control treatment of unmanipulated lake water. The samples (volume, 1000 ml in 2 l glass bottles) were incubated in the dark for a period of 48 h at ambient temperature (7°C) for a period of 48 h. Subsamples were fixed and prepared as described above, and the total cell numbers and proportions of *Flavobacteriaceae* in either treatment were determined by DAPI staining and CARD-FISH with probe CF319a.

Isolation of enriched bacteria

In view of the results from the dilution cultures, additional enrichments experiments were performed as described above during the spring phytoplankton bloom period 2007 with the purpose of isolating bacterial strains from the phylogenetic groups which grew most rapidly in the 2006 dilution experiments. After 72–120 h of enrichment subsamples (0.1–0.001 ml) were plated on complex media [YST: yeast extract, starch, peptone from casein, each 0.25 g l^{-1}; Plate-Count Agar (PCA, 20 g l^{-1}), PCA/10; Merck]. The plates were incubated for 1–3 days at 17°C and then at 8°C for several weeks to prevent overgrowth of more slowly growing visible colonies by more rapidly spreading ones. Morphologically distinguishable colonies were selected and repeatedly streaked and subcultured in order to obtain pure clonal cultures. The obtained set of isolates was screened by PCR with a group-specific primer set (Alonso *et al.*, 2007). All PCR-positive strains were subsequently identified by determination of their almost complete 16S rRNA gene sequences (> 1300 base pairs) following previously described procedures (Eilers *et al.*, 2000). Sequences were deposited in EMBL under the Accession No. FN179349–FN179365.

A phylogenetic analysis of almost full-length rRNA gene sequences of isolates affiliated to *Flavobacteriaceae* was

performed using the software ARB (Ludwig *et al.*, 2004). Phylogenies by Maximum Parsimony (MP) and Neighbour Joining (NJ) analysis were inferred using > 2500 almost complete sequences of *Flavobacteria* and related genera. A Maximum Likelihood (ML) tree was calculated on a subset of 650 most closely related sequences using the RaxML algorithm (Stamatakis *et al.*, 2005) as implemented in ARB (Hasegawa–Kishono–Yano model of nucleotide substitution). Several trees of each type were calculated using different filters custom made for *Flavobacteriaceae* (nucleotide conservation profiles, positional variability). A consensus tree based on the ML tree was constructed from the various analyses in which only bifurcations were maintained that were conserved in at least two of the three types of reconstruction approaches.

Acknowledgements

We thank Markus Steinkellner and Angela Mechsner for help with sample analysis and two anonymous reviewers for suggestions that improved the manuscript. The Zurich Water Supply Company is acknowledged for data on phytoplankton. This work was supported by a grant from the Foundation for Scientific Research of the University of Zurich, and by the Swiss National Fund (SNF No. 3100A0-117765).

References

Allgaier, M., and Grossart, H.P. (2006) Diversity and seasonal dynamics of *Actinobacteria* populations in four lakes in northeastern Germany. *Appl Environ Microbiol* **72:** 3489–3497.

Alonso, C., Warnecke, F., Amann, R., and Pernthaler, J. (2007) High local and global diversity of *Flavobacteria* in marine plankton. *Environ Microbiol* **9:** 1253–1266.

Amann, R.I., Ludwig, W., and Schleifer, K.H. (1995) Phylogenetic identification and *in situ* detection of individual microbial cells without cultivation. *Microbiol Rev* **59:** 143–169.

Beardsley, C., Pernthaler, J., Wosniok, W., and Amann, R. (2003) Are readily cultured bacteria in coastal North Sea waters suppressed by selective grazing mortality? *Appl Environ Microbiol* **69:** 2624–2630.

Bertoni, R., Callieri, C., Balseiro, E., and Modenutti, B. (2008) Susceptibility of bacterioplankton to nutrient enrichment of oligotrophic and ultraoligotrophic lake waters. *J Limnol* **67:** 120–127.

Bleiker, W., and Schanz, F. (1997) Light climate as the key factor controlling the spring dynamics of phytoplankton in Lake Zurich. *Aquat Sci* **59:** 135–157.

Böckelmann, U., Manz, W., Neu, T.R., and Szewzyk, U. (2000) Characterization of the microbial community of lotic organic aggregates ('river snow') in the Elbe River of Germany by cultivation and molecular methods. *FEMS Microbiol Ecol* **33:** 157–170.

Brosius, J., Dull, T.J., Sleeter, D.D., and Noller, H.F. (1981) Gene organization and primary structure of a ribosomal RNA operon from *Escherichia coli*. *J Mol Biol* **148:** 107–127.

Burkert, U., Warnecke, F., Babenzien, H.-D., Zwirnmann, E., and Pernthaler, J. (2003) Members of a readily enriched beta-proteobacterial clade are common in the surface waters of a humic lake. *Appl Environ Microbiol* **69:** 6550–6559.

Comte, J., Jacquet, S., Viboud, S., Fontvieille, D., Millery, A., Paolini, G., and Domaizon, I. (2006) Microbial community structure and dynamics in the largest natural French lake (Lake Bourget). *Microb Ecol* **52:** 72–89.

Cousin, S., Brambilla, E., Yang, J., and Stackebrandt, E. (2008) Culturable aerobic bacteria from the upstream region of a karst water rivulet. *Int Microbiol* **11:** 91–100.

Eiler, A., and Bertilsson, S. (2007) Flavobacteria blooms in four eutrophic lakes: linking population dynamics of freshwater bacterioplankton to resource availability. *Appl Environ Microbiol* **73:** 3511–3518.

Eilers, H., Pernthaler, J., Glöckner, F.O., and Amann, R. (2000) Culturability and *in situ* abundance of pelagic bacteria from the North Sea. *Appl Environ Microbiol* **66:** 3044–3051.

Elser, J.J., Stabler, L.B., and Hassett, R.P. (1995) Nutrient limitation of bacterial-growth and rates of bacterivory in lakes and oceans – a comparative-study. *Aquat Microb Ecol* **9:** 105–110.

Ferguson, R.L., Buckley, E.N., and Palumbo, A.V. (1984) Response of marine bacterioplankton to differential filtration and confinement. *Appl Environ Microbiol* **47:** 49–55.

Hahn, M.W., Lünsdorf, H., Wu, Q., Schauer, M., Höfle, M.G., Boenigk, J., and Stadler, P. (2003) Isolation of novel ultramicrobacteria classified as *Actinobacteria* from five freshwater habitats in Europe and Asia. *Appl Environ Microbiol* **69:** 1442–1451.

Hama, T., and Yanagi, K. (2001) Production and neutral aldose composition of dissolved carbohydrates excreted by natural marine phytoplankton populations. *Limnol Oceanogr* **46:** 1945–1955.

Hornak, K., Masin, M., Jezbera, J., Bettarel, Y., Nedoma, J., Sime-Ngando, T., and Simek, K. (2005) Effects of decreased resource availability, protozoan grazing and viral impact on a structure of bacterioplankton assemblage in a canyon-shaped reservoir. *FEMS Microbiol Ecol* **52:** 315–327.

Jezbera, J., Hornak, K., and Simek, K. (2006) Prey selectivity of bacterivorous protists in different size fractions of reservoir water amended with nutrients. *Environ Microbiol* **8:** 1330–1339.

Jüttner, F., Meon, B., and Köster, O. (1997) Quasi *in situ* separation of particulate matter from lakewater by hollow-fibre filters to overcome errors caused by short turnover times of dissolved compounds. *Water Res* **31:** 1637–1642.

Kirchman, D., Knees, E., and Hodson, R. (1985) Leucine incorporation and its potential as a measure of protein-synthesis by bacteria in natural aquatic systems. *Appl Environ Microbiol* **49:** 599–607.

Landry, M.R., and Hassett, R.P. (1982) Estimating the grazing impact of marine micro-zooplankton. *Mar Biol* **67:** 283–288.

Ludwig, W., Strunk, O., Westram, R., Richter, L., Meier, H., Yadhukumar, et al. (2004) ARB: a software environment for sequence data. *Nucleic Acids Res* **32:** 1363–1371.

Meon, B., and Juttner, F. (1999) Concentrations and dynamics of free mono- and oligosaccharides in a shallow

eutrophic lake measured by thermospray mass spectrometry. *Aquat Microb Ecol* **16:** 281–293.
Pernthaler, A., and Pernthaler, J. (2005) Diurnal variation of cell proliferation in three bacterial taxa from coastal North Sea waters. *Appl Environ Microbiol* **71:** 4638–4644.
Pernthaler, A., Pernthaler, J., and Amann, R. (2004) Sensitive multicolour fluorescence *in situ* hybridization for the identification of environmental organisms. In *Molecular Microbial Ecology Manual*, 2nd edn. Kowalchuk, G.A., De Bruijn, F.J., Head, I.M., Akkermans, A.D.L., and van Elsas, J.D. (eds). Dordecht, the Netherlands: Kluwer Academic Publishers, pp. 711–726.
Pernthaler, J. (2005) Predation on prokaryotes in the water column and its ecological implications. *Nat Rev Microbiol* **3:** 537–546.
Pernthaler, J., Sattler, B., Simek, K., Schwarzenbacher, A., and Psenner, R. (1996) Top-down effects on the size-biomass distribution of a freshwater bacterioplankton community. *Aquat Microb Ecol* **10:** 255–263.
Pernthaler, J., Glöckner, F.O., Unterholzner, S., Alfreider, A., Psenner, R., and Amann, R. (1998) Seasonal community and population dynamics of pelagic *Bacteria* and *Archaea* in a high mountain lake. *Appl Environ Microbiol* **64:** 4299–4306.
Porter, K.G., and Feig, Y.S. (1980) The use of DAPI for identifying and counting aquatic microflora. *Limnol Oceanogr* **25:** 943–948.
Posch, T., Pernthaler, J., Alfreider, A., and Psenner, R. (1997) Cell-specific respiratory activity of aquatic bacteria studied with the tetrazolium reduction method, cyto-clear slides and image analysis. *Appl Environ Microbiol* **63:** 867–873.
Posch, T., Mindl, B., Hornak, K., Jezbera, J., Salcher, M.M., Sattler, B., *et al.* (2007) Biomass reallocation within freshwater bacterioplankton induced by manipulating phosphorus availability and grazing. *Aquat Microb Ecol* **49:** 223–232.
Riemann, L., Steward, G.F., and Azam, F. (2000) Dynamics of bacterial community composition and activity during a mesocosm diatom bloom. *Appl Environ Microbiol* **66:** 578–587.
Salcher, M.M., Hofer, J., Hornak, K., Jezbera, J., Sonntag, B., Vrba, J., *et al.* (2007) Modulation of microbial predator–prey dynamics by phosphorus availability: growth patterns and survival strategies of bacterial phylogenetic clades. *FEMS Microbiol Ecol* **60:** 40–50.
Salcher, M.M., Pernthaler, J., Zeder, M., Psenner, R., and Posch, T. (2008) Spatio-temporal niche separation of planktonic *Betaproteobacteria* in an oligo-mesotrophic lake. *Environ Microbiol* **10:** 2074–2086.
Schanz, F. (1982) A fluorimetric method of determining chlorophyll *a* and phaeophytin a concentrations. *Arch Hydrobiol Beih* **16:** 91–100.
Sherr, B.F., Sherr, E.B., and McDaniel, J. (1992) Effect of protistan grazing on the frequency of dividing cells in bacterioplankton assemblages. *Appl Environ Microbiol* **58:** 4371–4378.
Sherr, B.F., Del Giorgio, P., and Sherr Evelyn, B. (1999) Estimating abundance and single-cell characteristics of respiring bacteria via the redox dye CTC. *Aquat Microb Ecol* **18:** 117–131.
Simek, K., and Chrzanowski, T.H. (1992) Direct and indirect evidence of size-selective grazing on pelagic bacteria by freshwater nanoflagellates. *Appl Environ Microbiol* **58:** 3715–3720.
Simek, K., Hornak, K., Jezbera, J., Masin, M., Nedoma, J., Gasol, J.M., and Schauer, M. (2005) Influence of top-down and bottom-up manipulations on the R-BT065 subcluster of beta-proteobacteria, an abundant group in bacterioplankton of a freshwater reservoir. *Appl Environ Microbiol* **71:** 2381–2390.
Simon, M., Tilzer, M.M., and Muller, H. (1998) Bacterioplankton dynamics in a large mesotrophic lake. I. Abundance, production and growth control. *Arch Hydrobiol* **143:** 385–407.
Simon, M., Glöckner, F.O., and Amann, R. (1999) Different community structure and temperature optima of heterotrophic picoplankton in various regions of the Southern Ocean. *Aquat Microb Ecol* **18:** 275–284.
Sommer, U. (1981) The role of r-selection and K-selection in the succession of phytoplankton in Lake Constance. *Acta Oecol Oecol Gener* **2:** 327–342.
Sommer, U., Gliwicz, Z.M., Lampert, W., and Duncan, A. (1986) The PEG-model of seasonal succession of planktonic events in fresh waters. *Arch Hydrobiol* **106:** 433–471.
Stamatakis, A., Ludwig, T., and Meier, H. (2005) RAxML-III: a fast program for maximum likelihood-based inference of large phylogenetic trees. *Bioinformatics* **21:** 456–463.
Sterner, R.W. (1994) Seasonal and spatial patterns in macronutrient and micronutrient limitation in Joe-Pool Lake, Texas. *Limnol Oceanogr* **39:** 535–550.
Urbach, E., Vergin, K.L., and Giovannoni, S.J. (1999) Immunochemical detection and isolation of DNA from metabolically active bacteria. *Appl Environ Microbiol* **65:** 1207–1213.
Warnecke, F., Sommaruga, R., Sekar, R., Hofer, J.S., and Pernthaler, J. (2005) Abundances, identity and growth state of actinobacteria in mountain lakes of different transparency. *Appl Environ Microbiol* **71:** 5551–5559.
Weinbauer, M.G. (2004) Ecology of prokaryotic viruses. *FEMS Microbiol Rev* **28:** 127–181.
Zöllner, E., Santer, B., Boersma, M., Hoppe, H.G., and Jürgens, K. (2003) Cascading predation effects of Daphnia and copepods on microbial food web components. *Freshwater Biol* **48:** 2174–2193.
Zweifel, U.L., and Hagström, A. (1995) Total counts of marine *Bacteria* include a large fraction of non-nucleoid-containing *Bacteria* (Ghosts). *Appl Environ Microbiol* **61:** 2180–2185.

7.5 Publication 6: Ecophysiological Differences of Betaproteobacterial Populations in two Hydrochemically Distinct Compartments of a Subtropical Lagoon.

Environmental Microbiology (2008) doi:10.1111/j.1462-2920.2008.01807.x

Ecophysiological differences of betaproteobacterial populations in two hydrochemically distinct compartments of a subtropical lagoon

Cecilia Alonso,[1,2]* Michael Zeder,[1] Claudia Piccini,[2] Daniel Conde[3] and Jakob Pernthaler[1]
[1]*Limnological Station, Institute of Plant Biology, Seestr. 187, CH-8802 Kilchberg, Switzerland.*
[2]*Instituto de Investigaciones Biológicas Clemente Estable, Avenida Italia 3318, CP11600, Montevideo, Uruguay.*
[3]*Facultad de Ciencias, Iguá 4225, CP11400, Montevideo, Uruguay.*

Summary

We studied the population sizes and substrate incorporation patterns of three phylogenetic groups of *Betaproteobacteria* in a coastal subtropical lagoon that is characterized by a sharp transition from humic freshwater to turbid brackish water. Various cellular processes were addressed by short-term incubations with four radiolabelled compounds and microautoradiographic assessment of substrate incorporation. Group-specific differences in the abundances and the respective physiological state of the three populations were observed upon transfer from the humic-rich compartment to the main body of the lagoon (estimated at 1–2 days). Members of the clade B of *Polynucleobacter* (PnecB) experienced only an insignificant change in cell numbers, but displayed a general metabolic downshift, carbon metabolism (glucose incorporation) being most affected. By contrast, bacteria from the closely related *Polynucleobacter* C clade (PnecC) clearly differed in total abundances and in the numbers of DNA-synthesizing or glucose incorporating cells. At the same time, PnecC bacteria maintained comparable levels of protein synthesis (leucine uptake) in both lagoon compartments, and the proportion of cells incorporating *N*-acetylglucosamine was even higher in the main body of the lagoon. Members of the R-BT lineage showed little changes in cell numbers, DNA synthesis and carbon metabolism. Altogether, the observed patterns of substrate metabolism suggest that different bacterial populations in the lagoon undergo specific physiological adjustments in response to changing environmental conditions.

Received 23 May, 2008; accepted 27 September, 2008. *For correspondence. E-mail calonso@iibce.edu.uy; Tel. (+598) 24 871 616 int. 148; Fax (+598) 24 875 548.

Introduction

Microbial abundances and activities in aquatic systems change with strong gradients of abiotic or biotic parameters, e.g. across the chemo- or oxycline of meromictic lakes (Cole *et al.*, 1993; Casamayor *et al.*, 2002), or along horizontal profiles of salinity (del Giorgio and Bouvier, 2002; Hewson and Fuhrman, 2004), turbidity (Selje and Simon, 2003), dissolved organic matter (Kirchman *et al.*, 2004) or primary production (Gasol *et al.*, 2002). These shifts at the level of the total microbial assemblage are typically paralleled by changes in community structure (Simek *et al.*, 2001a; Bouvier and del Giorgio, 2002; Gasol *et al.*, 2002; Crump *et al.*, 2004).

The taxonomic successions at changing environmental conditions might in parts be a consequence of species-specific mortality rates (Guixa-Boixereu *et al.*, 1999; Simek *et al.*, 2001b), but they are likely also related to the upregulation or downregulation of the growth rates of individual bacterial species. Such changes in growth rates currently cannot be directly determined *in situ*. However, sudden shifts in growth conditions (e.g. salinity or pH) likely affect various features of bacterial cell physiology (Booth, 1985; Ventosa *et al.*, 1998). A transition of microbial populations between different habitats thus probably induces an overall alteration of their physiological state. Some aspects of cell metabolism can be readily addressed *in situ*, e.g. DNA synthesis (Warnecke *et al.*, 2005), the functionality of the respiratory electron transport chain (Nielsen *et al.*, 2003), or the incorporation of particular substrates (Vila *et al.*, 2004). Ideally, various facets of microbial cell activity should be assessed simultaneously to reach a more synoptic conclusion about the growth state of populations. The combination of microautoradiography (MAR) and fluorescence *in situ* hybridization (FISH) allows for such a comparative assessment of various growth-related features at the single cell level, e.g. the sizes of subpopulations involved in DNA *de novo* synthesis (Cottrell and Kirchman, 2003), biomass production (Alonso and Pernthaler, 2006a), the degradation of

Table 1. Physicochemical parameters determined at the two sampling points.

	Conductivity[a] (mS cm^{-1})	TP (μg l^{-1})	SiO_2 (μg l^{-1})	TN (μg l^{-1})	SS (mg l^{-1})	OM (mg l^{-1})	F (UQ equiv.)	a_{320} (m^{-1})
Chafalote	1.8	26.9	3291.4	275.0	14.4	6.7	7326	43.3
Lagoon	6.7	50.5	2620.1	199.8	64.2	13.6	5993	26.4

a. Annual mean.
TP, total phosphorous; SiO_2, reactive silica; TN, total nitrogen, SS, suspended solids; OM, organic matter; F, fluorescence (UQ, ubiquinone); a_{320}, absorbance at 320 nm.

macromolecules (Cottrell and Kirchman, 2000), or of low molecular weight compounds (Alonso-Saez and Gasol, 2007).

So far, most studies about the growth state of bacterioplankton populations at contrasting environmental characteristics have only distinguished between large phylogenetic entities (Cottrell and Kirchman, 2000; Hornak *et al.*, 2006). However, these groups often harbour various taxa that may display very different patterns of substrate uptake (Alonso and Pernthaler, 2006b; Alonso-Saez and Gasol, 2007). Thus, ecophysiological investigations appear to be most meaningful if performed on phylogenetically narrow and physiologically coherent lineages of pelagic bacteria. In freshwaters, the *Betaproteobacteria* provide a good target for this purpose. Within this lineage there are several widely distributed groups, e.g. the *Rhodoferax* sp. BAL47/R-BT cluster (Simek *et al.*, 2001b; Zwart *et al.*, 2002) or the beta II/*Polynucleobacter* sp. clade (Glöckner *et al.*, 2000; Hahn, 2003). The former has been shown to consistently respond to food web manipulations in different lakes (Simek *et al.*, 2005; Salcher *et al.*, 2007). Within the latter clade, two species-like subpopulations have been identified that appear to differ in their preference for particular habitats (Hahn *et al.*, 2005a; Wu and Hahn, 2006).

We studied the sizes and substrate uptake patterns of three populations of freshwater *Betaproteobacteria* in a coastal subtropical lagoon (Laguna de Castillos, Uruguay, Fig. S1). This habitat is characterized by a natural separation between a humic freshwater and a turbid brackish water compartment (Pérez *et al.*, 1999). The two compartments are hydrologically tightly connected, thus providing the opportunity to assess the physiological plasticity within metapopulations that are divided by a strong environmental gradient. We specifically focused on the question if the preference patterns for different substrates are variable within these populations or if they are fixed irrespectively of environmental conditions.

Results

Differences between of sampling sites

The Chafalote compartment and the central area of the Castillos lagoon (Fig. S1) clearly differed in physicochemical characteristics (Table 1). While Chafalote featured higher concentrations of reactive silicate and total nitrogen, higher values of total phosphorous were found in the main body of the lagoon. The chromophoric dissolved organic matter (CDOM) from Chafalote exhibited higher fluorescence and absorbance values, indicating higher concentrations of humic substances in this compartment. By contrast, water in the main lagoon compartment contained a considerably larger amount of suspended solids and organic matter (Table 1).

Total microbial cell numbers and abundances of specific populations

The total abundances of prokaryotes (DAPI counts) were significantly higher in the main body of the lagoon ($1.1 \pm 0.1 \times 10^7$ cells ml^{-1}) than in the Chafalote ($8.4 \pm 0.3 \times 10^6$ cells ml^{-1} (Mann–Whitney *U*-test, $n = 6$, $P < 0.05$)). *Betaproteobacteria* accounted for $35 \pm 4.0\%$ and $14 \pm 1.4\%$ of total cells in the Chafalote and the main compartment of the lagoon respectively. All three studied betaproteobacterial lineages were significantly more abundant in the Chafalote compartment than in the main body of the Castillos lagoon ($P < 0.05$) and this difference was most pronounced for members of the PnecC clade (Fig. 1). The sum of the three specific groups accounted for 40–50% of all *Betaproteobacteria* in both compartments.

Incorporation of radiolabelled substrates

Incorporation of all four radiotracers could be observed in both compartments of the lagoon, albeit at very different rates (Fig. 2). Highest incorporation rates were observed for leucine and glucose in the Chafalote, whereas incorporation rates of *N*-acetylglucosamine (NAG) were low in both compartments. No pronounced differences of thymidine incorporation rates between sites were observed.

In general, the proportions of (DAPI-stained) cells that incorporated the offered tracers were rather low (Table 2) (average for all tracers, Chafalote, $7.9 \pm 3.3\%$; lagoon, $4.9 \pm 1.6\%$). In the Chafalote approximately three times more cells incorporated glucose and NAG than leucine, indicating that the high bulk uptake rates of this amino

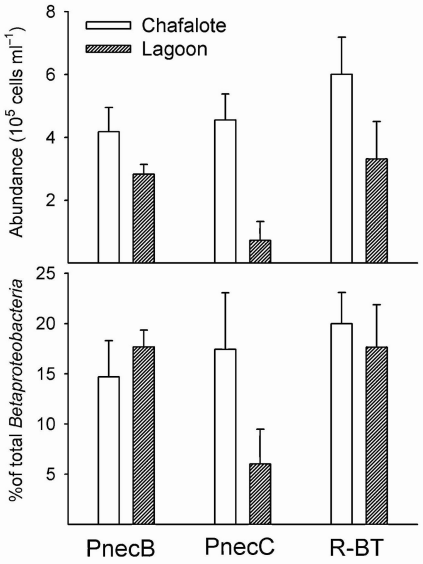

Fig. 1. Abundances of the three betaproteobacterial lineages in the two compartments (upper panel). Proportion of total *Betaproteobacteria* accounted for by the three lineages (lower panel).

acid (Fig. 2) was mainly due to a comparatively small but highly active population. Moreover, MAR-FISH revealed that most (> 80%) of these leucine-incorporating cells in the Chafalote were *Betaproteobacteria* (Table 2). By contrast, these bacteria only contributed to a small extent (< 10%) to cells with visible NAG uptake in both compartments (Table 2). The MAR-positive fractions of *Betaproteobacteria* ranged between 1.7 ± 0.6% for NAG and 10.1 ± 2.0% for thymidine. The proportion of thymidine incorporating *Betaproteobacteria* cells was significantly higher in the Chafalote ($P < 0.02$), whereas the fractions of MAR-positive cells did not significantly differ between compartments for the other tracers.

Radiotracer incorporation by betaproteobacterial populations

Bacteria from the three betaproteobacterial clades were found to incorporate all four radiolabelled substrates (Fig. 3). No substrate was unanimously preferred by all groups, and there were significant differences within groups in substrate preference between the compartments ($P < 0.01$). A larger proportion of cells from all three groups incorporated thymidine in the Chafalote than in the lagoon, but this was significant for populations PnecB and PnecC only. The highest proportion of thymidine incorporating cells was found in the PnecB cluster in both compartments. In general, the PnecB and PnecC bacteria appeared to be more active in the Chafalote than in the main body of the lagoon, as reflected by higher incorporation of three radiotracers (thymidine, leucine, glucose) by PnecB, and two (glucose, thymidine) by PnecC. By contrast, lower fractions of bacteria from the R-BT clade were observed to incorporate leucine in the Chafalote, whereas these bacteria significantly exceeded the other groups in uptake of both leucine and glucose in the main body of the lagoon. The differences in thymidine and glucose uptake of R-BT bacteria between compartments were not statistically significant. NAG was generally the least preferred substrate and the fractions of cells from the three studied lineages with visible incorporation of this tracer were low (< 10%). However, a significantly higher proportion of bacteria from the PnecC clade incorporated this tracer in the main body of the lagoon than in the Chafalote ($P < 0.01$).

The average proportion of MAR-positive cells (mean of all tracers) in the three betaproteobacterial lineages was generally higher than of the whole prokaryotic community (DAPI-stained cells) in both compartments (Table 2). This was however, not the case for NAG. Moreover, the fractions of glucose-incorporating cells in both *Polynucleobacter* populations were distinctly below community average in the lagoon. PnecB appeared to be the most active population in the Chafalote, i.e. this population displayed the highest average ratio of active bacteria to all MAR-positive cells. By contrast, this ratio was highest in R-BT bacteria in the main body of the lagoon. Both groups were particularly above the community average for thymidine and leucine incorporation.

Contribution of populations to active Betaproteobacteria

In the Chafalote, the three subpopulations clearly represented the majority of all *Betaproteobacteria* with visible incorporation of thymidine, leucine or glucose (Fig. 4),

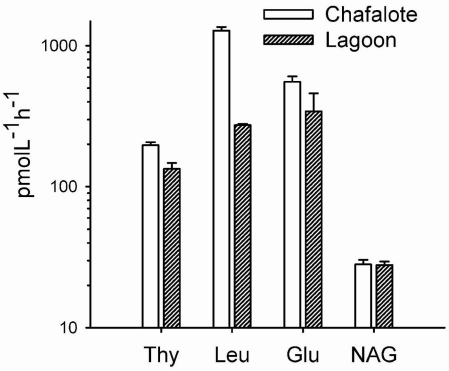

Fig. 2. Bulk incorporation rates of the four radiotracers in the two compartments.

Table 2. Proportions of all MAR-positive (MAR+) cells (i.e. of all DAPI-stained cells) and of MAR-positive *Betaproteobacteria* (i.e. of cell hybridized with probe BET42a) for the different substrates (mean ± 1 standard deviation); ratios of MAR-positive cells in the three studied lineages.

	% MAR+ cells	% MAR+ BET42a cells	% BET42a of total MAR+ cells	Ratio of MAR+ cells in group to total MAR+ cells		
				PnecB	PnecC	R-BT
Chafalote						
Thy	7.6 ± 1.0	5.7 ± 0.8	26	3.7	2.0	1.6
Leu	3.5 ± 0.4	8.5 ± 1.1	84	4.1	2.8	3.2
Glu	9.1 ± 1.8	8.3 ± 2.4	32	2.3	1.1	2.4
NAG	11.2	1.7 ± 0.6	5	0.1	0.1	0.3
Average of all tracers	7.9 ± 3.3	6.1 ± 3.2	37	2.6	1.5	1.8
Lagoon						
Thy	3.1 ± 1.1	10.1 ± 2.0	46	4.1	1.1	2.3
Leu	4.3 ± 2.2	7.6 ± 0.6	25	1.6	2.6	4.7
Glu	6.4 ± 1.4	6.2 ± 0.4	14	0.6	0.5	1.9
NAG	6.0 ± 1.7	3.0 ± 0.8	7	0.3	1.0	0.6
Average of all tracers	4.9 ± 1.6	6.7 ± 3.0	23	1.7	1.3	2.4

whereas their contribution to betaproteobacterial cells with NAG uptake approximately corresponded to their summed fraction of total betaproteobacterial abundances (Figs 1 and 4, lower panel). In the main body of the lagoon, a smaller number of active *Betaproteobacteria* was affiliated with the three studied groups, and, e.g. MAR-positive cells of the PnecB, PnecC and R-BT clades together formed less than one third of *Betaproteobacteria* with visible thymidine incorporation. Moreover, the relative importance of the three lineages within all active *Betaproteobacteria* appeared to differ between the two compartments. For example, PnecC were approximately one quarter of thymidine-incorporating *Betaproteobacteria* in the Chafalote, but only 1% in the main body of the lagoon, and a similar trend was also observed for leucine and glucose. By contrast, the contribution of leucine incorporating R-BT bacteria to all *Betaproteobacteria* approximately doubled between the compartments.

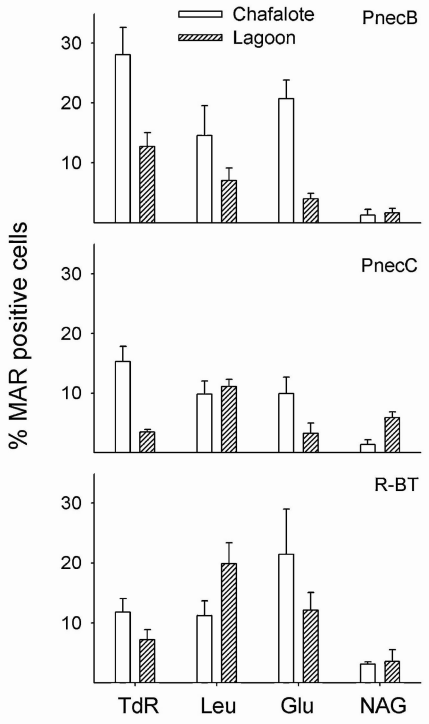

Fig. 3. Proportions of MAR-positive cells for the different tracers within each betaproteobacterial group in the two compartments.

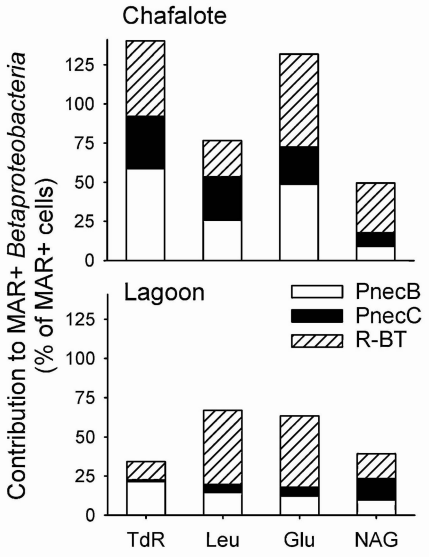

Fig. 4. Contribution of the three betaproteobacterial lineages to the total fraction of MAR-positive *Betaproteobacteria*.

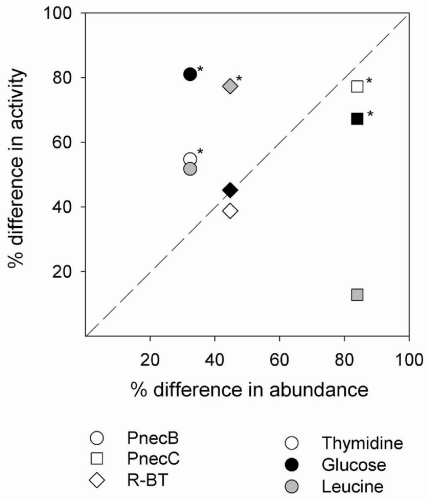

Fig. 5. Comparison of the changes between compartments in the respective proportions of MAR-positive and total cells of the three studied groups (three major substrates). Differences are expressed with reference to the values in the Chafalote compartment. Asterisks indicate statistical significance ($P < 0.05$).

Changes of abundances and of active subpopulations

Figure 5 compares the changes in the population sizes of PnecB, PnecC and R-BT bacteria between the two compartments of the Castillos lagoon with the changes in their respective fractions of MAR-positive cells. Changes in abundances and activity most closely matched in R-BT bacteria. By contrast, PnecB exhibited substantially higher shifts in activity than in abundances, and the total cell numbers of population PnecC tended to differ more strongly between compartments that their active fractions. In all three groups, changes in the fraction of thymidine incorporating cells generally closely resembled changes in abundance, whereas this was not the case for the other radiotracers.

Changes during short-term incubations

The three studied populations exhibited contrasting responses to short-term (2 h) incubations both in numbers and in their respective fractions of substrate incorporating cells (Fig. S2). Changes in total cell numbers of PnecB and R-BT were not significant, and a decrease in MAR-positive cells was observed in these bacteria for at least one radiotracer. By contrast, PnecC bacteria increased in numbers by approximately one-third and featured significantly higher proportions of thymidine and glucose incorporating cells at the end of the incubation period.

Discussion

The selected environment provided an ideal natural system for investigating ecophysiological properties of three cosmopolitan betaproteobacterial lineages in the context of a changing habitat.

Relevance of Betaproteobacteria *in the study system*

This is the first report on the *in situ* abundances of bacteria from two *P. necessarius* lineages and of microbes related to the R-BT cluster from the southern hemisphere. The three groups reached high cell numbers ($> 10^5$ ml^{-1}), and together they constituted 40–50% of *Betaproteobacteria* (Fig. 1). All three studied groups tended to be more abundant in the Chafalote than in the main body of the lagoon.

Bacteria affiliated with the R-BT cluster (targeted by the R-BT065 probe) have been detected in a range of different freshwater systems across Central and Northern Europe (Zwart *et al.*, 2003; Simek *et al.*, 2005; Warnecke *et al.*, 2005). These bacteria may account for a substantial proportion of the pelagic microbial communities in some freshwater systems (Simek *et al.*, 2005; Salcher *et al.*, 2008), but the scarce information about their *in situ* abundances in different habitat types still limits our understanding of the factors that determine their occurrence.

Bacteria from the freshwater Beta II lineage, i.e. cells hybridized with the probe BET2-870 (which targets *Polynucleobacter* and closely related sequence- types) could be exclusively assigned to two lineages of *Polynucleobacter* PnecB and PnecC (data not shown). Members of the various *P. necessarius* clades are common in a range of freshwater environments with different limnochemical properties (Burkert *et al.*, 2003; Hahn *et al.*, 2005b; Wu and Hahn, 2006). Cells related to the species-like PnecC lineage exhibited sixfold higher abundances in the Chafalote compartment (Fig. 1). The most obvious physicochemical differences between the compartments are the high humic content of the Chafalote and the high content of suspended solids in the main body of the lagoon (Table 1). It has been suggested that pH and temperature might be the main factors explaining the contrasting abundances of PnecB and PnecC populations in various freshwater habitats (Wu and Hahn, 2006). Our data suggest that other parameters, in particular the concentration of humic substances and salinity (i.e. conductivity), might also play a role in the respective success of these two groups.

Contribution of populations to active Betaproteobacteria

The three studied subpopulations accounted for the large majority of *Betaproteobacteria* with visible incorporation of

three of the tracers in the Chafalote compartment, but they contributed substantially less to MAR-positive beta-proteobacterial cells in the main body of the lagoon (Fig. 4). Moreover, the proportion of MAR-positive cells in the three populations (mean of all tracers) was higher than the community average (Table 2). This was most pronounced for leucine and thymidine, indicating that the three groups were key players in both compartments of the study system in terms of cell growth and biomass production.

Contrasting physiological state of metapopulations

In view of the rapid water transfer between the two sampling points, it can be assumed that the three studied populations were replaced daily at the sampling station in the main body of the lagoon by influx from the Chafalote. Therefore, it is likely that the comparative MAR-FISH analysis with the four substrates revealed specific alterations in the respective physiological state of each population that were induced by this transition (Fig. 3). It is conceivable that this might be a direct consequence of differential gene expression in response to changes in growth conditions such as nutrient availability, osmolarity, temperature, and interactions with other microorganisms (Cases and de Lorenzo, 2001).

Cells affiliated to the R-BT cluster showed small changes both of cell abundances and of several metabolic processes, and protein synthesis in this population even appeared to be enhanced after transfer to the lagoon. By contrast, members of the PnecB lineage showed only slightly lower abundances but were generally less active, i.e. a pronouncedly lower uptake of several tracers. This group exhibited a similar pattern of tracer uptake in both compartments, but all incorporation processes appeared to be reduced in the main body of the lagoon, with carbon metabolism being most strongly affected. Finally, bacteria affiliated to PnecC were clearly less in numbers and displayed significantly lower numbers of cells with visible DNA synthesis and carbon metabolism while maintaining similar levels of protein synthesis. Most strikingly, the proportion of NAG incorporating cells in this population was substantially higher, suggesting a metabolic rearrangement of substrate utilization patterns in order to exploit a major carbon source mainly available in that habitat. The enhanced utilization of NAG could moreover hint at the potential for a facultative anaerobic metabolism in these bacteria (Riemann and Azam, 2002). Members of PnecC were particularly active in amino acid uptake in the sub- and anoxic layers of a mesotrophic lake (Salcher *et al.*, 2008). Our findings thus point to a differential response of the studied groups to changes in the environmental conditions, which in turn may reflect different life strategies.

Generalists versus specialists?

Interestingly, populations PnecC and R-BT seemed to follow a somewhat similar growth pattern and the abundances of R-BT and PnecC bacteria in the Chafalote compartment and their respective proportions of MAR-positive cells were statistically indistinguishable for all the tracers (Figs 1 and 3). Members of the R-BT clade have been observed to rapidly respond to changes in growth conditions (Simek *et al.*, 2005). Our short-term incubation experiment (Fig. S2) suggests that this was also the case for the PnecC population from the Chafalote. Bacteria from this lineage have also been rapidly enriched in dilution cultures with unamended water from the humic lake Fuchskuhle (Burkert *et al.*, 2003).

However, there were also clear differences between the two lineages. R-BT was significantly less affected by the transition between the two environments both in abundance and activity (Fig. 5). This may indicate that the members of this group are capable of adapting to a wider range of physicochemical conditions. Bacteria from the R-BT cluster exhibited high growth potential in a eutrophic reservoir (Simek *et al.*, 2005), where they were particularly active in leucine uptake (Hornak *et al.*, 2006). High proportions of these bacteria could incorporate amino acids in a mesotrophic lake irrespective of the season (Salcher *et al.*, 2008).

By contrast, PnecC cells in our study exhibited the most pronounced decrease in abundance and in the proportion of MAR-positive cells in the main body of the lagoon (Figs 1 and 3), indicating that this group might thrive particularly well under humic conditions (as also indicated by our incubation experiment, Fig. S2). Hahn and co-workers reported that the *Polynucleobacter* community of a humic pond was exclusively composed by members of PnecC (Hahn *et al.*, 2005b). Moreover, PnecC bacteria might have a preference for particular substrates. This is suggested by the low proportions of glucose and leucine incorporating PnecC cells in the Chafalote compartment and the enhanced uptake of NAG by these bacteria in the main body of the lagoon (Fig. 3). In summary, the so far performed studies suggest that members of the R-BT cluster (Hornak *et al.*, 2006; Salcher *et al.*, 2008; this study) exhibit a growth pattern typical for generalists, whereas *Polynucleobacter* spp. appear to be particularly active under a more restricted set of environmental conditions, e.g. in humic habitats (Hahn *et al.*, 2005a; this study) or at low ambient oxygen concentrations (Salcher *et al.*, 2008). However, these conclusions should be regarded with caution, because the FISH probe R-BT065 still targets a relatively large set of sequence types.

Concluding remarks

The finding of differently sized subpopulations that

incorporated the various tracers within a single species-like population (e.g. PnecC) opens up the question whether in natural microbial populations there is one active 'core subpopulation' with different uptake rates for different tracers, or whether there is physiological variability within populations as previously observed for pure cultures (Rainey and Travisano, 1998). In the future, this might be addressed by combination of fluorescence activity tracers with MAR or NanoSIMS (Behrens *et al.*, 2008).

Experimental procedures

Study sites and sampling

Castillos lagoon (34°15′S–53°41′W) is the largest of the choked coastal lagoons of Uruguay (*c.* 90 km^2). Due to its pristine condition it is listed as a site in the Ramsar Convention of Wetlands and as a UNESCO Man and Biosphere Reserve. It is a very shallow (average depth 1.3 m) brackish (conductivity range from 0.5 to 23 mS cm^{-1}) system that is connected with the Atlantic Ocean through a 10 km stream (Fig. S1). The major freshwater input is the Chafalote stream which drains most of the 925 km^2 catchment of the lagoon. This stream discharges indirectly into the lagoon through the Chafalote marsh, which is a wind-protected compartment characterized by its low turbidity and by the high input of humic matter from littoral marshes of submerged and emergent macrophytes (Jorcin, 1999). In contrast, the main body of the lagoon is exposed to south-eastern winds, which cause re-suspension of the sediment and consequently high turbidity. These two tightly connected compartments also exhibit differences in other abiotic parameters such as conductivity and nutrient concentrations, whereas pH and temperature do not variate between them (D. Conde, unpubl. data). Under normal conditions the residence time of the lagoon is in the range of 40 days, and the estimated input from the Chafalote stream is 8–10 m^3 s^{-1}. From the surface area and the average depth of the mixing zone a total volume of water of 1–1.5 × 10^6 m^3 can be approximated. This results in an estimated water exchange period of 1–2 days between the sampling points. More detailed information on the lagoon is found elsewhere (Jorcin, 1999; Pérez *et al.*, 1999; Bonilla *et al.*, 2006).

In November 2004, water samples were taken from both compartments. Total and organic suspended solids were analysed gravimetrically (Eaton *et al.*, 2005). Samples were also analysed for ammonium (Koroleff, 1976), nitrite (Strickland and Parsons, 1972), nitrate and total nitrogen (Eaton *et al.*, 2005) (Valderrama, 1981), soluble reactive phosphorus (Murphy and Riley, 1962), total phosphorus (Valderrama, 1981) and reactive silicate (Mullin and Riley, 1955). The content of CDOM was estimated through optical water characteristics such as spectral absorptivity (*a*) and fluorescence (*F*) (Green and Blough, 1994; Ferrari and Dowell, 1998). Samples for the determination of the abundance of different bacterial populations by FISH were immediately fixed with freshly prepared buffered paraformaldehyde solution (PFA) at a final concentration of 1%. Portions of 1–5 ml were then filtered through polycarbonate filters (type GTTP, pore size, 0.2 μm, diameter 47 mm, Millipore, Eschborn, Germany). The filters were rinsed twice with sterile water and stored at –20°C until further analysis.

Bulk measurements of substrate incorporation

Incubations with either tritiated thymidine, leucine, NAG or glucose were performed within 1 h after sample collection. For every treatment type, triplicate 10 ml subsamples were incubated plus one control sample consisting in lagoon water fixed with PFA. Subsequently, either [6–^{3}H]Thymidine (Amersham, specific activity 3.11 TBq mmol^{-1}), L-[4,5–^{3}H]Leucine (Amersham, specific activity 2.26 TBq mmol^{-1}), *N*-Acetyl-D-[1–^{3}H]glucosamine (Amersham, specific activity 370 GBq mmol^{-1}), or d-[6–^{3}H]Glucose (Amersham, specific activity 1.29 TBq mmol^{-1}) were added to a final concentration of 10 nM. The incubations were run for 2 h in the dark at ambient water temperature (21°C). Subsequently, PFA was added to the samples to a final concentration of 1%.

Samples were then filtered onto cellulose mixed esters filters (type GSWP, pore size, 0.2 μm, diameter 25 mm, Millipore) and rinsed twice with ice-cold trichloroacetic acid and ethanol, as described by Kirchman (2001). Incorporation of radioactivity into bacterial biomass was measured in a Beckman LS5000TD liquid scintillation counter (Beckman, Fullerton, CA, USA). Measurements were corrected for quenching (internal standard method) and by subtraction of counts from the prefixed controls.

Substrate incorporation by specific bacterial populations

In order to assess substrate incorporation patterns by specific populations, additional triplicate incubations of 10 ml subsamples with radiolabelled substrates were performed as described above. In addition, an experiment was performed to assess the effects of short-term incubation on substrate incorporation patterns: Water from Chafalote was placed into sterile 300 ml bottles for two additional hours at *in situ* water temperature. The subsequent incubations with radiotracers (thymidine, leucine and glucose) in triplicate 10 ml subsamples were again carried out as described above. After fixation all samples were filtered through polycarbonate filters (type GTTP, pore size, 0.2 μm, diameter 25 mm, Millipore). The filters were rinsed twice with sterile phosphate-buffered saline and stored at –20°C until further analysis.

To study the substrate uptake by specific groups of *Betaproteobacteria*, we combined MAR and FISH as described previously (Alonso and Pernthaler, 2005). Triplicates samples of every treatment type were evaluated for each population, thus 132 filter pieces were analysed in total. FISH was combined with catalysed reporter deposition in order to improve signal strength (Pernthaler *et al.*, 2002). The following horseradish peroxidase labelled FISH probes were applied (all purchased from Biomers, Ulm, Germany): BET42a (most *Betaproteobacteria* (Amann *et al.*, 1995), R-BT065 (R-BT subcluster of the *Rhodoferax* sp. BAL47 lineage) (Simek *et al.*, 2001b), PnecB-23S-166 (*Polynucleobacter* subcluster B) (Wu and Hahn, 2006) and PnecC-16S-445 (*Polynucleobacter* subcluster C) (Hahn *et al.*, 2005b). Tyramides custom labelled with the fluorescent dye Alexa 488 (Molecular Probes, Leiden, the Netherlands) were used for signal amplification.

Different MAR exposure times (range: 4 h to 3 days) were tested to produce a maximum number of cells with silver grains (Alonso and Pernthaler, 2005). Optimal exposure time was 8 h for incubations with tritiated thymidine, leucine and glucose, and 24 h for incubations with tritiated NAG. All photochemicals were purchased from Kodak (Eastman Kodak, Rochester, NY, USA): autoradiography emulsion (type NTB-2), developer (type Dektol) and fixer. The development of the exposed slides followed the instructions of the manufacturer (2 min of development, 10 s rinsing with distilled water, 5 min in fixer, followed by 5 min washing with distilled water).

Evaluation of FISH and MAR-FISH samples

FISH and MAR-FISH preparations were embedded on microscopic slides in a previously described mounting medium containing 4,6-diamidino-2-phenylindole (DAPI, final concentration, 1 $\mu g\ ml^{-1}$) (Pernthaler *et al.*, 2002). Evaluation was carried out following the strategy outlined in Pernthaler and colleagues (2003) and Alonso and Pernthaler (2005) on a motorized microscopic system consisting of an epifluorescence microscope (AxioImager.Z1, Zeiss, Germany), a CCD Camera (Zeiss AxioCam MRm) and a motorized stage for eight microscopic slides (Zeiss WSB Piezodrive 05). Images were acquired using a 63× 'Plan-Apochromat' objective and the Zeiss filter sets 01 (DAPI) and 10 (Alexa 488). The microscope was linked to a personal computer with the image analysis software AxioVision 4.6 (Zeiss). Automation was achieved using the Visual Basic for Application module of AxioVision and comprised automated sample recognition and localization, multichannel image acquisition, image processing and cell counting routines for both FISH and MAR-FISH preparations (M. Zeder, unpubl. data). A manual verification of the results of automated counting in a subset of preparations was assisted by the free counting software 'ClickCounter' (http://www.kingdoms.ch).

Statistical analysis

The following hypotheses were addressed by statistical testing, using multivariate analysis of variance (MANOVA): (i) the three populations significantly differed in their incorporation of a particular substrate and this difference was influenced by the habitat; and (ii) there were differences in substrate incorporation within each population between the habitats. All percentages were arcsine transformed prior to MANOVA analyses in order to obtain normal distribution of variance (Kolmogorov–Smirnoff 1-sample test). In addition, a non-parametric one-way Kruskal–Wallis ANOVA was used to test for differences in the abundances of the studied populations between compartments. All statistical analyses were performed with SPSS v13 (SPSS, Chicago, IL, USA).

Acknowledgements

We would like to thank Paola Gómez for helping during the sampling, Tito Olivera for providing the field work logistics, and two anonymous reviewers for their helpful comments which substantially contributed to the improvement of an earlier version of this manuscript. This work was funded by the University of Zurich and the PDT program of the Uruguayan government.

References

Alonso, C., and Pernthaler, J. (2005) Incorporation of glucose under anoxic conditions by bacterioplankton from coastal North Sea surface waters. *Appl Environ Microbiol* **71:** 1709–1716.

Alonso, C., and Pernthaler, J. (2006a) Concentration-dependent patterns of leucine incorporation in coastal picoplankton. *Appl Environ Microbiol* **72:** 2141–2147.

Alonso, C., and Pernthaler, J. (2006b) Roseobacter and SAR11 dominate microbial glucose uptake in coastal North Sea waters. *Environ Microbiol* **8:** 2022–2030.

Alonso-Saez, L., and Gasol, J.M. (2007) Seasonal variations in the contributions of different bacterial groups to the uptake of low-molecular-weight compounds in northwestern Mediterranean coastal waters. *Appl Environ Microbiol* **73:** 3528–3535.

Amann, R.I., Ludwig, W., and Schleifer, K.H. (1995) Phylogenetic identification and *in situ* detection of individual microbial cells without cultivation. *Microbiol Rev* **59:** 143–169.

Behrens, S., Losekann, T., Pett-Ridge, J., Weber, P.K., Ng, W.-O., Stevenson, B.S., *et al.* (2008) Linking microbial phylogeny to metabolic activity at the single-cell level by using enhanced element labeling-catalyzed reporter deposition fluorescence *in situ* hybridization (EL-FISH) and NanoSIMS. *Appl Environ Microbiol* **74:** 3143–3150.

Bonilla, S., Conde, D., Aubriot, L., Rodriguez-Gallego, L., Piccini, C., *et al.* (2006) Procesos estructuradores de las comunidades biológicas en lagunas costeras de Uruguay. In *Bases para la conservación y el manejo de la costa Uruguaya*. Menafra, R., Rodríguez-Gallego, R., Scarabino-F., L., and Conde, D. (eds). Montevideo, Uruguay: Vida Silvestre Uruguay, pp. 611–630.

Booth, I.R. (1985) Regulation of cytoplasmic pH in bacteria. *Microbiol Rev* **49:** 359–378.

Bouvier, T.C., and del Giorgio, P.A. (2002) Compositional changes in free-living bacterial communities along a salinity gradient in two temperate estuaries. *Limnol Oceanogr* **47:** 453–470.

Burkert, U., Warnecke, F.H.-D.B., Zwirnmann, E., and Pernthaler, J. (2003) Members of a readily enriched beta-proteobacterial clade are common in the surface waters of a humic lake. *Appl Environ Microbiol* **69:** 6550–6559.

Casamayor, E.O., Pedros-Alio, C., Muyzer, G., and Amann, R. (2002) Microheterogeneity in 16S ribosomal DNA-defined bacterial populations from a stratified planktonic environment is related to temporal changes and to ecological adaptations. *Appl Environ Microbiol* **68:** 1706–1714.

Cases, I., and de Lorenzo, V. (2001) The black cat/white cat principle of signal integration in bacterial promoters. *EMBO J* **20:** 1–11.

Cole, J.J., Pace, M.L., Caraco, N.F., and Steinhart, G.S. (1993) Bacterial biomass and cell size distributions in lakes: more and larger cells in anoxic waters. *Limnol Oceanogr* **38:** 1627–1632.

Cottrell, M.T., and Kirchman, D.L. (2000) Natural assemblages of marine proteobacteria and members of the

Cytophaga-Flavobacter cluster consuming low- and high-molecular-weight dissolved organic matter. *Appl Environ Microbiol* **66:** 1692–1697.

Cottrell, M.T., and Kirchman, D.L. (2003) Contribution of major bacterial groups to bacterial biomass production (thymidine and leucine incorporation) in the Delaware estuary. *Limnol Oceanogr* **48:** 168–178.

Crump, B.C., Hopkinson, C.S., Sogin, M.L., and Hobbie, J.E. (2004) Microbial biogeography along an estuarine salinity gradient: combined influences of bacterial growth and residence time. *Appl Environ Microbiol* **70:** 1494–1505.

Eaton, A.D., Clesceri, L.S., Rice, E.W., Greenberg, A.E., and Franson, M.A.H., eds. (2005) *Standard Methods for the Examination of Water and Wastewater: Centennial Edition*. Washington DC, USA: American Public Health Association.

Ferrari, G.M., and Dowell, M.D. (1998) CDOM absorption characteristics with relation to fluorescence and salinity in coastal areas of the southern baltic sea. *Estuarine, Coast Shelf Sci* **47:** 91–105.

Gasol, J.M., Comerma, M., Garcia, J.C., Armengol, J., Casamayor, E.O., Kojecka, P., and Simek, K. (2002) A transplant experiment to identify the factors controlling bacterial abundance, activity, production, and community composition in a eutrophic canyon-shaped reservoir. *Limnol Oceanogr* **47:** 62–77.

del Giorgio, P.A., and Bouvier, T.C. (2002) Linking the physiologic and phylogenetic successions in free- living bacterial communities along an estuarine salinity gradient. *Limnol Oceanogr* **47:** 471–486.

Glöckner, F.-O., Zaichikov, E., Belkova, N., Denissova, L., Pernthaler, J., Pernthaler, A., and Amann, R. (2000) Comparative 16S rRNA analysis of lake bacterioplankton reveals globally distributed phylogenetic clusters including an abundant group of *Actinobacteria*. *Appl Environ Microbiol* **66:** 5053–5065.

Green, S.A., and Blough, N.V. (1994) Optical Absorption and fluorescence properties of chromophoric dissolved organic matter in natural waters. *Limnol Oceanogr* **39:** 1903–1916.

Guixa-Boixereu, N., Lysnes, K., and Pedros-Alio, C. (1999) Viral lysis and bacterivory during a phytoplankton bloom in a coastal water microcosm. *Appl Environ Microbiol* **65:** 1949–1958.

Hahn, M.G. (2003) Isolation of strains belonging to the cosmopolitan *Polynucleobacter necessarius* cluster from freshwater habitats located in three climatic zones. *Appl Environ Microbiol* **69:** 5248–5254.

Hahn, M., Pöckl, M., and Wu, Q. (2005a) Low Intraspecific diversity in a polynucleobacter subcluster population numerically dominating bacterioplankton of a freshwater pond. *Appl Environ Microbiol* **71:** 4539–4547.

Hahn, M.W., Pockl, M., and Wu, Q.L. (2005b) Low intraspecific diversity in a polynucleobacter subcluster population numerically dominating bacterioplankton of a freshwater pond. *Appl Environ Microbiol* **71:** 4539–4547.

Hewson, I., and Fuhrman, J.A. (2004) Richness and diversity of bacterioplankton species along an estuarine gradient in Moreton Bay, Australia. *Appl Environ Microbiol* **70:** 3425–3433.

Hornak, K., Jezbera, J., Nedoma, J., Gasol, J., and Simek, K. (2006) Effects of resource availability and bacterivory on leucine incorporation in different groups of freshwater bacterioplankton, assessed using microautoradiography. *Aquat Microb Ecol* **45:** 277–289.

Jorcin, A. (1999) Temporal and spatial variability in the macrobenthic community along a salinity gradient in the Castillos lagoon (Uruguay). *Arch Hydrobiol* **146:** 369–384.

Kirchman, D. (2001) Measuring bacterial biomass production and growth rates from leucine incorporation in natural aquatic environments. In *Methods in Microbiology*. Paul, J.H. (ed.). London, UK: Academic Press, pp. 227–237.

Kirchman, D.L., Dittel, A.I., Findlay, S.E.G., and Fischer, D. (2004) Changes in bacterial activity and community structure in response to dissolved organic matter in the Hudson River, New York. *Aquat Microbial Ecol* **35:** 243–257.

Koroleff, F. (1976) Determination of ammonia. In *Methods of Seawater Analysis*. Grasshoft, K. (ed.). Weinheim, Germany: Verlag Chemie, pp. 126–133.

Mullin, J.B., and Riley, P. (1955) The spectrophotometric determination of silicate-silicon in natural waters with special reference to sea water. *Anal Chim Acta* **12:** 162–170.

Murphy, J., and Riley, J.P. (1962) A modified single solution method for the determination of phosphate in natural waters. *Anal Chim Acta* **27:** 31–36.

Nielsen, J.L., de Muro, M.A., and Nielsen, P.H. (2003) Evaluation of the redox dye 5-cyano-2,3-tolyl-tetrazolium chloride for activity studies by simultaneous use of microautoradiography and fluorescence in situ hybridization. *Appl Environ Microbiol* **69:** 641–643.

Pérez, M.C., Bonilla, S., Smarda, J., and Komárek, J. (1999) A bloom of Nodularia baltica-spumigena group (*Cyanobacteria*) in a shallow coastal lagoon of Uruguay, South America. *Algol Stud* **93** (Suppl. 128)**:** 91–101.

Pernthaler, A., Pernthaler, J., and Amann, R. (2002) Fluorescence *in situ* hybridization and catalyzed reporter deposition for the identification of marine bacteria. *Appl Environ Microbiol* **68:** 3094–3101.

Pernthaler, J., Pernthaler, A., and Amann, R. (2003) Automated enumeration of groups of marine picoplankton after fluorescence in situ hybridization. *Appl Environ Microbiol* **69:** 2631–2637.

Rainey, P., and Travisano, M. (1998) Adaptive radiation in a heterogeneous environment. *Nat Rev Genet* **394:** 69–72.

Riemann, L., and Azam, F. (2002) Widespread *N*-acetyl-D-glucosamine uptake among pelagic marine bacteria and its ecological implications. *Appl Environ Microbiol* **68:** 5554–5562.

Salcher, M., Hofer, J., Hornak, K., Jezbera, J., Sonntag, B., Vrba, J., *et al.* (2007) Modulation of microbial predator–prey dynamics by phosphorus availability: growth patterns and survival strategies of bacterial phylogenetic clades. *FEMS Microb Ecol* **60:** 40–50.

Salcher, M., Pernthaler, J., Zeder, M., Psenner, R., and Posch, T. (2008) Spatio-temporal niche separation of planktonic *Betaproteobacteria* in an oligomesotrophic lake. *Environ Microbiol* **10:** 2074–2086.

Selje, N., and Simon, M. (2003) Composition and dynamics of particle-associated and free-living bacterial communities in the Weser estuary, Germany. *Aquat Microbial Ecol* **30:** 221–237.

Simek, K., Armengol, J., Comerma, M., Garcia, J.C., Kojecka, P., Nedoma, J., and Hejzlar, J. (2001a) Changes

in the epilimnetic bacterial community composition, production, and protist-induced mortality along the longitudinal axis of a highly eutrophic reservoir. *Microb Ecol* **42:** 359–371.

Simek, K., Pernthaler, J., Weinbauer, M., Hornak, K., Dolan, J., Nedoma, J., *et al.* (2001b) Changes in bacterial community composition, dynamics and viral mortality rates associated with enhanced flagellate grazing in a mesoeutrophic reservoir. *Appl Environ Microbiol* **67:** 2723–2733.

Simek, K., Hornak, K., Jezbera, J., Masin, M., Nedoma, J., Gasol, J., and Schauer, M. (2005) Influence of top-down and bottom-up manipulations on the R-BT065 subcluster of {beta}-*Proteobacteria*, an abundant group in bacterioplankton of a freshwater reservoir. *Appl Environ Microbiol* **71:** 2381–2390.

Strickland, J.D.H., and Parsons, T.R. (1972) A practical handbook of sea water analysis. *Fish Res Bd Can Bull* **167:** 207–211.

Valderrama, J.C. (1981) The simultaneous analysis of total N and P in natural waters. *Mar Chem* **10:** 1009–1022.

Ventosa, A., Nieto, J., and Oren, A. (1998) Biology of moderately halophilic aerobic bacteria. *Microbiol Mol Biol Rev* **62:** 504–544.

Vila, M., Simo, R., Kiene, R.P., Pinhassi, J., González, J.A., Moran, M.A., and Pedros-Alio, C. (2004) Use of microautoradiography combined with fluorescence in situ hybridization to determine dimethylsulfoniopropionate incorporation by marine bacterioplankton taxa. *Appl Environ Microbiol* **70:** 4648–4657.

Warnecke, F., Sommaruga, R., Hofer, J.S., and Pernthaler, J. (2005) Abundances, identity and growth state of *Actinobacteria* in mountain lakes of different transparency. *Appl Environ Microbiol* **71:** 5551–5559.

Wu, Q., and Hahn, M. (2006) Differences in structure and dynamics of polynucleobacter communities in a temperate and a subtropical lake, revealed at three phylogenetic levels. *FEMS Microbiol Ecol* **57:** 67–79.

Zwart, G., Crump, B.C., Agterveld, M., Hagen, F., and Han, S.K. (2002) Typical freshwater bacteria: an analysis of available 16S rRNA gene sequences from plankton of lakes and rivers. *Aquat Microbiol Ecol* **28:** 141–155.

Zwart, G., van Hannen, E.J., Kamst-van Agterveld, M.P., Van der Gucht, K., Lindstrom, E.S., Van Wichelen, J., *et al.* (2003) Rapid screening for freshwater bacterial groups by using reverse line blot hybridization. *Appl Environ Microbiol* **69:** 5875–5883.

Supporting information

Additional Supporting Information may be found in the online version of this article:

Fig. S1. Map of Laguna de Castillos. The two sampling points in the Chafalote compartment (C) and the main body of the lagoon (L) are indicated by dots.

Fig. S2. Upper panel: Changes in abundance and the activity of the three lineages during a short-term incubation experiment. Lower panel: Percent deviation in the fractions of MAR-positive cells before and after the short-term incubations for three substrates.

Please note: Wiley-Blackwell are not responsible for the content or functionality of any supporting materials supplied by the authors. Any queries (other than missing material) should be directed to the corresponding author for the article.

7.6 Publication 7: Spatio-Temporal Niche Separation of Planktonic **Betaproteobacteria** *in an Oligo-Mesotrophic Lake.*

Environmental Microbiology (2008) **10**(8), 2074–2086 doi:10.1111/j.1462-2920.2008.01628.x

Spatio-temporal niche separation of planktonic *Betaproteobacteria* in an oligo-mesotrophic lake

Michaela M. Salcher,[1]* Jakob Pernthaler,[1] Michael Zeder,[1] Roland Psenner[2] and Thomas Posch[1]

[1]*Department of Limnology, Institute of Plant Biology, University of Zurich, Seestrasse 187, CH-8802 Kilchberg, Switzerland.*

[2]*Institute of Ecology, University of Innsbruck, Technikerstrasse 25, A-6020 Innsbruck, Austria.*

Summary

We investigated the diversity of planktonic *Betaproteobacteria* and the seasonal population changes of betaproteobacterial taxa in an oligo-mesotrophic lake (Piburger See, Austria). Focus was put on the vertical distribution of the investigated populations and on differences between their respective cell fractions with apparent amino acid incorporation. On average, 66% of betaproteobacterial cells and 73% of their diversity could be attributed to four clades within three lineages that were further analysed by fluorescence *in situ* hybridization. The numbers of bacteria from the R-BT subclade of the beta I lineage and from the PnecB subgroup of the beta II lineage were rather constant throughout the water column. In contrast, members of another subgroup of beta II (PnecC) and bacteria related to *Methylophilus* (beta IV) were particularly numerous in the oxygen-depleted zone. In general, only moderate seasonal changes in abundance were observed in the upper water layers, whereas there was a clear relationship between decreasing oxygen levels and the rise of bacteria from the PnecC and beta IV clades in deeper strata. On average, almost 80% of beta I bacteria, but < 15% of cells from the beta IV clade, showed amino acid incorporation. Our results suggest that the studied populations occupy distinct vertical and ecophysiological niches in Piburger See.

Introduction

Seasonality of freshwater bacterioplankton at the community level has been the topic of numerous studies. It has been shown that bacterial abundances, biomasses and bulk production may follow seasonal patterns of phytoplankton development and/or physicochemical changes (e.g. Coveney and Wetzel, 1995; Simon *et al.*, 1998). However, the seasonal successions of lake bacterioplankton are much less understood than that of phyto- or zooplankton (Sommer *et al.*, 1986). This is mainly due to the limited information on temporal changes of the taxonomic composition of freshwater microbial assemblages.

There is, however, first evidence that different freshwater bacteria exhibit specific seasonal succession patterns. For example, a species-like clade within *Betaproteobacteria* showed pronounced summer maxima of population sizes that were tightly correlated with water temperature (Hahn *et al.*, 2005; Wu and Hahn, 2006a,b). *Actinobacteria* from a typical freshwater lineage may form spring and autumn maxima in temperate lakes (Burkert *et al.*, 2003; Allgaier and Grossart, 2006), and a rise of filamentous bacteria affiliated with *Saprospiraceae* was observed in parallel with the decay of phytoplankton spring bloom (Schauer *et al.*, 2006). Short-lived peaks of filamentous morphotypes related to *Sphingobacteria* and *Alphaproteobacteria* were also found during periods of high densities of bacterivorous nanoflagellates (Pernthaler *et al.*, 2004; Nishimura and Nagata, 2007).

One drawback of many seasonal studies is the exclusive focus on the surface water layers (e.g. Burkert *et al.*, 2003; Wu and Hahn, 2006a). Thermally stratified lakes typically exhibit pronounced depth gradients of physicochemical parameters, and higher abundances and biomasses of microorganisms can be found in deeper water layers (Cole *et al.*, 1993). The oxygen-depleted hypolimnion may represent a niche for specialized microorganisms, such as fermenting bacteria, denitrifiers, methanotrophs, methylotrophs or autotrophic sulfur bacteria (Casamayor *et al.*, 2000; Lehours *et al.*, 2007). Moreover, some heterotrophic bacteria from the oxic layers may be capable of a facultative anaerobic metabolism (Alonso and Pernthaler, 2005). Such ecophysiological questions can be addressed by combining phylogenetic identification with the assessment of single-cell activity (Lee *et al.*, 1999).

Betaproteobacteria are a prominent group of freshwater bacterioplankton that may form high abundances in

Received 14 November, 2007; accepted 7 March, 2008. *For correspondence. E-mail msalcher@limnol.uzh.ch; Tel. (+41) 44 716 12 21; Fax (+41) 44 716 12 25.

lakes of different trophic status (Glöckner *et al*., 1999; Wu *et al*., 2006). Several authors have defined four to six phylogenetic clusters of freshwater *Betaproteobacteria* (Glöckner *et al*., 2000; Zwart *et al*., 2002). So far, research has mainly been focused on the ecology of bacteria from the beta I (also called *Rhodoferax* and GKS16) and beta II (also called *Polynucleobacter necessarius*) clades (Šimek *et al*., 2001; 2006; Burkert *et al*., 2003; Wu and Hahn, 2006a,b; Pérez and Sommaruga, 2006; 2007; Wu *et al*., 2006). In contrast, less is known about the cosmopolitan betaproteobacterial clusters beta III and beta IV (Glöckner *et al*., 2000).

We investigated the diversity of *Betaproteobacteria* and the seasonal abundance fluctuations of different betaproteobacterial lineages in a prealpine soft water lake in the context of changes in physicochemical parameters and chlorophyll *a* concentrations. As this lake is characterized by stable summer stratification and an anaerobic hypolimnetic layer, focus was also put on vertical distribution patterns. In addition, potential differences between the studied populations in their preferences for amino acids were assessed.

Results

Seasonal changes of water chemistry and chlorophyll a

Piburger See was ice-covered from the beginning of our study in February 2005 until March 2005 and again from December 2005 until the end of the investigation period in February 2006. Spring mixis occurred in April 2005, but the oxygen profiles suggested only partial hypolimnetic oxygen replenishment. The lake was stratified between May and November 2005, and the metalimnion extended from 3 m depth in May to 12 m depth in November (Fig. 1). Oxygen was strongly depleted in the hypolimnion during stratification, and the anoxic water body extended up to a depth of 18 m in November 2005 (Fig. 1). Autumnal mixis occurred in early December and the aerobic zone expanded to at least 21 m depth in January 2006. Dissolved phosphorus concentrations ranged from 1.7 μg l^{-1} in 3 m in August to a maximum of 40.9 μg l^{-1} in 24 m depth in March. Nitrate was presumably consumed by algae in the upper layers of the lake during the growing season, whereas its concentrations in the hypolimnion strongly decreased with oxygen depletion (Fig. 1), concomitant with an accumulation of ammonium during late summer and autumn (data not shown).

Two pronounced peaks of chlorophyll *a* concentrations were observed in June–July and September–November respectively. The first maximum was mainly formed by *Chrysophyceae*. A second, late autumn phytoplankton bloom almost exclusively consisted of the diatom *Asterionella* sp.

Diversity and phylogenetic affiliation of freshwater Betaproteobacteria

Altogether 39 nearly full-length and eight partial 16S rRNA gene sequences affiliated with *Betaproteobacteria* were obtained in four clone libraries from different sampling depths and dates by screening 229 clones in total. Three almost complete sequences were subsequently identified as chimeras and excluded from further analysis. Our sequencing effort was sufficient to sample a high proportion of the total diversity of *Betaproteobacteria* in the libraries at 98% of sequence similarity. This was indicated by: (i) a high value of Good's coverage (> 0.9) and (ii) a stable estimate of total predicted phylotypes (Chao1 estimator: 13 predicted versus 11 observed) after the analysis of at least 30 sequence types.

The majority of sequences (55%) were related to two well-separated branches within a phylogenetic lineage that is targeted by fluorescence *in situ* hybridization (FISH) probe MET1217 (Fig. 2). One of these subgroups (beta IVa) exclusively consisted of sequence types from the pelagic zone of freshwaters, whereas the other one (beta IVb) contained sequence types from a variety of habitats (wastewater treatment pools, groundwater, sediments, soil and the like), but none from the water column. Nine per cent of our sequences fell into the branch of beta I bacteria detectable by probe R-BT065 and 9% into the beta II clade (targeted by probe Bet2-870). All clones affiliated with the beta II clade were related to the species-like subcluster PnecC and targeted by probe PnecC-445. Of the remaining 12 sequences, two were affiliated with the beta III clade (GKS98 cluster), and the rest with the beta I lineage, although not detectable by probe R-BT065: two sequences were related to the *Rhodoferax* sp. BAL47 clade (Zwart *et al*., 2002), two to *Coccomonas*, four to *Rhodoferax fermentans* and one to the GKS16 clade (Zwart *et al*., 2002) and to *Leptothrix* respectively.

Seasonal and vertical distribution patterns of different lineages of Betaproteobacteria

Between 34% and 100% of all *Betaproteobacteria* could be assigned to three phylogenetic groups by FISH with specific oligonucleotide probes (annual mean: 66%, Table 1). Microbes of the R-BT branch of the beta I lineage formed one-third of all *Betaproteobacteria* in 3 and 9 m depth, but their contribution was significantly smaller in the hypolimnetic layers (Table 1). By contrast, the fractions of *Betaproteobacteria* affiliated with the beta II clade significantly increased with depth. This was even more pronounced for beta IV bacteria, which formed only a small proportion of *Betaproteobacteria* in the epi- and metalimnion, but over 40% in the anoxic layer.

Members of the R-BT sublineage of the beta I clade were present throughout the whole water column

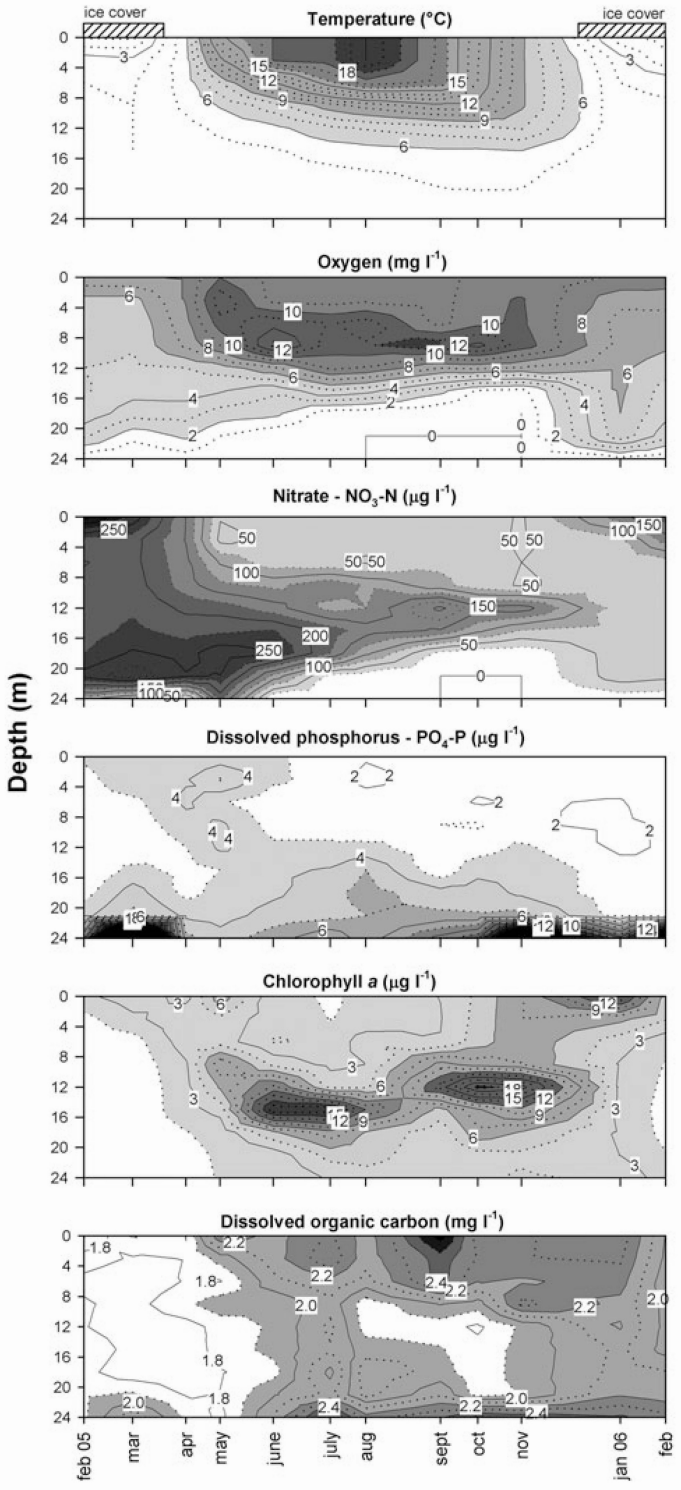

Fig. 1. Seasonal and vertical fluctuations of different environmental parameters in Piburger See during the study period (February 2005–February 2006).

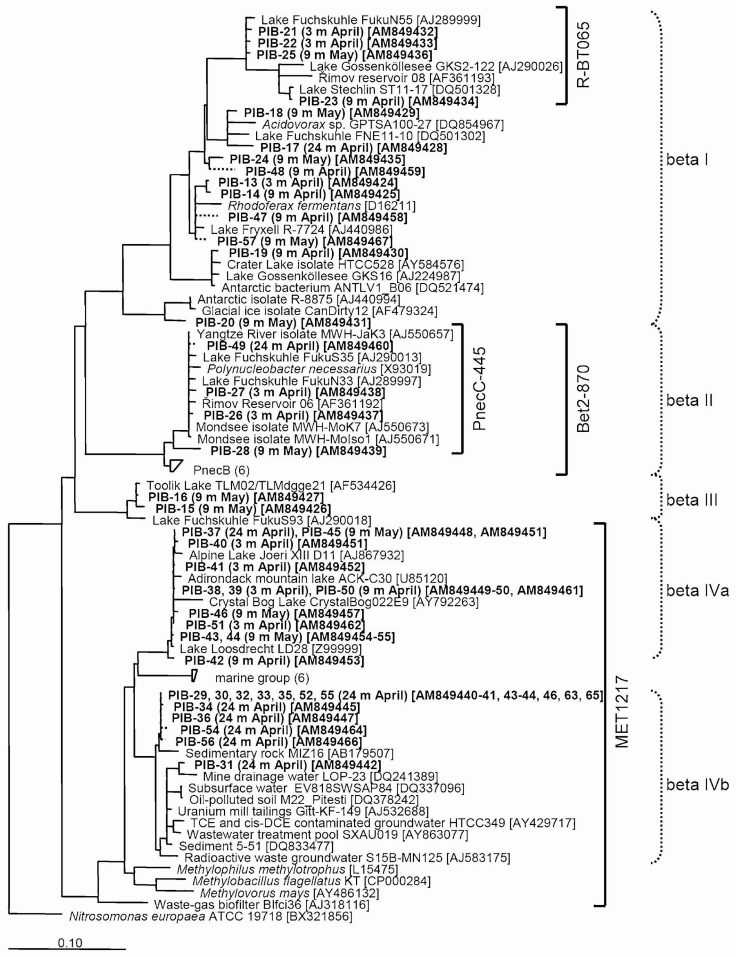

Fig. 2. Phylogenetic affiliation of betaproteobacterial sequence types from four 16S rRNA gene clone libraries obtained at different time points and depths (in bold). Partial sequences are shown with dotted lines, and identical sequences (similarity 99.9% or higher) are presented in one line. The scale bar represents 10% estimated sequence divergence.

(Table 2, Fig. 3), where they constituted between 1.4% and 7.6% of total (4,6-diamidino-2-phenylindole, DAPI) cell counts. These bacteria showed seasonal fluctuations in the epilimnion with two maxima between April and June (3 m), and between October and November (3 and 9 m). Distinctly higher abundances of R-BT bacteria were observed in the anoxic hypolimnetic water body (24 m) during summer stratification (June and July).

Bacteria from the beta II and beta IV clades (Probes Bet2-870 and MET1217) were both most abundant in hypolimnetic, oxygen-depleted waters (Figs 4 and 5). Members of the beta II clade occurred in rather low densities in the oxygenated water column (Fig. 4). In 18 m depth, their numbers increased approximately threefold in parallel to the progressing oxygen depletion between June and July (Fig. 1). Here, they maintained high abundances until November and subsequently decreased to

Table 1. Annual means of the relative contributions of the studied populations to all *Betaproteobacteria* (i.e. cells hybridized with probe Bet42a) and to *Betaproteobacteria* with visible amino acid incorporation (MAR+ cells) of the studied sampling depths.

Depth	R-BT065	Bet2-870	MET1217	Sum
% of total Betaproteobacteria				
3 m	33.0 (A)	19.3 (A)	5.0 (A)	57.4
9 m	34.7 (A)	22.8 (AB)	6.3 (A)	63.8
18 m	17.6 (B)	22.7 (AB)	17.9 (B)	58.3
24 m	15.2 (B)	28.1 (B)	41.2 (C)	84.4
% of MAR+ Betaproteobacteria				
3 m	54.4 (A)	15.5 (A)	ND	69.9
9 m	58.0 (A)	13.2 (A)	ND	71.2
18 m	27.9 (B)	30.2 (AB)	9 (A)	67.1
24 m	28.9 (B)	27.6 (B)	13.7 (A)	70.2

Different letters in brackets indicate significant differences between the different depths (one way ANOVA, $P < 0.01$).
ND, no MAR data were determined for bacteria hybridized with probe MET1217 in these layers.

Table 2. Means and annual ranges (in brackets) of relative abundances (in percentage of DAPI) and of cells with visible amino acid incorporation (MAR+ cells) (in percentage of MAR+ DAPI) of the studied betaproteobacterial clades.

Depth	BET42a	R-BT065	Bet2-870	MET1217	PnecB	PnecC
Relative abundance (% of DAPI)						
3 m	10.9 (8–15)	3.5 (2.3–7.6)	2.1 (0.6–3.6)	0.6 (0–1.2)	0.8 (0.3–1.5)	0.8 (0.4–1.4)
9 m	9.2 (5–14)	3.0 (1.4–6.2)	2.0 (1.4–2.9)	0.6 (0.1–1.3)	0.6 (0.2–1.3)	0.6 (0.2–1.2)
18 m	14.4 (9–21)	2.4 (1.4–3.5)	3.4 (1.2–6.6)	2.7 (0.4–6)	0.6 (0.3–0.9)	2.9 (0.8–7.3)
24 m	21.5 (13–31)	3.4 (1.5–5.2)	5.7 (2.7–9.1)	8.7 (4.4–12.2)	0.5 (0.2–0.9)	5.6 (3.4–7.1)
Relative abundance of MAR+ (% of MAR+ DAPI)						
3 m	36 (12–63)	19.6 (7.9–32.8)	5.2 (2.9–12.9)	ND	ND	ND
9 m	25.9 (5–39)	14.3 (6.3–22.6)	3.4 (1.1–6.1)	ND	ND	ND
18 m	32.8 (12–63)	9.6 (7.7–12.6)	8.9 (1.2–22.2)	2.9 (0.7–5.2)	ND	ND
24 m	57.9 (22–94)	18.7 (8.3–31.2)	17.7 (5.5–28.2)	7.4 (3.7–10.7)	ND	ND

ND, no MAR data were determined.

initial numbers (0.6×10^5 cells ml^{-1}). In 24 m, beta II bacteria increased in numbers between May and June and remained stable thereafter. Virtually all bacteria hybridized with probe Bet2-870 could be assigned to the sum of two specific probes for two subclades within beta II (PnecB, PnecC, Table 2). Moreover, clear differences in the vertical distribution of the two sublineages were observed. While bacteria affiliated to PnecB and PnecC occurred in roughly equal abundances in the oxygenated water column, the bloom of beta II bacteria in the sub- and anoxic layers of Piburger See could be almost entirely attributed to microbes related to PnecC (Fig. 4).

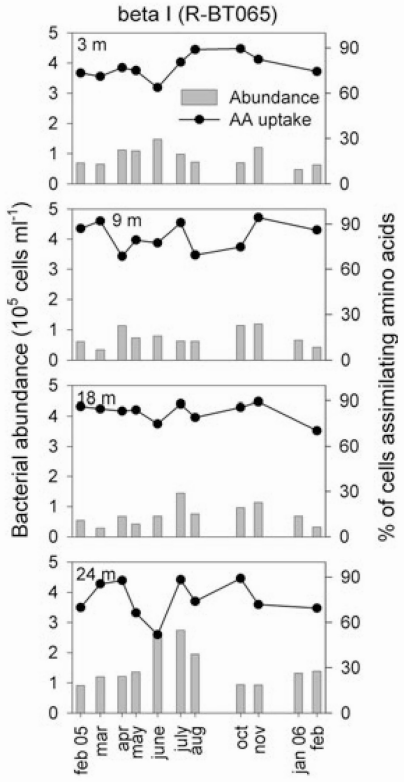

Fig. 3. Seasonal and vertical patterns of abundance (10^5 cells ml^{-1}) and amino acid uptake activity (AA uptake, in per cent of all probe-positive cells) of bacteria from the beta I clade (as detected by probe R-BT065).

A similar trend as observed for PnecC but even more pronounced was found for microbes affiliated with the beta IV lineage (Fig. 5). In the epi- and metalimnion (3–9 m), these bacteria were close to the lower limit of precise quantification by our FISH approach (i.e. below 0.8% of total counts) throughout the investigation period [mean ± standard deviation, $(0.15 \pm 0.1) \times 10^5$ cells ml^{-1}]. Beta IV bacteria increased in numbers by > 20 times in 18 m depth between May and June, maintained high densities until November and sharply declined thereafter. By contrast, bacteria from this lineage were always abundant in 24 m depth (between 2.6×10^5 and 5×10^5 cells ml^{-1}), forming distinct maxima in early summer and late winter (June and February respectively).

Incorporation of amino acids by different groups of Betaproteobacteria

On average, 76% of all *Betaproteobacteria* with visible incorporation of amino acids were members of the studied subgroups. While beta I and beta IV bacteria showed only slight changes in amino acid uptake activity, microbes of the beta II lineage exhibited pronounced temporal and vertical fluctuations (Table 2, Figs 3–5).

Bacteria from the beta I clade had significantly higher fractions of active cells than the other two groups (ANOVA, $P < 0.001$), and on average 79% (minimum: 52%, maximum: 94%) of cells hybridized by probe R-BT065 incorporated amino acids (Fig. 3). These bacteria represented almost 60% of all active *Betaproteobacteria* in the upper layers (3 and 9 m depth), but less than one-third in the hypolimnion (18 and 24 m depth, Table 1). Bacteria from the beta II clade showed the opposite trend, with higher contributions to active *Betaproteobacteria* in 24 m depth than in the epilimnion (Table 1). On average,

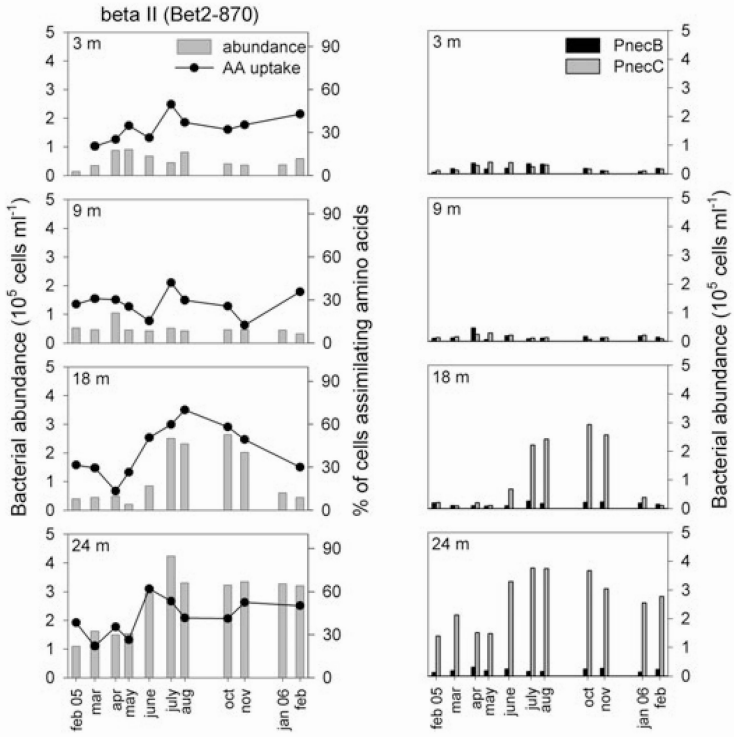

Fig. 4. Seasonal and vertical patterns of abundance (10^5 cells ml^{-1}) and amino acid uptake activity (AA uptake, in per cent of all probe-positive cells) of bacteria from the beta II clade (as detected by probe Bet2-870, left panels) and abundances of bacteria from the PnecB and PnecC subclades of beta II (10^5 cells ml^{-1}, right panels).

approximately one-third of these bacteria incorporated amino acids (mean: 36%, minimum: 13%, maximum: 70%) (Fig. 4). The highest fractions of active beta II cells were found between June and November in 18 m, and between June and February in 24 m depth respectively. Because of the low abundances of beta IV bacteria in the upper water body, it was not possible to determine microautoradiography (MAR)-positive fractions of these bacteria in 3 and 9 m depth. Members of this lineage showed significantly (ANOVA, $P < 0.001$) lower amino acid uptake activity (mean 13%, minimum: 7%, maximum: 20%) than the other studied groups in 18 and 24 m. Consequently, their contribution to total MAR-positive *Betaproteobacteria* was low (Table 1).

Relationship between environmental parameters and distribution patterns of different Betaproteobacteria

The first two axes of the redundancy analysis (RDA) model explained 99.1% of the variability in abundance and amino acid uptake of the different betaproteobacterial groups (Fig. 6). Axis 1 explained 93% of the variability and was found to correlate most highly with oxygen concentrations ($r = -0.85$) and dissolved phosphorus ($r = 0.68$). The second axis explained only 6.1% of the variability. Dissolved organic carbon and chlorophyll *a* concentrations were identified as the most important second axis variables ($r = -0.40$ each). Population sizes of beta IV and PnecC bacteria were clearly separated from R-BT and PnecB bacteria on the first axis of RDA, and from each other on the second one. By contrast, the abundances of R-BT bacteria were mainly related to the second axis, where they aligned with PnecC bacteria. RDA did not significantly explain changes in the fractions of active cells in either R-BT or beta II bacteria.

Discussion

Occurrence of Betaproteobacteria *as detected by FISH and clone libraries*

While over 80% of all *Betaproteobacteria* could be hybridized by the applied set of probes in the anoxic water body of Piburger See, FISH coverage was substantially lower in the epi- and metalimnetic samples (Table 1). Thus, other *Betaproteobacteria* might also form large populations in the lake at least seasonally. This is also suggested by sequence analysis: approximately one quarter of the sequence types in our 16S rRNA gene clone libraries were not detected by the specific FISH probes (Fig. 2). Most of these sequences were affiliated to other branches of the highly diversified beta I lineage (10) plus two

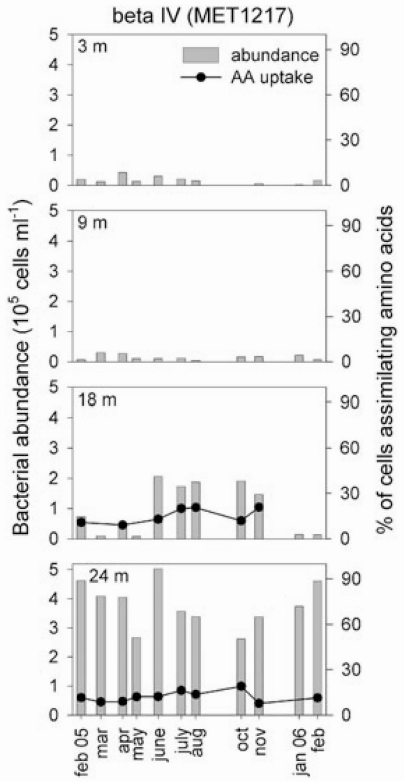

Fig. 5. Seasonal and vertical patterns of abundance (10^5 cells ml^{-1}) and amino acid uptake activity (AA uptake, in per cent of all probe-positive cells) of bacteria from the beta IV clade (as detected by probe MET1217). No MAR data were produced for fractions of probe-positive cells below 1.5% of total (DAPI) counts.

sequence types from 9 m depth related to the beta III (GKS98) clade. Interestingly, bacteria from the species-like PnecB lineage of beta II could be detected by FISH throughout the investigation (Fig. 4). However, no corresponding PnecB genotypes were present in our sequence collection, although different indices suggested that most betaproteobacterial diversity in the libraries at the species level had been covered.

Substrate incorporation patterns of different Betaproteobacteria

The three studied betaproteobacterial populations clearly differed in their respective incorporation of radiolabelled amino acids (Tables 1 and 2, Figs 3–5). In the epi- and metalimnion, the fractions of active bacteria from the R-BT clade were always larger than from the beta II clade, and there were always fewer MAR-positive cells in the beta IV lineage than in the beta II lineage in anoxic waters. This suggests that there might be consistent, growth rate-independent differences in the preference of the three populations for amino acids characteristic of their respective ecophysiological niches.

Unfortunately, it was not possible to incubate MAR samples at strictly ambient oxygen conditions in the suboxic and anoxic layers of Piburger See (18–24 m). Therefore, the high fractions of MAR-positive cells from the beta I and II lineages (Figs 3 and 4) might not accurately reflect their *in situ* levels of activity, but rather indicate their potential for a facultatively anaerobic lifestyle. As amino acid uptake is dependent on ATP-driven transporter systems (Hosie and Poole, 2001), oxygen-independent energy sources might be used by these bacteria for the incorporation of the offered substrates. A facultative anaerobic metabolism of beta I and beta IV bacteria in 18 m depth was also suggested by the rather constant percentages of active cells in this layer throughout the season irrespective of the drastic changes in ambient oxygen concentrations (Figs 1, 3 and 5).

Members of the R-BT subclade of Betaproteobacteria

All sequences affiliated with the R-BT subcluster (and detected by probe R-BT065) originated from clone libraries from 3 or 9 m depth, suggesting that these bacteria preferably inhabited the oxygenated layers of Piburger See. However, R-BT bacteria were also present and highly active in hypolimnetic layers of the lake (Fig. 3). This hints at high ecological plasticity within this lineage, as has been observed for other freshwater *Betaproteobacteria* (Hahn 2006).

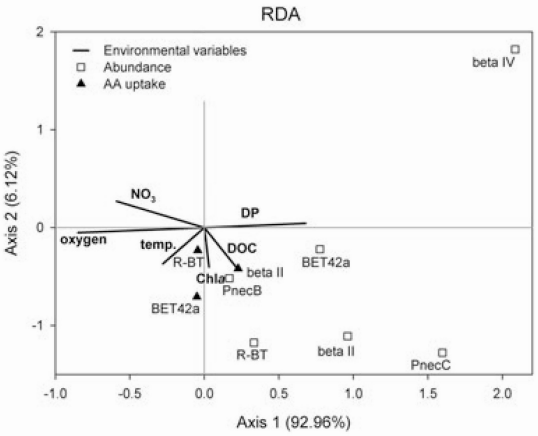

Fig. 6. Redundancy analysis biplot showing the different betaproteobacterial clades in cell numbers (□) and visible amino acid incorporation (▲) in relation to the strongest environmental variables. The eigenvalues of the two axes are given in brackets. Oxygen, oxygen concentrations; DP, dissolved phosphorus concentration; temp, temperature; Chl*a*: chlorophyll *a* concentrations; NO_3: nitrate concentration.

The population sizes of R-BT bacteria in Piburger See showed some seasonal variability both in the epi- and hypolimnion (Fig. 3). This was also reflected in their alignment with the second axis of redundancy analysis (Fig. 6), which is most strongly related to seasonal parameters, such as chlorophyll *a* and dissolved organic carbon (DOC) concentrations (Fig. 1). Bacteria detectable with probe R-BT065 are preferably ingested by heterotrophic nanoflagellates (Jezbera *et al.*, 2006), and they are typically enriched if protistan predators are eliminated via size fractionation (Šimek *et al.*, 2001, 2005) or dilution (Pérez and Sommaruga, 2006). In fact, these microbes may compensate predation mortality by their unusually high growth rates (Šimek *et al.*, 2001, 2005; Horňák *et al.*, 2006). The R-BT bacteria were observed to rapidly multiply after addition of phosphorus (Šimek *et al.*, 2006; Salcher *et al.*, 2007), algal-derived DOC (Pérez and Sommaruga, 2007) or if transplanted from nutrient-poor to nutrient-richer environments (Šimek *et al.*, 2006). Altogether, these findings indicate that microbes from this phylogenetic lineage follow an 'opportunistic' life strategy, i.e. they respond to environmental changes by rapid increase in growth rates, but are also tightly controlled by predation.

Beta II subgroup of Betaproteobacteria

Bacteria related to the beta II lineage have been found in various freshwater habitats in different climatic zones (Hahn, 2003; Wu *et al.*, 2006). Water chemistry, in particular pH and salinity, has been identified as an important factor for the ecological differentiation of two subclusters within this lineage, PnecB and PnecC (Wu and Hahn, 2006a,b). Numerous strains of free-living, aerobic, heterotrophic ultramicrobacteria from this lineage (predominantly from the PnecC and PnecD subclades) have been isolated from various freshwaters (Hahn, 2003; Hahn *et al.*, 2005; Wu and Hahn, 2006a; Vannini *et al.*, 2007). The generally small cell sizes of beta II bacteria have also been confirmed *in situ* (Wu and Hahn, 2006a), and some strains seem to range at the lower size-dependent uptake limit of heterotrophic nanoflagellates (Boenigk *et al.*, 2004).

In the upper layers of Piburger See, the subgroups PnecB and PnecC each approximately represented half of all beta II bacteria respectively (Fig. 4). Microbes related to PnecB were present in low numbers throughout the year in all depth layers, and no pronounced seasonality could be observed. In contrast, distinct seasonality of PnecB bacteria was found in surface waters of Lakes Mondsee and Taihu, with maxima in summer and winter respectively (Wu and Hahn, 2006a). The species-like PnecC subcluster of the beta II clade harbours ecologically distinct free-living strains as well as phylogenetically closely related obligate endosymbionts of the freshwater ciliate *Euplotes* sp. (*P. necessarius*) (Hahn, 2003; Vannini *et al.*, 2007). PnecC bacteria may persistently occur in humic lakes (Newton *et al.*, 2006), where they can form pronounced seasonal fluctuations (Burkert *et al.*, 2003) and transient blooms of up to 60% of total cells (Hahn *et al.*, 2005). However, members of PnecC are widespread across various freshwaters and have also been reported to form seasonal blooms in a shallow eutrophic subtropical lake (Wu and Hahn, 2006a).

So far, there is no information about the vertical distribution of PnecC bacteria in freshwaters. Our findings thus expand the current knowledge about the ecology of these bacteria by illustrating their potential preference for oxygen-depleted and anoxic waters: members of the PnecC lineage formed a distinct summer maximum in 18 m depth in Piburger See, and they were significantly more numerous in 24 m depth than in the two epi- and metalimnetic layers (Fig. 4). Moreover, $>$ 50% of all cells affiliated to beta II from anoxic waters (and thus presumably to PnecC) readily incorporated amino acids, indicating *de novo* biomass production by these bacteria. It is therefore likely that members of the PnecC clade can use other electron acceptors than oxygen, or that they are capable of fermentation.

Bacteria affiliated with the beta IV lineage

All 16S rRNA gene sequences from the beta IV lineage obtained from Piburger See fell into two well-separated branches (Fig. 2). One clade (beta IVa) exclusively contains freshwater sequences of the beta IV (Glöckner *et al.*, 2000) or LD28 cluster (Zwart *et al.*, 2002). The majority of betaproteobacterial sequences in our 24 m clone library were affiliated with a second lineage (beta IVb) that harbours sequences from habitats such as wastewater treatment plants, contaminated groundwater, mine drainage water, sedimentary rocks or oil-polluted soils (e.g. Connon *et al.*, 2005; Battaglia-Brunet *et al.*, 2006). The closest taxonomically described relative of beta IV bacteria is *Methylophilus methylotrophus*. It is an obligate type I methylotrophic bacterium isolated from activated sludge (Jenkins *et al.*, 1987) which can grow only on one-carbon organic compounds, such as methanol or formaldehyde, but does not use methane as substrate (Anthony, 1982). Members of the family *Methylophilaceae* are important denitrifyers in wastewater treatment plants and some of these bacteria use methanol as a substrate *in situ* (Ginige *et al.*, 2004). Stable isotope probing in lake sediment microcosms with the ^{13}C-labelled C1 substrates methanol, methylamine and formaldehyde selectively yielded sequence types related to *Methylophilaceae* (Nercessian *et al.*, 2005).

The FISH probe MET1217 was independently designed by Friedrich and colleagues (2003) and Ginige and colleagues (2004) for studying bacteria in an industrial biofilter and in an anoxic methanol-fed sequencing batch reactor respectively. The catalysed reported deposition-FISH (CARD-FISH) revealed a distinct vertical pattern of these bacteria in Piburger See (Fig. 5). While cells hybridized with probe MET1217 were almost absent in the epi- and metalimnion, they formed the dominant fraction of *Betaproteobacteria* in the hypolimnion (Table 2, Fig. 5). Because of the rather broad specificity of the probe (Fig. 2), it remains unclear if bacteria from both branches of beta IV shared the same vertical distribution. Recently, eight strains of the beta IVa cluster have been isolated from three German lakes on a mix of organic substrates under aerobic conditions (Gich *et al*., 2005), indicating that these bacteria might be more important in epilimnetic waters. All our 16S rRNA gene sequences affiliated to the beta IVb lineage were exclusively derived from 24 m depth and other sequences from this subclade were mainly obtained from anoxic habitats (Fig. 2). Therefore, we hypothesize that predominantly methylotrophic bacteria affiliated with the beta IVb lineage were abundant in the suboxic and anoxic layers of Piburger See. This is also supported by the low fractions of cells hybridized with probe MET1217 that could incorporate amino acids (Fig. 5).

Conclusions

The numerical importance of beta IV and PnecC bacteria in anoxic waters of Piburger See would have been missed by sampling of the upper layers only. Thus, a vertical profiling of freshwaters might substantially expand our knowledge of which bacteria are typical components of lake bacterioplankton. Moreover, we recommend studying bacterial communities at a high-resolution level, as even bacteria of such closely related clades as PnecB and PnecC or beta IVa and beta IVb might substantially differ in their niche occupation.

Experimental procedures

Study site and sampling

Piburger See is an oligo-mesotrophic dimictic lake situated in the Tyrolean Alps, Austria, at 913 m above sea level. Further information on the lake can be found elsewhere (Tolotti and Thies, 2002). Water samples were taken monthly over a period of 1 year (from February 2005 to February 2006) at the deepest part of the lake (24.6 m) from 3, 9, 18 and 24 m depths with a 5 l Schindler-Patalas sampler. Furthermore, samples for chemical and phytoplankton analyses were taken in a 3 m interval (nine samples from 0 to 24 m depths). Water temperature was directly determined during sampling. No samples could be collected in December 2005 because of the unstable ice coverage of the lake.

Portions of 40 ml from each sample were fixed either with formaldehyde (2% final concentration) for determination of bacterial abundance, or with freshly prepared buffered paraformaldehyde (pH 7.4, 2% final concentration) for analysis by CARD-FISH. All formaldehyde-fixed samples were stored at 4°C until further processing. In addition, unfixed water samples were collected for MAR-FISH (MAR combined with CARD-FISH) analyses (40 ml), for the construction of 16S rRNA gene clone libraries (1 l), and for chemical analyses (2 l). These samples were delivered to the lab at *in situ* temperature within 2 h. The following chemical parameters were evaluated: oxygen concentrations (mg l^{-1}; Winkler's method, detection limit: 0.1 mg l^{-1}), concentrations of chlorophyll *a* (μg l^{-1}; spectrophotometric measurement), nitrate (NO_3-N, μg l^{-1}; spectrophotometrical determination after reduction with sodium salicilate Seignette salt), dissolved phosphorus (PO_4-P, μg l^{-1}; molybdate method after digestion with H_2SO_4 and H_2O_2) and DOC (mg l^{-1}; high-temperature catalytic oxidation with a Shimadzu TOC analyser). Samples for phytoplankton analysis (100 ml) were fixed with Lugol's solution and counted with an inverted microscope with phase contrast.

Bacterial abundances

A total of 2–2.5 ml of formaldehyde-fixed samples were stained with DAPI (6.7 μg ml^{-1} final concentration, Porter and Feig, 1980), filtered onto black polycarbonate filters (Osmonics, 0.22 μm pore size, 25 mm diameter) and evaluated with an epifluorescence microscope (Zeiss Axioplan, Carl Zeiss, Germany). At least 1000 bacteria (Zeiss filter set 01) were counted per sample at a total magnification of 1600×.

16S rRNA gene clone libraries and phylogenetic sequence analysis

Unfixed water samples were pre-filtered through 3 μm filters to remove larger organisms. Subsequently, 300–600 ml were filtered onto white polycarbonate filters (Millipore, Type GTTP, 0.2 μm pore size, 47 mm diameter). Filters were air-dried and stored at −80°C until further processing. Samples taken in spring 2005 from different depths (i.e. April: 3, 9 and 24 m depths, and May: 24 m depth) were processed to produce four clone libraries. Small pieces of the filters were used as template for polymerase chain reaction (PCR) as previously described (Kirchman *et al*., 2001) using the primers GM3F and GM4R (*Escherichia coli* positions 8–24 and 1492–1507; Muyzer *et al*., 1995). The PCR products were purified with the QIAquick PCR purification kit (QIAGEN), inserted into TOPO vectors (TOPO TA cloning kit for sequencing; Invitrogen) and cloned into competent cells of *E. coli* according to the manufacturer's instructions. After screening of the clones for right-sized inserts, plasmid preparations were done with the QIAprep Spin Miniprep Kit (QUIAGEN) or with the Montage Plasmid Miniprep96 Kit (Millipore). The sequencing reactions were accomplished with the M13F vector primer and the ABI BigDye chemistry on an ABI 3130x Genetic Analyzer (Applied Biosystems). Partial sequences were first analysed with the

BLAST queuing system (http://www.ncbi.nlm.nih.gov/blast/) for their phylogenetic affiliations. Nearly full-length sequences of all unique sequence types affiliated with *Betaproteobacteria* were obtained by additional sequencing with vector primer M13R (Messing, 1983) and primer GM1 F (Muyzer *et al.*, 1993).

Partial sequences were assembled with the Sequencher software (Gene Codes) and checked for chimeric origin using the software Pintail (Ashelford *et al.*, 2005). Phylogenetic analyses were performed with the ARB software package (Ludwig *et al.*, 2004). The ARB database was complemented with betaproteobacterial sequences deposited in GenBank that were closely related to our sequences. All sequences were first automatically aligned using the ARB tool FAST_ALIGNER and alignments were subsequently manually optimized. For the reconstruction of phylogenetic trees, only nearly full-length (i.e. longer than 1400 nucleotides) sequences were considered. A 50% base frequency filter and a filter designed with betaproteobacterial sequences were used to exclude highly variable positions. Maximum parsimony, neighbour-joining and maximum likelihood analyses were performed with the respective ARB tools. The resulting trees were compared manually to obtain a consensus tree. Partial sequences were added to this consensus tree in accordance with maximum parsimony criteria, without allowing changes in the tree topology.

Abundances of different Betaproteobacteria

A total of 10–15 ml of paraformaldehyde-fixed samples were filtered onto white polycarbonate filters (Millipore, Type GTTP, 0.2 μm pore size, 47 mm diameter), rinsed with distilled water, air-dried and stored at –20°C until further processing. CARD-FISH was carried out as previously described (Sekar *et al.*, 2003) with horseradish peroxidase-labelled oligonucleotide probes specific for *Betaproteobacteria* (BET42a, used in combination with the unlabelled competitor GAM42a, Amann *et al.*, 1995) and three subclades within this group: R-BT065 (closely related to *Rhodoferax* sp. BAL47, belonging to the beta I cluster, Šimek *et al.*, 2001), Bet2-870 (*P. necessarius* or beta II cluster, Burkert *et al.*, 2003) and MET1217 (order *Methylophilales*, Friedrich *et al.*, 2003) which includes freshwater bacteria from the beta IV cluster (Glöckner *et al.*, 2000). In addition, the probes PnecB-23S-116 and PnecC-445 (Wu and Hahn, 2006a) were used for the discrimination of two subclusters within the beta II clade. Signal amplification was performed using tyramides labelled with Alexa488 (Invitrogen). Filter sections were counterstained with DAPI (1 μg ml^{-1}) and inspected with an epifluorescence microscope (Axiophot, Carl Zeiss) at a magnification of 1250× and the filter sets 01 (DAPI) and 10 (Alexa 488). For manual evaluation of the fractions of hybridized cells, at least 500–1000 DAPI-stained cells were counted.

The majority of FISH and MAR-FISH preparations were evaluated by automated cell counting using a set of manual counts for system calibration (Pernthaler *et al.*, 2003). Evaluations were performed with a fully automated system consisting of an epifluorescence microscope (AxioImager.Z1, Carl Zeiss) with a motorized stage for eight microscopic slides (Zeiss WSB Piezodrive 05) and a CCD Camera (AxioCam MRm, Carl Zeiss), linked to a personal computer with the image analysis software AxioVision 4.6 (Carl Zeiss). A 63× 'PlanApo' objective was used for image acquisition. Automation was achieved using the Visual Basic for Application module of AxioVision (M. Zeder, unpublished). Briefly, the microscope was loaded with up to eight slides, overview images were automatically acquired using a 1× EC 'Plan-Neofluar' objective and filter pieces were detected. A x,y-position list was generated containing a user-defined number of locations equally distributed on each filter piece. Two images (DAPI and Alexa 488 fluorescence) were acquired at each microscopic field. After image acquisition and an automated quality control routine to discard images of low quality, a counting routine automatically processed all images and detected the fractions of hybridized bacteria within all DAPI-stained cells.

In order to better assess counting precision, five duplicate hybridizations were evaluated for each probe. Only insignificant differences between duplicate determinations were observed (paired *t*-test, $P > 0.2$).

Microautoradiography combined with CARD-FISH

Five millilitres of samples were incubated with [^{3}H]-amino acids (5 nM final concentration, 48 Ci $mmol^{-1}$ specific activity, Amersham) for 1 h at *in situ* temperatures. After fixation with buffered paraformaldehyde (pH 7.4, 2% final concentration) duplicate subsamples of 2 ml were filtered onto white polycarbonate filters (Millipore, type GTTP, 0.2 μm pore size, 25 mm diameter), rinsed twice with sterile water and stored at –20°C until further processing. After CARD-FISH staining of filter sections (see above), MAR was performed as previously described (Alonso and Pernthaler, 2005). Briefly, filter sections were glued onto glass slides with 2% agarose (Seakem), dipped into autoradiography emulsion (NTB emulsion, Kodak) in the darkroom, placed on ice for 10 min and exposed in the dark at 4°C for 2–4 days. Thereafter, slides were developed with Dektol developer (Kodak) and Kodak fixer (Kodak) following the manufacturer's instructions. After drying, filters were embedded in a mounting medium containing DAPI (1 μg ml^{-1}). The evaluation of MAR-FISH filters was carried out by fully automated image analysis as described above, but an additional stack of nine bright field images in 0.5 μm steps above the z-position of the DAPI image was acquired to detect the silver grains (M. Zeder, unpublished). No samples for MAR-FISH were collected in January 2006, and no MAR-FISH samples were evaluated in which the fractions of probe-positive cells were below 1.5% of total (DAPI) counts.

Statistical analyses

Prior to statistical analyses, all data of relative abundances (percentages) were arcsine-transformed to obtain normal distribution, whereas cell numbers and chemical variables were $\log(x + 1)$-transformed. We used ANOVA to test for significant differences between the different depth layers and for differences in the amino acid uptake between betaproteobacterial clades. Furthermore, paired *t*-tests were carried out. The programme R (http://www.r-project.org) was used for these statistical analyses.

The coverage of the diversity of *Betaproteobacteria* in our clone libraries (Good's C index, Good, 1953) and the estimated total diversity (S_{Chao1} estimator, Chao, 1984) were calculated using 98% of sequence similarity as cut-off for the classification of different sequence types. Analyses were performed with the online input form created by Kemp and Aller (2004).

Redundancy analysis was used to determine the effects of environmental variables on betaproteobacterial abundances and the fraction of cells with visible amino acid incorporation (Stewart and Love, 1968). Only those environmental variables exhibiting a significant correlation ($P < 0.001$) to betaproteobacterial abundances or amino acid uptake were included in the analysis. Activity patterns of beta IV bacteria were excluded from analysis because of the high number of missing data points. The significance of added variables was tested by a Monte Carlo permutation test (499 permutations, $P < 0.001$). Analyses were performed with the Microsoft EXCEL add-in program XLSTAT-ADA (http://www.xlstat.com).

Nucleotide sequence accession numbers

All 16S rRNA gene sequences have been deposited to EMBL under the Accession Numbers AM849424 to AM849467.

Acknowledgements

We thank Josef Franzoi for chemical analyses and help during sampling and Pamela Analetti for the determination of algal abundances and biomasses. Claudia Piccini is cordially thanked for help with cloning and sequencing, and Rudi Amann is thanked for hosting M.M.S. in his lab. Maite Pérez is acknowledged for assistance during sampling, and we appreciate the helpful comments of three anonymous reviewers. This study was supported by the Austrian Science Fund (Project FWF P17554-B06 awarded to R.P.).

References

Allgaier, M., and Grossart, H.P. (2006) Diversity and seasonal dynamics of *Actinobacteria* populations in four lakes in northeastern Germany. *Appl Environ Microbiol* **72:** 3489–3497.

Alonso, C., and Pernthaler, J. (2005) Incorporation of glucose under anoxic conditions by bacterioplankton from coastal North Sea surface waters. *Appl Environ Microbiol* **71:** 1709–1716.

Amann, R., Ludwig, W., and Schleifer, K.H. (1995) Phylogenetic identification and *in situ* detection of individual microbial cells without cultivation. *Microbiol Rev* **59:** 143–169.

Anthony, C. (1982) *The Biochemistry of Methylotrophs*. New York, NY, USA: Academic Press.

Ashelford, K.E., Chuzhanova, N.A., Fry, J.C., Jones, A.J., and Weightman, A.J. (2005) At least 1 in 20 rRNA sequence record currently held in public repositories is estimated to contain substantial anomalies. *Appl Environ Microbiol* **71:** 7724–7736.

Battaglia-Brunet, F., Itard, Y., Garrido, F., Delorme, F., Crouzet, C., Greffie, C., and Joulian, C. (2006) A simple biogeochemical process removing arsenic from a mine drainage water. *Geomicrobiol J* **23:** 201–211.

Boenigk, J., Stadler, P., Wiedlroither, A., and Hahn, M.W. (2004) Strain-specific differences in the grazing sensetivities of closely related ultramicrobacteria affiliated with the *Polynucleobacter* cluster. *Appl Environ Microbiol* **70:** 5787–5793.

Burkert, U., Warnecke, F., Babenzien, D., Zwirnmann, E., and Pernthaler, J. (2003) Members of a readily enriched β-Proteobacterial clade are common in surface waters of a humic lake. *Appl Environ Microbiol* **69:** 6550–6559.

Casamayor, E.O., Schäfer, H., Baneras, L., Pedrós-Alió, C., and Muyzer, G. (2000) Identification of and spatio-temporal differences between microbial assemblages from two neighboring sulfurous lakes: comparison by microscopy and denaturing gradient gel electrophoresis. *Appl Environ Microbiol* **66:** 499–508.

Chao, A. (1984) Non-parametric estimation of the number of classes in a population. *Scand J Stat* **11:** 265–270.

Cole, J.J., Pace, M.L., Caraco, N.F., and Steinhart, G.S. (1993) Bacterial biomass and cell size distributions in lakes: more and larger cells in anoxic waters. *Limnol Oceanogr* **38:** 1627–1632.

Connon, S.A., Tovanabootr, A., Dolan, M., Vergin, K., Giovannoni, S.J., and Semprini, L. (2005) Bacterial community composition determined by culture-independent and –dependent methods during propane-stimulated bioremediation in trichloroethene-contaminated groundwater. *Environ Microbiol* **7:** 165–178.

Coveney, M.F., and Wetzel, R.G. (1995) Biomass, production, and specific growth rate of bacterioplankton and coupling to phytoplankton in an oligotrophic lake. *Limnol Oceanogr* **40:** 1187–1200.

Friedrich, U., Van Langenhove, H., Altendorf, K., and Lipski, A. (2003) Microbial community and physicochemical analysis of an industrial waste gas biofilter and design of 16S rRNA-targeting oligonucleotide probes. *Environ Microbiol* **5:** 183–201.

Gich, F., Schubert, K., Bruns, A., Hoffelner, H., and Overmann, J. (2005) Specific detection, isolation, and characterization of selected, previously uncultured members of the freshwater bacterioplankton community. *Appl Environ Microbiol* **71:** 5908–5919.

Ginige, M.P., Hugenholtz, P., Daims, H., Wagner, M., Keller, J., and Blackall, L.L. (2004) Use of stable-isotope probing, full-cycle rRNA analysis, and fluorescence *in situ* hybridization-microautoradiography to study a methanol-fed denitrifying microbial community. *Appl Environ Microbiol* **70:** 588–596.

Glöckner, F.O., Fuchs, B.M., and Amann, R. (1999) Bacterioplankton compositions of lakes and oceans: a first comparison based on fluorescence *in situ* hybridization. *Appl Environ Microbiol* **65:** 3721–3726.

Glöckner, F.O., Zaichikov, E., Belkova, N., Denissova, L., Pernthaler, J., Pernthaler, A., and Amann, R. (2000) Comparative 16S rRNA analysis of lake bacterioplankton reveals globally distributed phylogenetic clusters including an abundant group of *Actinobacteria*. *Appl Environ Microbiol* **66:** 5053–5065.

Good, I.J. (1953) The population frequencies of species and

the estimation of population parameters. *Biometrika* **40:** 237–264.
Hahn, M.W. (2003) Isolation of strains belonging to the cosmopolitan *Polynucleobacter necessarius* cluster from freshwater habitats located in three climatic zones. *Appl Environ Microbiol* **69:** 5248–5254.
Hahn, M.W. (2006) The microbial diversity of inland waters. *Curr Opin Biotechnol* **17:** 256–261.
Hahn, M.W., Pöckl, M., and Wu, Q.L. (2005) Low intraspecific diversity in a *Polynucleobacter* subcluster population numerically dominating bacterioplankton of a freshwater pond. *Appl Environ Microbiol* **71:** 4539–4547.
Horʃák, K., Jezbera, J., Nedoma, J., Gasol, J.M., and Šimek, K. (2006) Effects of resource availability and bacterivory on leucine incorporation in different groups of freshwater bacterioplankton, assessed using microautoradiography. *Aquat Microb Ecol* **45:** 277–289.
Hosie, A.H.F., and Poole, P.S. (2001) Bacterial ABC transporters of amino acids. *Res Microbiol* **152:** 259–270.
Jenkins, O., Byrom, D., and Jones, D. (1987) *Methylophilus* – a new genus of methanol-utilizing bacteria. *Int J Syst Bacteriol* **37:** 446–448.
Jezbera, J., Horňák, K., and Šimek, K. (2006) Prey selectivity of bacterivorous protists in different size fractions of reservoir water amended with nutrients. *Environ Microbiol* **8:** 1330–1339.
Kemp, P.F., and Aller, J.Y. (2004) Estimating prokaryotic diversity: when are 16S rDNA libraries large enough? *Limnol Oceanogr Meth* **2:** 114–125.
Kirchman, D.L., Yu, L., Fuchs, B.M., and Amann, R. (2001) Structure of bacterial communities in aquatic systems as revealed by filter PCR. *Aquat Microb Ecol* **26:** 13–22.
Lee, N., Nielsen, P.H., Andreasen, K.H., Juretschko, S., Nielsen, J.L., Schleifer, K.H., and Wagner, M. (1999) Combination of fluorescent *in situ* hybridization and microautoradiography – a new tool for structure-function analyses in microbial ecology. *Appl Environ Microbiol* **65:** 1289–1297.
Lehours, A.C., Evans, P., Bardot, C., Joblin, K., and Gerard, F. (2007) Phylogenetic diversity of *Archaea* and *Bacteria* in the anoxic zone of a meromictic lake. *Appl Environ Microbiol* **73:** 2016–2019.
Ludwig, W., Strunk, O., Westram, R., Richter, L., Meier, H., Yadhukumar, *et al.* (2004) ARB: a software environment for sequence data. *Nucleic Acid Res* **32:** 1363–1371.
Messing, J. (1983) New M13 vectors for cloning. *Methods Enzymol* **101:** 20–78.
Muyzer, G., De Waal, E.C., and Uitterlinden, A.G. (1993) Profiling of complex microbial populations by denaturing gradient gel electrophoresis analysis of polymerase chain reaction-amplified genes coding for 16S rRNA. *Appl Environ Microbiol* **59:** 695–700.
Muyzer, G., Teske, A., Wirsen, C.O., and Jannasch, H.W. (1995) Phylogenetic relationship of *Thiomicrospira* species and their identification in deep-sea hydrothermal vent samples by denaturing gel electrophoresis of 16S rDNA fragments. *Arch Microbiol* **164:** 165–172.
Nercessian, O., Noyes, E., Kalyzhnaya, M.G., Lidstrom, M.E., and Chistoserdova, L. (2005) Bacterial populations active in metabolism of C1 compounds in the sediment of Lake Washington, a freshwater lake. *Appl Environ Microbiol* **71:** 6885–6899.
Newton, R.J., Kent, A.D., Triplett, E.W., and McMahon, K.D. (2006) Microbial community dynamics in a humic lake: differential persistence of common freshwater phylotypes. *Environ Microbiol* **8:** 956–970.
Nishimura, Y., and Nagata, T. (2007) Alphaproteobacterial dominance in a large mesotrophic lake (Lake Biwa, Japan). *Aquat Microb Ecol* **48:** 231–240.
Pérez, M.T., and Sommaruga, R. (2006) Differential effect of algal- and soil-derived dissolved organic matter on alpine lake bacterial community composition and activity. *Limnol Oceanogr* **51:** 2527–2537.
Pérez, M.T., and Sommaruga, R. (2007) Interactive effects of solar radiation and dissolved organic matter on bacterial activity and community structure. *Environ Microbiol* **9:** 2200–2210.
Pernthaler, J., Pernthaler, A., and Amann, R. (2003) Automated enumeration of groups of marine picoplankton after fluorescence *in situ* hybridization. *Appl Environ Microbiol* **69:** 2631–2637.
Pernthaler, J., Zöllner, E., Warnecke, F., and Jürgens, K. (2004) Bloom of filamentous bacteria in a mesotrophic lake: identity and potential controlling mechanism. *Appl Environ Microbiol* **70:** 6272–6281.
Porter, K.G., and Feig, Y.S. (1980) The use of DAPI for identifying and counting aquatic microflora. *Limnol Oceanogr* **25:** 943–948.
Salcher, M.M., Hofer, J.S., Horňák, K., Jezbera, J., Sonntag, B., Vrba, J., *et al.* (2007) Modulation of microbial predator-prey dynamics by phosphorus availability: growth patterns and survival strategies of bacterial phylogenetic groups. *FEMS Microbiol Ecol* **60:** 40–50.
Schauer, M., Jiang, J., and Hahn, M.W. (2006) Recurrent seasonal variations in abundance and composition of filamentous SOL cluster bacteria (*Saprospiraceae*, *Bacteroidetes*) in oligomesotrophic lake Mondsee (Austria). *Appl Environ Microbiol* **72:** 4704–4712.
Sekar, R., Pernthaler, A., Pernthaler, J., Warnecke, F., Posch, T., and Amann, R. (2003) An improved protocol for quantification of freshwater *Actinobacteria* by fluorescence *in situ* hybridization. *Appl Environ Microbiol* **69:** 2928–2935.
Šimek, K., Horʃák, K., Jezbera, J., Masin, M., Nedoma, J., Gasol, J.M., and Schauer, M. (2005) Influence of top-down and bottom-up manipulation on the R-BT065 subcluster of beta-proteobacteria, an abundant group in bacterioplankton of a freshwater reservoir. *Appl Environ Microbiol* **71:** 2381–2390.
Šimek, K., Pernthaler, J., Weinbauer, M.G., Horňák, K., Dolan, J.R., Nedoma, J., *et al.* (2001) Changes in bacterial community composition and dynamics and viral mortality rates associated with enhanced flagellate grazing in a mesoeutrophic reservoir. *Appl Environ Microbiol* **67:** 2723–2733.
Šimek, K., Horňák, K., Jezbera, J., Nedoma, J., Vrba, J., Straskrabová, V., *et al.* (2006) Maximum growth rates and possible life strategies of different bacterioplankton groups in relation to phosphorus availability in a freshwater reservoir. *Environ Microbiol* **8:** 1613–1624.
Simon, M., Tilzer, M.M., and Müller, H. (1998) Bacterioplank-

ton dynamics in a large mesotrophic lake: I. abundance, production and growth control. *Arch Hydrobiol* **143:** 385–407.

Sommer, U., Gliwicz, Z.M., Lampert, W., and Duncan, A. (1986) The PEG-model of seasonal sucession of planktonic events in fresh waters. *Arch Hydrobiol* **106:** 443–471.

Stewart, D.K., and Love, W.A. (1968) A general canonical correlation index. *Psychol Bull* **70:** 160–163.

Tolotti, M., and Thies, H. (2002) Phytoplankton community and limnochemistry of Piburger See (Tyrol, Austria) 28 years after lake restoration. *J Limnol* **61:** 77–88.

Vannini, C., Pöckl, M., Petroni, G., Wu, Q.L., Lang, E., Stackebrandt, E., *et al.* (2007) Endosymbiosis in statu nascendi: close phylogenetic relationship between obligately endosymbiotic and obligately free-living *Polynucleobacter* strains (*Betaproteobacteria*). *Environ Microbiol* **9:** 347–359.

Wu, Q.L., and Hahn, M.W. (2006a) Differences in structure and dynamics of *Polynucleobacter* communities in a temperate and a subtropical lake, revealed at three phylogenetic levels. *FEMS Microbiol Ecol* **57:** 67–79.

Wu, Q.L., and Hahn, M.W. (2006b) High predictability of the seasonal dynamics of a species-like *Polynucleobacter* population in a freshwater lake. *Environ Microbiol* **8:** 1660–1666.

Wu, Q.L., Zwart, G., Schauer, M., Kamst-van Agterveld, M.P., and Hahn, M.W. (2006) Bacterioplankton community composition along a salinity gradient of sixteen high-mountain lakes located on the Tibetan plateau, China. *Appl Environ Microbiol* **72:** 5478–5485.

Zwart, G., Crump, B.C., Kamst-van Agterveld, M.P., Hagen, F., and Han, S.K. (2002) Typical freshwater bacteria: an analysis of available 16S rRNA gene sequences from plankton of lakes and rivers. *Aquat Microb Ecol* **28:** 141–155.

8 Acknowledgments

I wish to thank Jakob Pernthaler for giving me the opportunity to do my Ph.D. thesis at the Limnological Station. I highly appreciated his profound interest in my work, that he always had time for discussions and that he taught me how to write. I deeply admire his way of scientific and philosophical thinking and I enjoyed the relaxed atmosphere of collaboration and friendship.

I would like to thank my co-Ph.D.s and Post-docs Michaela Salcher, Judith Blom and Cecilia Alonso for their friendship, stimulating discussions and a lot of other things.

I would like to thank the students I had the pleasure to work with, Simone Peter, Silke van den Wyngaert, Tanja Shabarova, Ester Eckert, and Esther Kohler, who were all amazingly motivated and talented. My time at the Station would not have been the same without them.

I wish to thank Eugon Loher for his great support in all technical matters, his engineering skills and his relaxed and optimistic mode.

Evi Hofer is greatly acknowledged for showing me the way to object oriented programming and for her friendship.

Thomas Posch, Ferdinand Schanz and Friedrich Jüttner are acknowledged for interesting discussions and input about ecology other things.

I wish to thank my friends and co workers and the guests and members of the Limnological Station in Kilchberg, Astrid, Markus, Angela, Stefan, Bettina, Yannik, Seraina, Kasia, Karel and all others for the nice time.

Finally and most importantly, I would like to thank Kathrin and my family for being there and supporting me during this time, which was sometimes not the easiest.

9 Curriculum Vitae and List of Publications

Name	Michael Zeder
Title	Dipl. Natw. ETH
Date of birth	7. October 1979
Current position	PhD student
Nationality	Switzerland
Phone	+41 79 4071538
Email	mzeder@limnol.uzh.ch
Website	www.kingdoms.ch

Education:

2000 – 2005	Studies in Biology (Biochemistry, Microbiology) Swiss Federal Institute of Technology (ETHZ)
2005	Diploma in Biochemistry/Microbiology (ETHZ) Thesis: "Cyclic peptides in cyanobacteria and their effects on apoptosis enzymes of eukaryotes" Supervisor: Prof. em. Dr. F. Jüttner Dr. J. Blom
11.2005 – 04.2006	Internship with Roche Diagnostics, Microtechnology Center, Rotkreuz, Switzerland
04.2006 – 09.2009	Ph.D. student, University of Zürich Institute of Plant Biology, Department of Limnology Thesis: "Development of methods and technology for automated high-throughput multi-parameter analysis of single cells by fluorescence microscopy" Supervisor: Prof. Dr. J. Pernthaler

List of Publications

Zeder M, Pernthaler J.
Multi-spot live-image autofocusing for high-throughput microscopy of fluorescently stained bacteria. Cytom Part A. *in press* 2009

Zeder M, Peter S, Shabarova T, Pernthaler J.
A small population of planktonic *Flavobacteria* with disproportionally high growth during the springphytoplankton bloom in a prealpine lake. Environ Microbiol. *in press* 2009

Felder KM, Hoelzle K, Wittenbrink MM, Zeder M, Ehricht R, Hoelzle LE.
A DNA microarray facilitates the diagnosis of *Bacillus anthracis* in environmental samples. Lett Appl Microbiol. 2009

Alonso C, Zeder M, Piccini C, Conde D, Pernthaler J.
Ecophysiological differences of betaproteobacterial populations in two hydrochemically distinct compartments of a subtropical lagoon. Environ Microbiol. 2009

Salcher MM, Pernthaler J, Zeder M, Psenner R, Posch T.
Spatio-temporal niche separation of planktonic *Betaproteobacteria* in an oligo-mesotrophic lake. Environ Microbiol. 2008

Connor EC, Rott AS, Zeder M, Jüttner F, Dorn S.
13C-labelling patterns of green leaf volatiles indicating different dynamics of precursors in Brassica leaves. Phytochemistry. 2008

10 Abbreviations

AO	Acridine orange
BP	Bandpass
BrdU	5-bromo-2-deoxyuridine
CAD	Computer aided design
CARD	Catalyzed reporter deposition
CCD	Charge-coupled device
DAPI	4’6-diamidino-2-phenylindole
Em	Emission
Ex	Excitation
FISH	Fluorescence *in situ* hybridization
FOV	Field of view
FT	Farbteiler (Beam splitter)
LED	Light Emitting Diode
LP	Lowpass
MAR	Microautoradiography
m.a.s.l.	Meters above sea level
OOP	Object oriented Programming
Pixel	Picture element
RAM	Random access memory
VB.NET	Visual Basic .NET
VBA	Visual Basic for Applications

11 References

Alfreider A, Pernthaler J, Amann R, Sattler B, Glockner FO, Wille A, Psenner R (1996) Community analysis of the bacterial assemblages in the winter cover and pelagic layers of a high mountain lake by in situ hybridization. Applied and Environmental Microbiology 62:2138-2144

Alonso C, Pernthaler J (2005) Incorporation of glucose under anoxic conditions by bacterioplankton from coastal North Sea surface waters. Applied and Environmental Microbiology 71:1709-1716

Alonso C (2005) Identity and activity of marine microbial populations as revealed by single cell techniques. Dissertation

Alonso C, Zeder M, Piccini C, Conde D, Pernthaler J (2008) Ecophysiological differences of betaproteobacterial populations in two hydrochemically distinct compartments of a subtropical lagoon. Environ Microbiol

Amann RI, Krumholz L, Stahl DA (1990) Fluorescent-oligonucleotide probing of whole cells for determinative, phylogenetic, and environmental studies in microbiology. J Bacteriol 172:762-770

Amann RI, Ludwig W, Schleifer KH (1995) Phylogenetic Identification and in-Situ Detection of Individual Microbial-Cells without Cultivation. Microbiological Reviews 59:143-169

Andreatta S, Hofer JS, Sommaruga R, Psenner R (2002) Analysis and high speed sorting of free viruses by flow cytometry. Cytometry:69-69

Azam F, Fenchel T, Field JG, Gray JS, Meyerreil LA, Thingstad F (1983) The ecological role of water-column microbes in the sea. Mar. Ecol.-Prog. Ser. 10:257-263

Bartels PH, Bahr GF, Bibbo M, Wied GL (1972) Objective Cell Image Analysis. Journal of Histochemistry & Cytochemistry 20

Beling A, Jannasch H (1955) Hydrologische Untersuchungen der Fulda unter Anwendung der Membranfiltermethode. Hydrobiologia 7:36-51

Bjornsen PK (1986) Automatic Determination of Bacterioplankton Biomass by Image Analysis. Appl Environ Microbiol 51:1199-1204

Blackburn N, Hagstrom A, Wikner J, Cuadros-Hansson R, Bjornsen PK (1998) Rapid determination of bacterial abundance, biovolume, morphology, and growth by neural network-based image analysis. Applied and Environmental Microbiology 64:3246-3255

Bloem J, Veninga M, Shepherd J (1995) Fully-Automatic Determination of Soil Bacterium Numbers, Cell Volumes, and Frequencies of Dividing Cells by Confocal Laser-Scanning Microscopy and Image-Analysis. Applied and Environmental Microbiology 61:926-936

Blom JF, Robinson JA, Juttner F (2001) High grazer toxicity of [D-Asp(3) (E)-Dhb(7)]microcystin-RR of Planktothrix rubescens as compared to different microcystins. Toxicon 39:1923-1932

Blom JF, Bister B, Bischoff D, Nicholson G, Jung G, Sussmuth RD, Juttner F (2003) Oscillapeptin J, a new grazer toxin of the freshwater cyanobacterium Planktothrix rubescens. Journal of Natural Products 66:431-434

Bossard P, Gammeter S, Lehmann C, Schanz F, Bachofen R, Burgi HR, Steiner D, Zimmermann U (2001) Limnological description of the Lakes Zurich, Lucerne, and Cadagno. Aquatic Sciences 63:225-249

Boyde A, Williams RA (1971) Estimation of Volumes of Bacterial Cells by Scanning Electron Microscopy. Archives of Oral Biology 16

Brock TD (1967) Bacterial growth rate in the sea - direct analysis by thymidine autoradiography. Science 155

Chorus I, Falconer IR, Salas HJ, Bartram J (2000) Health risks caused by freshwater cyanobacteria in recreational waters. Journal of Toxicology and Environmental Health-Part B-Critical Reviews 3:323-347

Cole JJ, Findlay S, Pace ML (1988) Bacterial production in fresh and saltwater ecosystems - a cross-system overview. Mar. Ecol.-Prog. Ser. 43:1-10

Collins TJ (2007) ImageJ for microscopy. Biotechniques 43

Cottrell MT, Kirchman DL (2000) Natural assemblages of marine proteobacteria and members of the Cytophaga-Flavobacter cluster consuming low- and high-molecular-weight dissolved organic matter. Applied and Environmental Microbiology 66:1692-1697

Culverhouse PF, Williams R, Benfield M, Flood PR, Sell AF, Mazzocchi MG, Buttino I, Sieracki M (2006) Automatic image analysis of plankton: future perspectives. Mar. Ecol.-Prog. Ser. 312:297-309

Daims H, Wagner M (2007) Quantification of uncultured microorganisms by fluorescence microscopy and digital image analysis. Applied Microbiology and Biotechnology 75:237-248

DeLong EF, Wickham GS, Pace NR (1989) Phylogenetic stains: ribosomal RNA-based probes for the identification of single cells. Science 243:1360-1363

Ernst B, Hitzfeld B, Dietrich D (2001) Presence of Planktothrix sp and cyanobacterial toxins in Lake Ammersee, Germany and their impact on whitefish (Coregonus lavaretus L.). Environmental Toxicology 16:483-488

Fastner J, Neumann U, Wirsing B, Weckesser J, Wiedner C, Nixdorf B, Chorus I (1999a) Microcystins (hepatotoxic heptapeptides) in German fresh water bodies. Environmental Toxicology 14:13-22

Fastner J, Erhard M, Carmichael WW, Sun F, Rinehart KL, Ronicke H, Chorus I (1999b) Characterization and diversity of microcystins in natural blooms and strains of the genera Microcystis and Planktothrix from German freshwaters. Archiv Fur Hydrobiologie 145:147-163

Ferguson RL, Buckley EN, Palumbo AV (1984) Response of marine bacterioplankton to differential filtration and confinement. Appl Environ Microbiol 47:49-55

Forster B, Van de Ville D, Berent J, Sage D, Unser M (2004) Complex wavelets for extended depth-of-field: A new method for the fusion of multichannel microscopy images. Microscopy Research and Technique 65:33-42

Fuchs BM, Zubkov MV, Sahm K, Burkill PH, Amann R (2000) Changes in community composition during dilution cultures of marine bacterioplankton as assessed by flow cytometric and molecular biological techniques. Environmental Microbiology 2:191-201

Giovannoni SJ, DeLong EF, Olsen GJ, Pace NR (1988) Phylogenetic group-specific oligodeoxynucleotide probes for identification of single microbial cells. J Bacteriol 170:720-726

Giovannoni SJ, Tripp HJ, Givan S, Podar M, Vergin KL, Baptista D, Bibbs L, Eads J, Richardson TH, Noordewier M, Rappe MS, Short JM, Carrington JC, Mathur EJ (2005) Genome streamlining in a cosmopolitan oceanic bacterium. Science 309:1242-1245

Glöckner FO, Amann R, Alfreider A, Pernthaler J, Psenner R, Trebesius K, Schleifer KH (1996) An in situ hybridization protocol for detection and identification of planktonic bacteria. Systematic and Applied Microbiology 19:403-406

Gmür R, Guggenheim B, Giertsen E, Thurnheer T (2000) Automated immunofluorescence for enumeration of selected taxa in supragingival dental plaque. European Journal of Oral Sciences 108:393-402

Hamasaki K, Long RA, Azam F (2004) Individual cell growth rates of marine bacteria, measured by bromodeoxyuridine incorporation. Aquatic Microbial Ecology 35:217-227

Henrici AT (1933) Studies of freshwater bacteria I A direct microscopic technique. Journal of Bacteriology 25:277-287

Hersch J (1976) Die Hoffnung Mensch zu sein. Benziger Verlag Zürich, Köln

Hobbie JE, Daley RJ, Jasper S (1977) Use of nucleopore filters for counting bacteria by fluorescence microscopy. Applied and Environmental Microbiology 33:1225-1228

Hoeger SJ, Hitzfeld BC, Dietrich DR (2005) Occurrence and elimination of cyanobacterial toxins in drinking water treatment plants. Toxicology and Applied Pharmacology 203:231-242

Jones JG (1974) Some Observations on Direct Counts of Freshwater Bacteria Obtained with a Fluorescence Microscope. Limnol. Oceanogr. 19:540-543

Jurgens K, Pernthaler J, Schalla S, Amann R (1999) Morphological and compositional changes in a planktonic bacterial community in response to enhanced protozoan grazing. Applied and Environmental Microbiology 65:1241-1250

Krambeck C, Krambeck HJ, Overbeck J (1981) Microcomputer-Assisted Biomass Determination of Plankton Bacteria on Scanning Electron-Micrographs. Applied and Environmental Microbiology 42:142-149

Lee N, Nielsen PH, Andreasen KH, Juretschko S, Nielsen JL, Schleifer KH, Wagner M (1999) Combination of fluorescent in situ hybridization and microautoradiography - a new tool for structure-function analyses in microbial ecology. Applied and Environmental Microbiology 65:1289-1297

Legendre L, Courties C, Troussellier M (2001) Flow cytometry in oceanography 1989-1999: Environmental challenges and research trends. Cytometry 44:164-172

Liu J, Dazzo FB, Glagoleva O, Yu B, Jain AK (2001) CMEIAS: A computer-aided system for the image analysis of bacterial morphotypes in microbial communities. Microbial Ecology 41:173-194

Neto JC, Meyer GE, Jones DD, Samal AK (2006) Plant species identification using Elliptic Fourier leaf shape analysis. Computers and Electronics in Agriculture 50:121-134

Noble RT, Fuhrman JA (1998) Use of SYBR Green I for rapid epifluorescence counts of marine viruses and bacteria. Aquatic Microbial Ecology 14:113-118

Nowak HP (1984) Geschichte des Mikroskops. Selbstverlag

Oppenheimer JR (1966) Drei Krisen der Physiker. Walter-Verlag

Ouverney CC, Fuhrman JA (1999) Combined Microautoradiography-16S rRNA probe technique for determination of radioisotope uptake by specific microbial cell types in situ. Applied and Environmental Microbiology 65:1746-1752

Pace ML, Cole JJ (1996) Regulation of bacteria by resources and predation tested in whole-lake experiments. Limnol. Oceanogr. 41:1448-1460

Pernthaler A, Pernthaler J, Schattenhofer M, Amann R (2002a) Identification of DNA-synthesizing bacterial cells in coastal North Sea plankton. Applied and Environmental Microbiology 68:5728-5736

Pernthaler A, Pernthaler J, Amann R (2002b) Fluorescence in situ hybridization and catalyzed reporter deposition for the identification of marine bacteria. Applied and Environmental Microbiology 68:3094-3101

Pernthaler J, Alfreider A, Posch T, Andreatta S, Psenner R (1997) In situ classification and image cytometry of pelagic bacteria from a high mountain lake (Gossenkollesee, Austria). Applied and Environmental Microbiology 63:4778-4783

Pernthaler J, Glockner FO, Unterholzner S, Alfreider A, Psenner R, Amann R (1998) Seasonal community and population dynamics of pelagic bacteria and archaea in a high mountain lake. Applied and Environmental Microbiology 64:4299-4306

Pernthaler J, Posch T, Simek K, Vrba J, Pernthaler A, Glockner FO, Nubel U, Psenner R, Amann R (2001) Predator-specific enrichment of actinobacteria from a cosmopolitan freshwater clade in mixed continuous culture. Applied and Environmental Microbiology 67:2145-2155

Pernthaler J, Pernthaler A, Amann R (2003) Automated enumeration of groups of marine picoplankton after fluorescence in situ hybridization. Applied and Environmental Microbiology 69:2631-2637

Pernthaler J (2005) Predation on prokaryotes in the water column and its ecological implications. Nat Rev Microbiol 3:537-546

Pernthaler J, Amann R (2005) Fate of heterotrophic microbes in pelagic habitats: focus on populations. Microbiol Mol Biol Rev 69:440-461

Pincus Z, Theriott JA (2007) Comparison of quantitative methods for cell-shape analysis. Journal of Microscopy-Oxford 227:140-156

Porter KG, Feig YS (1980) The Use of Dapi for Identifying and Counting Aquatic Microflora. Limnol. Oceanogr. 25:943-948

Posch T, Pernthaler J, Alfreider A, Psenner R (1997) Cell-specific respiratory activity of aquatic bacteria studied with the tetrazolium reduction method, cyto-clear slides, and image analysis. Applied and Environmental Microbiology 63:867-873

Posch T, Loferer-Krossbacher M, Gao G, Alfreider A, Pernthaler J, Psenner R (2001) Precision of bacterioplankton biomass determination: a comparison of two fluorescent dyes, and of allometric and linear volume-to-carbon conversion factors. Aquatic Microbial Ecology 25:55-63

Posch T, Mindl B, Hornak K, Jezbera J, Salcher MM, Sattler B, Sonntag B, Vrba J, Simek K (2007) Biomass reallocation within freshwater bacterioplankton induced by manipulating phosphorus availability and grazing. Aquatic Microbial Ecology 49:223-232

Posch T, Franzoi J, Prader M, Salcher MM (2009) New image analysis tool to study biomass and morphotypes of three major bacterioplankton groups in an alpine lake. Aquatic Microbial Ecology 54:113-126

Psenner R, Sommaruga R (1992) Are rapid changes in bacterial biomass caused by shifts from top-down to bottom-up control. Limnol. Oceanogr. 37:1092-1100

Salcher MM, Pernthaler J, Zeder M, Psenner R, Posch T (2008) Spatio-temporal niche separation of planktonic Betaproteobacteria in an oligo-mesotrophic lake. Environmental Microbiology 10:2074-2086

Schattenhofer M (2009) Distribution of major bacterioplankton groups in the Atlantic Ocean. Dissertation

Schattenhofer M, Fuchs BM, Amann R, Zubkov MV, Tarran GA, Pernthaler J (2009) Latitudinal distribution of prokaryotic picoplankton populations in the Atlantic Ocean. Environ Microbiol

Schlegel HG (2004) Geschichte der Mikrobiologie. Deutsche Akademie der Naturforscher Leopoldina

Sekar R, Pernthaler A, Pernthaler J, Warnecke F, Posch T, Amann R (2003) An improved protocol for quantification of freshwater Actinobacteria by fluorescence in situ hybridization. Applied and Environmental Microbiology 69:2928-2935

Sekar R, Fuchs BM, Amann R, Pernthaler J (2004) Flow sorting of marine bacterioplankton after fluorescence in situ hybridization. Applied and Environmental Microbiology 70:6210-6219

Shapiro HM (1995) Practical flow cytometry. Wiley-Liss

Sieracki ME, Johnson PW, Sieburth JM (1985) Detection, Enumeration, and Sizing of Planktonic Bacteria by Image-Analyzed Epifluorescence Microscopy. Applied and Environmental Microbiology 49:799-810

Sieracki ME, Viles CL, Webb KL (1989) Algorithm to Estimate Cell Biovolume Using Image Analyzed Microscopy. Cytometry 10:551-557

Singleton S, Cahill JG, KeithWatson G, Allison C, Cummins D, Thurnheer T, Guggenheim B, Gmur R (2001) A fully automated microscope bacterial enumeration system for studies of oral microbial ecology. Journal of Immunoassay & Immunochemistry 22:253-274

Smith EM, del Giorgio PA (2003) Low fractions of active bacteria in natural aquatic communities? Aquatic Microbial Ecology 31:203-208

Sommer U, Gliwicz ZM, Lampert W, Duncan A (1986) The Peg-Model of Seasonal Succession of Planktonic Events in Fresh Waters. Archiv Fur Hydrobiologie 106:433-471

Urbach E, Vergin KL, Giovannoni SJ (1999) Immunochemical detection and isolation of DNA from metabolically active bacteria. Applied and Environmental Microbiology 65:1207-1213

Warnecke F, Sommaruga R, Sekar R, Hofer JS, Pernthaler J (2005) Abundances, identity, and growth state of actinobacteria in mountain lakes of different UV transparency. Applied and Environmental Microbiology 71:5551-5559

Wiggins PM (1990) Role of water in some biological processes. Microbiological Reviews 54:432-449

Wilkinson MHF (1998) Digital image analysis of microbes imaging, morphometry, fluorometry and motility techniques and applications. Wiley

Young KD (2006) The selective value of bacterial shape. Microbiology and Molecular Biology Reviews 70:660-+

Zeder M, Peter S, Shabarova T, Pernthaler J (2009) Cultivable planktonic Flavobacteria that are highly active during the spring phytoplankton bloom in Lake Zurich. Environmental Microbiology:*in press*